Tampere University

Sami Seppälä

EFFECTS OF MARINE FUEL SULFUR RESTRICTIONS ON PARTICLE PROPERTIES IN ATMOSPHERIC AEROSOL AT THE BALTIC SEA

Faculty of Engineering and Natural Sciences
Master of Science thesis
February 2020

ABSTRACT

Sami Seppälä: Effects of marine fuel sulfur restrictions on particle properties in atmospheric aerosol at the Baltic Sea
Master of Science Thesis
Tampere University
Master's degree Programme in Science and Engineering
February 2020

Emissions produced by shipping have been shown to have a significant effect on the climate and the human health especially in coastal areas. It is estimated that typically the emissions produced by shipping have in total a cooling effect on the climate as negative radiative forcing (RF) induced by refractive particulate matter (PM) negates the warming effect of greenhouse gases (GHGs) emitted in shipping. However, this effect is not uniform and, in some areas, for example in the Arctic the net effect of shipping on the climate might also be warming. The shipping emissions also contribute to the acidification of marine environments. The effects of shipping emissions on the human health are negative. The shipping emissions have been shown to lead to increased premature mortality and numerous respiratory diseases.

This work focuses on the effects of the different marine fuel sulfur restrictions of 1.50 %, 1.00 % and 0.10 % on the atmospheric aerosol and ship plumes in the Baltic Sea Sulfur Emission Control Area (SECA). The discussed properties are total particle number concentration (PNC), particle number concentration over background particle number concentration during plume (PNC_{pl}), the direct contribution of the PNC_{pl} to the total PNC, the number size distribution of the plume particles (NSD_{pl}), the number size distribution of the background particles (NSD_{bg}), the surface area concentration of the plume particles (PSC_{pl}) and plume aging. The NSD_{pl}s are also compared to NSDs from direct emission measurements. The measurement data used in this work is differential mobility particle sizer (DMPS) data measured by the Finnish Meteorological Institute at the measurement station of Utö in the Baltic Sea between 11.1.2007-31.12.2016. The DMPS data was used with the Automatic Identification System (AIS) and weather data to produce the results. In this work the plumes were analyzed from three different sectors with the plumes arriving from different distances on average. The goal of this work was to study if the ship plumes are detectable in the atmospheric measurement data and how the sulfur restrictions influence the particle properties of the atmospheric aerosol. This work may give better understanding what kind of an effect the sulfur restrictions have on the atmospheric aerosol and how the measurement system at Utö could be developed in the future.

In total 43503 analyzable plumes were detected from the DMPS data. The sulfur restrictions were found to be effective, reducing both the PNCs and average particle diameters. The effect of the change in the sulfur restriction from 1.50 % to 1.00 % was much smaller than the effect of the later change in the sulfur restriction from 1.00 % to 0.10 %. These effects of the sulfur restriction changes were observed both in the plumes and the background aerosol particles. The most significant effects of the changes in the sulfur restrictions were: 1) The increase of the PNC_{pl}s in particles sizes smaller than 35 nm, while the PNC_{pl}s in total decreased. This increase was related to the reduced size of the particles produced in the combustion process. 2) The sulfur restrictions were found to decrease the largest average PNC_{pl}s. Especially the PNC_{pl}s of the plumes with the largest diameters of the maximums of the NSD_{pl}s were reduced. 3) The lower sulfur contents in marine fuels led to larger relative increases of the PNC_{pl}s in the smaller particles in the plume aging compared to the higher sulfur contents. 4) The stricter sulfur reductions shifted the maximums of the NSD_{bg}s to smaller particle sizes and reduced the PNC_{bg}s indicating that the effect of the shipping emissions on the atmospheric aerosol is a lot larger than what only the direct effects would suggest. 5) The measurement cycle of the DMPS (5 min 20 s) was found to be too long for the optimal plume detection and using an instrument with a shorter time resolution would be beneficial.

Keywords: sulfur restriction, atmospheric aerosol, ship emission, ship plume.

The originality of this thesis has been checked using the Turnitin OriginalityCheck service.

TIIVISTELMÄ

Sami Seppälä: Laivapolttoaineen rikkirajoitusten vaikutus ilmakehän aerosolipartikkelien ominaisuuksiin Itämerellä
Diplomityö
Tampereen yliopisto
Teknis-luonnontieteellinen tutkinto-ohjelma
Helmikuu 2020

Laivaliikenteessä syntyvillä päästöillä on osoitettu olevan merkittävä vaikutus ilmastoon ja ihmisten terveyteen varsinkin rannikkoalueilla. On arvioitu, että tyypillisten laivapäästöjen vaikutus ilmastoon on viilentävä johtuen heijastavien partikkelipäästöjen aiheuttamasta lisääntyneestä negatiivisesta säteilypakotteesta (engl. radiative forcing, RF), joka on suurempi kuin laivaliikenteessä syntyvien kasvihuonekaasujen (engl. greenhouse gas, GHG) lämmittävä vaikutus. Tämä vaikutus ei kuitenkaan ole yhtenäinen ja joillakin alueilla, kuten esimerkiksi Arktiksella, laivapäästön vaikutus ilmastoon voi olla myös lämmittävä. Laivapäästöt myös lisäävät merialueiden happamoitumista. Laivapäästöjen vaikutus ihmisten terveyteen on negatiivinen lisäten ennenaikaista kuolleisuutta ja useita hengitys- ja verenkiertoelimistön sairauksia.

Tämä työ keskittyy 1,50 %, 1,00 %, ja 0,10 % rikkirajoitusten vaikutuksiin ilmakehän aerosoliin ja laivojen savuvanoihin (pluumeihin) Itämeren rikkipäästöjen rajoitusalueella (engl. sulfur emission control area, SECA). Tutkitut ominaisuudet ovat kokonaishiukkaslukumääräkonsentraatio (engl. particle number concentration, PNC), pluumin aikainen taustahiukkaslukumääräkonsentraation ylittävä hiukkaslukumääräkonsentraatio (PNC_{pl}), PNC_{pl}:n suora vaikutus kokonais-PNC:hen, pluumipartikkelien lukumääräkokojakauma (engl. number size distribution, NSD_{pl}), taustan lukumääräkokojakauma (NSD_{bg}), pluumi partikkelien pinta-alakonsentraatio (engl. particle surface area concentration (PSC_{pl}), pluumien ikääntyminen ja pluumien lukumääräkokojakaumien vertailu suorien päästömittausten lukumääräkokojakaumiin. Tässä työssä käytetty mittausdata oli Suomen Ilmatieteenlaitoksen Utön mittaus asemalla aikaväillä 11.1.2007-31.12.2016 mittaamaa differentiaalisen liikkuvuusanalysaattorin (engl. differential mobility analyzer, DMPS) dataa. Dataa käytettiin yhdessä laivojen automaattisen tunnistusjärjestelmä (engl. automatic identification system, AIS) datan ja säädatan kanssa tulosten tuottamiseksi. Tässä työssä pluumeja tutkittiin kolmelta eri sektorilta, joilta tulevat pluumit olivat keskimäärin lähtöisin eri etäisyyksiltä. Tämän työn tavoitteena oli tutkia, ovatko laivapluumit havaittavissa ilmakehän mittausdatasta ja kuinka rikkirajoitukset vaikuttavat näihin. Tämä työ voi lisätä ymmärrystä rikkirajoitusten vaikutuksista ilmakehän aerosoliin ja antaa uutta tietoa, kuinka Utön mittaus laitteistoa voitaisiin kehittää tulevaisuudessa.

Kokonaisuudessaan 43503 analysoitavaksi kelpaavaa pluumia löydettiin DMPS datasta. Rikkirajoitusten huomattiin olleen toimivia, vähentäen niin PNC:itä kuin hiukkasten keskimääräisiä halkaisijoita. Rikkirajoituksen muutoksen vaikutuksen 1,50 %:sta 1,00 %:iin huomattiin olleen paljon pienempi kuin myöhemmän suuremman rajoituksen muutoksen 1.00 %:sta 0,10 %:iin. Rikkirajoitusten vaikutukset olivat nähtävissä niin laivapluumeissa kuin tausta-aerosolin hiukkasissa. Merkittävimmät rikkirajoitusten vaikutukset olivat: 1) PNC_{pl}:t lisääntyivät kokoluokassa alle 35 nm, samalla kun PNC_{pl}:t kokonaisuudessaan laskivat. Tämä konsentraation kasvu yhdistettiin entistä pienempien hiukkasten syntymiseen paloprosessissa. 2) Rikkirajoitusten huomattiin vähentävän suurimpia keskimääräisiä PNC_{pl}:tä. Varsinkin PNC_{pl}:t, joilla oli suurimmat NSD_{pl}:n maksimit, pienenivät. 3) Matalammat rikkipitoisuudet johtivat suurempaan suhteelliseen kasvuun aerosolin ikääntymisessä PNC_{pl}:ssä pienemmillä partikkeleilla verrattuna korkeampiin rikkipitoisuuksiin. 4) Rikkirajoituksen siirsivät NSD_{bg}:n maksimeja pienemmille hiukkasko'oille ja vähensivät PNC_{bg}: itä vihjaten, että laivapäästöjen vaikutus ilmakehän aerosoliin on paljon suurempi kuin suorien vaikutusten perusteella voisi olettaa. 5) DMPS:n mittaussyklin (5 min 30 s) huomattiin olleen liian pitkä optimaaliseen pluumien tunnistamiseen datasta. Tulevaisuudessa lyhyemmän mittaussyklin omaavan laitteen käytöstä voisi olla hyötyä.

Avainsanat: rikkirajoitukset, ilmakehän aerosoli, laivapäästö, laivapluumi

Tämän työn alkuperäisyys on tarkastettu käyttäen Turnitin OriginalityCheck palvelua.

ACKNOWLEDGEMENTS

This thesis work was done at Finnish Meteorological Institute's unit of Atmospheric Composition Research, in Atmospheric Aerosols group. This thesis was an individual research funded by research infrastructure ACTRIS (European Research Infrastructure for observation of Aerosol, Clouds and Trace Gases). DMPS and weather data used in this thesis was measured by Finnish Meteorological Institute in atmospheric measurement station at Utö between 11.1.2007-31.12.2016. I did not take part in the measurements myself and I would like to thank everyone who contributed in making the measurements and made this work possible.

First, I would like to thank Professor Jorma Keskinen from Aerosol Physics Laboratory at Tampere University for acting as the main examiner of this thesis and for valuable comments and ideas. From the Finnish Meteorological Institute, I would like to thank Docent Hilkka Timonen for acting as the second examiner of this thesis and for valuable comments according to this work. I would like to also thank the supervisors of this thesis Antti-Pekka Hyvärinen and Sanna Saarikoski for irreplaceable help on data processing and refining of the thesis. Special thanks go also to Niku Kivekäs for providing the codes on which the data analysis was based on and helping greatly in the data analysis.

Finally, I would like to thank my beloved wife Liisa Harni for the irreplaceable help in finding this master's thesis workplace and the continuous support and encouragement in the thesis process.

Helsinki, 4.2.2020

Sami Seppälä

TABLE OF CONTENTS

ABBREVIATIONS AND MARKINGS

Abbreviations

ACTRIS	European Research Infrastructure for observation of Aerosol, Clouds and Trace Gases
AIS	Automatic Identification System
BC	Black carbon
CPC	Condensation particle counter
DMA	Differential mobility analyzer
DMPS	Differential mobility particle sizer
DSC	Digital selective calling
EPA	United States Environmental Protection Agency
FMI	Finnish Meteorological Institute
GHG	Greenhouse gas
GT	Gross tonnage
HELCOM	Baltic Marine Environment Protection Commission
HFO	Heavy fuel oil
ICRP	International Commission on Radiological Protection
IFO	Intermediate fuel oil
IMO	International Maritime Organization
LDSA	Lund deposited surface area
LNG	Liquefied natural gas
LPG	Liquefied petroleum gas
MARPOL	International Convention for the Prevention of Pollution from Ships
MDO	Marine diesel oil
MMO	Metal oxides
MMSI	Maritime mobile service identity
NSD	Particle number size distribution
NSD_{bg}	Background particle number size distribution
NSD_e	Excess number size distribution (total NSD subtracted with NSD_{bg})
NSD_{pl}	Particle number size distribution of plumes (total NSD subtracted with NSD_{bg} during plumes)
NMVOC	Non-methane volatile organic compounds
OM	Organic matter
PA	Primary aerosol
PM	Particulate matter
$PM_{0.15}$	Particulate matter smaller than 0.15 µm in diameter
PM_1	Particulate matter smaller than 1 µm in diameter
$PM_{2.5}$	Particulate matter smaller than 2.5 in diameter
PM_{10}	Particulate matter smaller than 10 µm in diameter
PNC	Particle number concentration
PNC_{bg}	Background particle number concentration
PNC_e	Excess particle number concentration
PNC_{pl}	Particle number concentration of plumes (total PNC subtracted with PNC_{bg})
PNSD	Particle number size distribution
PSC	Particle surface area concentration
R_e	Ratio of total PNC to PNC_{bg}
RF	Radiative forcing
RORO	Roll-on/roll-off
SA	Secondary aerosol
SCR	Selective catalytic reduction
SECA	Sulfur Emission Control Area

SMPS	Scanning mobility particle sizer
SOA	Secondary organic aerosol
TSP	Total Suspended Particulate
VOC	Volatile Organic Compound

Symbols

CMD	Count median diameter
d_p	Particle diameter
$\mathrm{d}d_p$	Differential width of size bin
$\mathrm{d}\log d_p$	Differential width of size bin on a logarithmic scale
$\mathrm{d}N$	Number of particles in a size bin with differential width
GSD	Geometric standard deviation
σ_g	Geometric standard deviation
$n(d_p)$	Particle number distribution
$n(\ln d_p)$	Log-normal particle number distribution
N_T	Total number concentration of particles

Chemical compounds

Al	Aluminum
C	Carbon
Ca	Calcium
CFC	Anthropogenic chlorofluorocarbon
Cl	Chlorine
Cl_2	Molecular chlorine
ClO	Chlorine monoxide
CO	Carbon monoxide
CO_2	Carbon dioxide
Fe	Iron
H	Hydrogen
HC	Hydrocarbons
HClO	Hydrochloride monoxide
HO_2	Hydroperoxyl
H_2O	Water
N	Nitrogen
NH_3	Ammonia
$\mathrm{NH_4^+}$	Ammonium
Ni	Nickel
NO_x	Nitrogen oxides
NO_2	Nitrogen dioxide
NO_3	Nitrate radical
O	Oxygen
OH	Hydroxyl radical
O_2	Oxygen molecule
O_3	Ozone
S	Sulfur
Si	Silicon
SO_x	Sulfur oxides
SO_2	Sulfur dioxide
$\mathrm{SO_4^{2-}}$	Sulfate
V	Vanadium

1. INTRODUCTION

Ambient concentrations of airborne particulate matter (PM) have long been known to be a large factor in increasing cardiorespiratory mortality and morbidity. This has been shown in multiple studies including, but not limited to, Pope (1996), Schwartz et al. (1996) and Landis et al. (2001). Eyring et al. (2010) reported shipping to cause air quality problems through formation of ground level ozone (O_3), sulfur (S) emissions and PM. These problems were found significant as nearly 70 % of all maritime emissions are produced within 400 km from coastlines. Eyring et al. also stated that the problems are mostly located around heavily trafficked shipping lanes and harbor areas, but the O_3 and aerosol precursor emissions can be transported even several hundreds of kilometers inland.

The ship emissions have been shown to have impacts on the climate in multiple studies including, but not limited to, Fugelstvedt et al. (2009), Eyring et al. (2010), Headey et al. (2010), and Dessens et al. (2014). The ship emissions cool the climate by altering the reflectivity of clouds and forming light reflecting sulfur particles from sulfur dioxide (SO_2) of marine fuels (Fugelstvedt, et al., 2009; Eyring, et al., 2010). This results to negative radiative forcing (RF). The cooling effect of the negative RF outweighs climate warming effects of carbon dioxide (CO_2) and other greenhouse gases produced by shipping.

The ship emissions have long been unregulated. According to Chu Van et al. (2019) the International Convention for the Prevention of Pollution from Ships (MARPOL) was initiated by the International Maritime Organization (IMO) and adopted in 1973. Chu Van et al. also state that the regulations set by the convention aim to reduce nitrogen oxides (NO_x), sulfur oxides (SO_x) and PM from marine engines and that these regulations have been effective since May 19th, 2005. They also stated that additional stricter emission restrictions have been presented by some nations or set for vulnerable areas. For example, Sulphur Emission Control Areas (SECAs) have been set in the Baltic Sea, the North Sea area, the North American region, and the United States Caribbean Sea areas.

This work aims to study the effectiveness of two changes in the sulfur content of the marine fuels in the Baltic Sea SECA. The changes of the sulfur restrictions were from 1.50 % to 1.00 % in July 1st, 2010 and from 1.00 % to 0.10 % in January 1st, 2015 (Antturi, et al., 2016). Large positive effects of the sulfur restrictions of the marine fuels on air quality have been reported before in Hong Kong harbor area by Mason et al. (2019).

Similar studies have not been made before in the Baltic Sea SECA. Another goal of is this study is to figure how well the ship plumes can be detected and separated from the atmospheric measurement data in marine environments. This has been studied earlier by Kivekäs et al. (2014) and the plume detection method used in this thesis is based on that article. These results produce valuable information, that can be used in developing the marine atmospheric particle measurement setup in Utö and evaluating the effects, that the sulfur restrictions have on the atmospheric aerosol particle properties in the Baltic Sea.

The discussed effects of the sulfur restrictions in this thesis are the total particle number concentration (PNC), particle number concentration over background particle number concentration during plumes (PNC_{pl}), direct contribution of the PNC_{pl} to the total PNC, the number size distribution of the plumes (NSD_{pl}), the number size distribution of the background (NSD_{bg}), the surface area concentration of the plume particles (PSC_{pl}) and plume aging. The NSD_{pl}s are also compared to NSDs from direct emission measurements. The atmospheric measurement data used in this study was measured by the Finnish Metrological Institute (FMI) in the atmospheric measurement station at Utö between 11.1.2007-31.12.2016. The direct emission measurement data was attained from Kuittinen (2016).

2. ATMOSPHERIC AEROSOLS

The atmosphere of Earth is mostly composed of gases, but also contains PM from liquid and solid substances. Together these particles and gases form an atmospheric aerosol (Boucher, et al., 2013). According to Hinds (1999) the atmospheric aerosol is a complex and dynamic mixture, where new primary particles are continuously emitted into and secondary particles formed in. The atmospheric aerosol particles may undergo evaporation, growth by different mechanisms, chemical reactions, or get removed from the atmosphere through numerous removal mechanisms (Hinds, 1999; Grythe, 2017). One of the most relevant quantities concerning the atmospheric aerosols is the particle concentration. The common particle concentrations to be measured are particle number, mass, surface area and volume concentrations (Kulkarni et al., 2011).

2.1 Sources of atmospheric aerosols

The sources of the atmospheric aerosols are numerous and widely spread in both space and time (Potier, et al., 2019). According to Boucher et al. (2013), all the atmospheric aerosols are formed through two pathways, by direct emissions or by the formation of secondary particulate matter from precursor gases. In the atmosphere the particles can grow to larger sizes through vapor condensation or by coagulation with other particles (Hinds, 1999). The most significant removal mechanism of particles from atmosphere is precipitation (Grythe, 2017).

The atmospheric aerosols can be further classified to two distinct categories according to their sources, natural and anthropogenic aerosols (Hinds, 1999; Grythe, 2017). The natural aerosol is the background aerosol that is not the result of human activities (Hinds, 1999). Common natural aerosol sources are sea spray, botanical debris, volcanic dust, forest fires, gas-to-particle conversion, and photochemical processes (Hinds, 1999; Spracklen and Rap, 2013). The contribution of the natural aerosols in the atmosphere is significant and the natural aerosols are distributed all around the globe (Hinds, 1999; Grythe, 2017). The largest of the natural aerosol sources are the large sea areas of Earth followed by deserts and vegetation (Hinds, 1999).

According to Hinds (1999) the anthropogenic aerosol is the aerosol that is produced by or related to human activities. Anthropogenic aerosol sources consist of primary emissions, particles formed by gas-to-particle conversions and photochemical reactions (Hinds, 1999). Huang et al. (2014) estimated that 35 % of the global emissions of the

total suspended particulate (TSP) in 2007 were from the anthropogenic sources. The sources of the anthropogenic aerosols are more concentrated to the industrialized regions of the world where the levels of the anthropogenic aerosols can be higher than the natural background aerosol levels (Hinds, 1999). For example, in South Asia 37 ± 20 % of the particulate matter smaller than 2.5 µm ($PM_{2.5}$) have been measured being vehicular emissions, 23 ± 16 % industrial emissions, 22 ± 12 % SA and only 20 ± 15 % natural aerosols (Singh, et al., 2017).

The areal variation of aerosol concentrations is large. For example, in measurements made in Delhi, India by Tiwari et al. (2011), the hourly mean values of TSP varied between 395 µg/m^3 and 980 µg/m^3. In turn, Zhu et al. (2018) measured in the southeastern Tibetan plateau where the TSP levels varied between 12.5 ± 5.5 µg/m^3 and 19.1 ± 8.3 µg/m^3. According to Kulkarni et al. (2011) when the aerosol concentrations are considered, the total aerosol concentrations in polluted urban areas are typically in the order of 10^5 #/cm^3 being even in the order of 10^7 #/cm^3 near emission sources and in order of 10^4 #/cm^3 in less polluted areas.

2.2 Particle size distribution

For particle sizes, size distributions and size distribution functions the reader is referred to John (2011). The particle size is usually characterized by the diameter of the particle. Depending on the circumstances, the particle diameter may refer to multiple different diameters, for example, a geometric diameter, an aerodynamic diameter, a Stokes diameter, an electrical mobility diameter or an optical diameter. All these diameters have different definitions and can be different for the same exact particle and the optical diameter is even dependent on the used measurement instrument. The particles in an aerosol have a wide size range from about 10^{-9} m to 10^{-4} m. As the particle sizes range over 6 orders of magnitude, dividing the particles to smaller size classes is useful. One classification made by United States Environmental Protection Agency (EPA) is listed in Table 1.

Table 1 The different particle size classes according to EPA adapted from Castranova (2011).

Particle Type	Aerodynamic diameter
Ultrafine	<0.1 μm
Fine	0.1-2.5 μm
Coarse	2.5-10 μm
Supercoarse	>10 μm

The particle diameter is a key parameter in many aerosol processes such as particle transport and deposition. That is why it is often useful to study a particle size distribution. If all particles in an aerosol are the same size, the size distribution is called a monodisperse size distribution. In real aerosols the particles are seldom only one size, but many different sizes. The only aerosols with even nearly monodisperse particle distributions are usually created in a laboratory. The particle size distribution that consists of many different sized particles is called a polydisperse size distribution.

The simplest form of presenting the particle size distribution of aerosol particles is to form size bins for the aerosol particles, measure the aerosol particle numbers for all the size bins and plot a histogram. This kind of histogram can be hard to interpret because the particle numbers of the size bins are dependent on the width of the size bins. When the size bins are fine enough the size distribution is called a differential size distribution. Since the plotted quantity is the particle number for each of the differential size bins, the distribution is called a number distribution. The particle number distribution $n(d_p)$ is defined as

$$\mathrm{d}N = n(d_p)\mathrm{d}d_p,$$

where the $\mathrm{d}N$ is the number of the particles, in a differential size bin with the width of the $\mathrm{d}d_p$. The $n(d_p)$ is the size distribution function. In many situations the sizes of the aerosol particles can range over several orders of magnitude. That is why it is useful to replace the $\mathrm{d}d_p$ with the logarithmic differential bin width $\mathrm{dlog}d_p$ and therefore the previous equation can be expressed as

$$\mathrm{d}N = n(d_p)\mathrm{dlog}d_p.$$

In many cases it is convenient to fit the data with a function to characterize the distribution by only a few variables. Many natural sources have also been shown to fit well to a log-normal distribution

$$n(\ln d_p) = \frac{N_T}{\sqrt{2\pi}\ln\sigma_g} e^{\frac{-(\ln d_p - \ln CMD)^2}{2(\ln\sigma_g)}}.$$

Where N_T is the total number concentration of the particles, σ_g is the geometric standard deviation and the CMD is the count median diameter. This log-normal distribution is widely used in aerosol science.

When atmospheric aerosol particle number size distribution (NSD) is transformed into volume distribution typically at least three distinct size modes are revealed. Those three modes are nuclei mode 0.005-0.1 µm, accumulation mode 0.1-2 µm and coarse mode >2 µm. Hinds (1999) states the following concerning the formation of the particles in the different modes: The particles in the nuclei mode are mostly combustion particles from direct emission sources or formed straight from gas through gas-to-particle conversion i.e. nucleation. The particles in the accumulation mode are direct combustion particles, smog or nuclei mode particles that have coagulated with particles from the accumulation mode. The particles in coarse mode are mostly windblown dust, salt particles formed from sea spray and mechanically generated anthropogenic particles for example from surface mining or agriculture.

2.3 Primary and secondary aerosols

There are two types of atmospheric aerosols, primary aerosols (PAs) and secondary aerosols (SA) (Hinds, 1999). The PAs are emitted directly into atmosphere and SAs are formed in the atmosphere trough the chemical reactions of gaseous components (Hinds, 1999; Grythe, 2017). The contribution of the SAs in the atmosphere for both, natural and anthropogenic sources is significant (Hinds, 1999). PA sources consist of wide variety of natural and anthropogenic sources. According to Hallquist et al. (2009) the PAs are produced by biomass burning, fossil fuel combustion, volcanic eruptions, the wind driven suspension of soil, mineral dust, sea salt and biological materials. Hallquist et al. (2009) also state that there are no direct sources for the SAs, but they are formed by gas-to-particle conversion processes, such as the nucleation, the condensation, and heterogenous and multiphase chemical reactions.

The formation of the SAs from inorganic gases such as SO_2, nitrogen dioxide (NO_2), and ammonia (NH_3) is quite well known, but there is a large uncertainty concerning the production of secondary organic aerosol (SOA) from volatile organic compounds (VOCs) (Hallquist, et al., 2009). Fossil fuel combustion has been shown to be a large source of the SOA (Gentner, et al., 2012). The SOA is formed from condensable oxidation products

of VOCs and is known to be a significant and widespread factor of the atmospheric aerosol (Kanakidou, et al., 2005; Zieman and Atkinson, 2012; Ehn, et al., 2014). The SOA is also noted having an important effect on the climate change and to the overall air quality (Hong, et al., 2019).

The SOA is formed in the atmosphere when the VOCs are oxidized to less volatile oxidation products, that condensate on existing particles to establish equilibrium between the gas and aerosol phases (Seinfeld and Pandis, 2006). The VOCs are oxidized by reactions with hydroxyl radicals (OH), O_3, nitrate radicals (NO_3) or chlorine atoms (Cl) (Zieman and Atkinson, 2012). The SOA formation is different during the day and the night (Warneke et al., 2004). The VOCs emitted in the atmosphere are oxidized with chemical processes of photolysis and reactions with the OH during daytime, with NO_3 during evening and with O_3 during nighttime (Zieman and Atkinson, 2012).

2.4 Health effects of aerosol particles

For the health effects of particles, the reader is referred to Hinds (1999) and Castranova (2011). Particles can cause negative health effects when they are inhaled. The harmfulness of the inhaled particles depends on multiple variables including their size, shape, surface chemistry, and deposition place and residence time in the respiratory system. PM concentrations have been related to negative health effects in many studies, including but not limited to, Donaldson et al. (2005), Kim et al. (2019) and Lu et al. (2019). The PNC of particles in the size range of 50-500 nm and lung-deposited particle surface area (LDSA) have also been linked to natural and cardiovascular mortality (Hennig, et al., 2018).

In the respiratory system, the particles can deposit to three different regions. The first region is the head airways region that includes the nose, the mouth, the pharynx and the larynx. The second region is the lung airways region, that includes the airways from trachea to the terminal bronchioles. The third region is the alveolar region, that includes the pulmonary alveolus where the gas exchange between inhaled air and blood takes place.

The deposition of particles is determined by five deposition mechanisms, impaction, settling, diffusion, intersection and electrostatic deposition. From these five, the last two are important only in special situations. The deposition can be modelled with the International Commission on Radiological Protection (ICRP) model. The different deposition functions for the model have been represented in Figure 1. The deposition fractions to the different areas of the respiratory system as well as the total deposition are presented as the function of particle diameter using ICRPN equations.

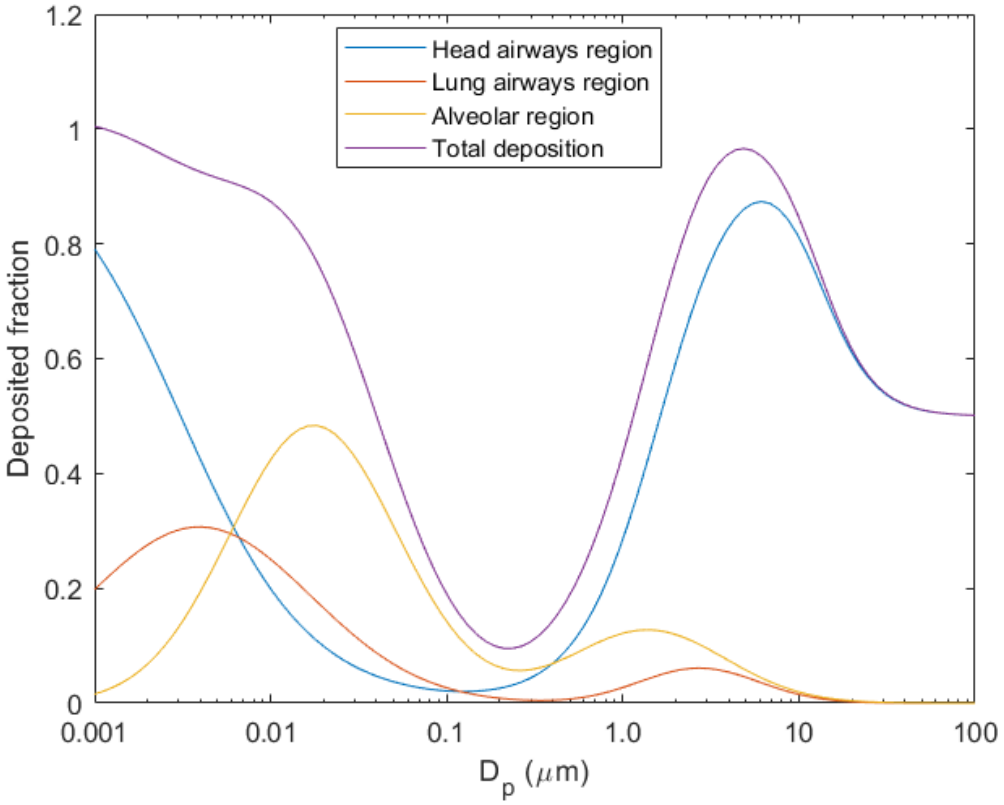

Figure 1 The deposition fractions of particles in the respiratory system according to the ICPR model equations adapted from Hinds (1999).

In the respiratory systems particles that contact the airway walls get deposited and are retained there for varying times depending on the location and the clearance mechanism involved. Particles deposited in the first two regions are removed in a matter of hours. Particles that are deposited into alveolar region are removed very slowly over the period of months and years.

The initiation and progression of pathogenic processes leading to disease induced by the inhaled aerosol are governed by the site of the particle deposition in the respiratory system, the residence time in the lungs and reactivity with lung cells. The harmfulness of the inhaled particles is reduced if the particles are removed rapidly and pronounced if the residence time is long. The particles deposited in the pulmonary region are more likely to be harmful than the particles deposited in the other parts of the respiratory system. Once the particle is deposited in the lung the surface properties of the particle are the decisive factor in particle-cell interaction and thus affect the bioactivity and pathogenicity of the particle. Examples of the PM induced diseases are parenchyneal cancer, interstitial fibrosis and emphysema.

Particles that are smaller than 100 nm in diameter are called nanoparticles. These particles have some differences to other fine particles considering health effects. Because of

their smaller size they have virtually no mass or inertia and are not deposited in the respiratory tract by the impaction or sedimentation, but mostly by the diffusion caused by Brownian motion. As the nanoparticles are small, they can be inhaled deep in the lungs and when they reach the alveoli they get deposited on the alveolar surface by diffusion as seen in Figure 1. This increases their residence time and harmfulness in the respiratory system.

2.5 PM climate effects

The atmospheric aerosols have a large effect on the climate, influencing two major atmospheric processes, global warming and O_3 depletion (Hinds, 1999). PM interacts with solar radiation through two processes, absorption and scattering. The interactions are stronger with solar radiation than with the long wave terrestrial radiation, leading to cooling effect (Boucher, et al., 2013). Hinds (1999) lists two ways how aerosols can scatter light. Firstly, the aerosols scatter light back to the space by direct scattering where the aerosol itself directly scatters the solar light. Secondly, the aerosols scatter light as acting as cloud condensation nuclei forming more clouds that scatter the light. Both of these effects have a cooling effect on the climate of the Earth, and their total effect is called a "white house" effect. Hinds (1999) states that the estimates of the magnitude of this effect vary between 20-100 % of the heating effects due the greenhouse gases. Although, according to Boucher et al. (2013) there are large uncertainties concerning the net radiative feedback of the clouds.

The effect of the aerosols in the troposphere (the lower level of atmosphere) on the climate can be warming or cooling depending on the aerosol. If the aerosol is absorbing for example black carbon (BC) the effect is warming (Kanakidou, et al., 2005; Gao, et al., 2014). According to Gao et al. (2014), if the aerosol is refractive such as sulfate (SO_4^{2-}), NO_3 or ammonium (NH_4^+), the effect on the climate is cooling. Gao et al. also state that the warming effect of the absorbing BC negates approximately half of the cooling effects of the refractive aerosols related to the anthropogenic aerosols. A significant difference between gases and particles in atmosphere is that particles have a lifetime of approximately a week, while greenhouse gases have a lifetime of decades (Hinds, 1999).

This paragraph has been adapted from Hinds (1999) who states that whereas most aerosol mass is located in the troposphere, aerosols in the stratosphere often also have significant effects on the climate. Naturally produced aerosols in stratosphere can have a significant impact on the radiative balance of the Earth. Major volcanic eruptions can increase the stratospheric concentrations of PM up to two magnitudes. The primary source of aerosols in stratosphere is the formation of sulfuric acid droplets by gas-to-

particle conversion of SO_2 injected there by volcanic eruptions. These aerosols scatter incoming light back to the space meanwhile having little effect on the terrestrial long-wave radiation, cooling the lower levels of atmosphere and the surface of the Earth. These particles in stratosphere have half-lives of a year and may have a cooling effect of the same magnitude as the greenhouse gases have warming effect.

This paragraph has been adapted from Hinds (1999) who states that the second climate effect of atmospheric aerosols, O_3 depletion happens in the polar stratosphere during winter at low temperatures. In this process nitric acid and water vapors condense and form stratospheric clouds. The surfaces of these cloud droplets act as catalytic sites for conversion of chlorine compounds such as anthropogenic chlorofluorocarbons (CFCs), molecular chlorine (Cl_2) and hydrochloride monoxide (HClO). In the spring sunlight photodissociates these compounds forming Cl, which then reacts with O_3 forming oxygen (O_2) and chlorine monoxide (ClO). After that ClO is photolyzed back to Cl and the process repeats itself destroying even more O_3. The stratospheric aerosols enhance this process by migrating to the poles of the Earth and acting as an additional surface for catalytic activation of the Cl.

3. SHIPPING: ENGINES, EMISSIONS AND CONTROL

According to Lehtoranta et al. (2019) shipping is an efficient way to transport goods globally, and because of this, most of the global trade volume is transported by ships. Emissions produced in the shipping have a significant and growing contribution to the total emissions of the global transportation (Eyring, et al., 2010; Viana el al., 2014). Fugelstvedt et al. (2009) stated that in 2009, 80 % of world trade was transported by ships. They also predicted that the importance of the emissions produced by shipping may become greater in the future, as new shipping lanes might open in more sensitive areas. Shipping activity all over the world has been growing since. The commercial shipping fleet of the world has grown between 3 % and 10 % annually and nowadays the shipping fleet of the world consist over 94 000 vessels and is responsible of transportation of over 80 % of the world trade (UNCTAD, 2018).

According to Viana et al. (2014) the contribution of the shipping emissions to the total levels of PM and NO_2 are significant in the coastal areas of Europe. They state that the shipping emissions are responsible for 1-7 % of the levels of PM smaller than 10 µm in diameter (PM_{10}), 1-14 % of the levels of PM smaller than 2.5 µm in diameter ($PM_{2.5}$), at least 11 % of the levels of PM smaller than 1 µm in diameter (PM_1) and 7-24 % of the levels of NO_2. In busy port areas these contributions can be even higher. Wang et al. (2019) reported that shipping contributed 36.4 % to the levels SO_2, 0.7 % to the levels of NO, 5.1 % to the levels of NO_2, 5.9 % to the levels of $PM_{2.5}$, and 49.5 % to the vanadium (V) particle concentrations in the Shanghai port. Kivekäs et al. (2014) found that during days when wind was blowing over a shipping lane, the shipping was responsible of 11-19 % of PNCs and 9-18 % of $PM_{0.15}$ in Høvsøre, Denmark, 25 to 60 km from the shipping lane. When these numbers were extrapolated over the whole year, including days when the wind was blowing from inland, the fractions caused by the ship plumes were 5-8 % for PNC and 4-8 % for $PM_{0.15}$. In another study by Ausmeel et al. (2019) the shipping emissions contributed 18 % to PNC during the winter (January-February) and 10 % during the summer (May-July) of 2016 in the Baltic Sea SECA in southern Sweden, 7-20 km downwind from a shipping lane. Also, time periods when the shipping line was not affecting the station were included in the calculation of the contributions.

3.1 Ship engines and fuels

Ushakov et al. (2013) state that diesel engines are a preferred choice in heavy-duty machinery because of their better fuel efficiency, higher power output and durability. They also state that the diesel engines emit lower levels of carbon monoxide (CO) and hydrocarbons (HC) compared to engines operated with a spark ignition. Despite of this, shipping still produces a wide range of pollutants that have been shown to have a clear impact on the human health and the climate (Sofiev, et al., 2018). Especially the PM emissions from the diesel engines are significant (Ushakov, et al., 2013). The diesel engines also emit BC, which is a result of incomplete combustion (Kholod Evans 2016). Gentner et al. (2012) found that, compared to gasoline engines, the diesel engines also produce approximately 6.7 ± 2.9 times more SOA for the same mass of unburned fuel.

This paragraph has been written mainly in accordance with Ntziachristos et al. (2016) who state that the diesel combustion in large marine engines is significantly different to smaller engines used on-road. Most of these differences occur because of the different operational speeds of on-road and the marine engines. The typical on-road engines may have maximum power outputs for example at 1800-2400 rpm (Thiruvengadam, et al., 2014). In contrast to this, the typical medium sized marine engines do not usually exceed 750 rpm and the large marine engines do not exceed even 130 rpm. The marine engines and especially large two-stroke engines typically also have much larger stroke/bore ratios compared to the ratios of the on-road diesel engines, the ratios being 3:1 and 1.3:1, respectively. These two factors together allow combustion products to spend longer time in cylinders at high temperatures, which increases oxidation. The marine engines also have much higher air-to-fuel ratios. While the on-road diesel engines rarely exceed the air-to-fuel ratios of 20:1 the air-to-fuel ratios of marine engines often exceed 40:1. This further increases the oxidation in the combustion process as there is more oxygen available. Fuels used in ships are also different. For example, a typical fuel used in ships, the heavy fuel oil (HFO) contains ash-forming components and is much less flammable and harder to vaporize than the full distillate products used on-road. Together these differences lead the marine and the engines used on-road to have different exhaust profiles.

According to Goldsworthy and Goldsworthy (2015) there are two kinds of engines used in ships for different task, the main engines that produce the propulsive power of the ship and the auxiliary engines that are used for energy generation, lightning cooking, air conditioning, heating, and other auxiliary jobs. They also state that one important difference between the engine types is that, while the main engines are used mostly only in the open sea, the auxiliary engines are often running also when the ship is at berth. Low-speed two-stroke engines are mainly used in big containerships as the main engines

while medium or high-speed 4-stroke engines are usually used in cruisers as well as coastal and inland fishing boats (Molland, 2008; Buhaug, et al., 2009; Zhou, et al., 2019,). The main engines are responsible for most of the fuel consumption of ships (Goldsworthy and Goldsworthy, 2015).

The emissions produced in shipping are highly dependent on used fuel type, as the different fuels produce different amounts of CO_2 and other pollutants per a unit of work done (Buhaug, et al., 2009). One often used fuel in the marine engines is HFO (Corbett and Koehler, 2003). The HFO is a left-over product of refinery processes that contains typically numerous chemical elements (S, N, C, H, O, Fe, Si, Ni, V and Ca), asphaltenes, ash and other sediments such as water and micro carbon residue (Jiang, et al., 2019). Another often used fuel in the slow-speed two-stroke and the medium-speed four-stroke marine diesel engines is the relatively inexpensive intermediate fuel oil (IFO) (Di Natale and Carotenuto, 2015). IFO is a mix of low-cost residual oil from petroleum refining and distillate gas in proper proportions to match the needed specifications (Hsieh, et al., 2013) The IFO also contains many impurities including heavy metals (V, Al, Si, Ni and Fe), ash and sulfur (Hsieh, et al., 2013). Other used fuels in the marine engines include liquefied natural gas (LNG), marine diesel oil (MDO), and various kinds of biofuels (Buhaug, et al., 2009). According to Buhaug et al. (2009) the benefits of the LNG compared to the HFO and the IFO are the lower emissions of NO_x, SO_x, PM and CO_2 and that the LNG is also similarly inexpensive to the HFO. Buhaug et al. lists the problems related with the usage of the LNG being the needed space on ship for fuel storage and that at the availability of the LNG in harbors is limited. The benefit of the MDO in comparison to the HFO is the lower sulfur content of the MDO (Peterson and Woessmann, 2014). Buhaug et al. (2009) state that the biofuels consist of multiple different fuels of biological origin. For example, fuels are made from sugar, starch, vegetable oils or animal fats. According to Buhaug et al. (2009) there are multiple problems related to using the biofuels such as stability during storage, acidity, the lack of water-shedding, the plugging of fuel filters, wax formation and more. Wind and solar energy are also used for generating power on ships (Buhaug, et al., 2009).

3.2 Composition of exhaust emissions from ship

The key components of ship exhaust are HC, NO_x CO, CO_2, SO_2, VOCs and PM (Eyring et al., 2005; Goldsworthy and Goldsworthy, 2015). The most important greenhouse gas (GHG) emitted in shipping is CO_2 (Buhaug et al., 2009). Most of the PM emissions pro-

duced in shipping are composed of inorganic ions such as SO_4^{2-}, NO_3, NH_3, carbonaceous matter (organic and elemental carbon) and metal oxides (MMO) (Zhang et al., 2014; Aakko-Saksa, et al., 2016; Ntzhiachsitos, et al., 2016, Wang, et al., 2019).

A large variation in the composition of emissions is observed depending on the fuel type, the engine and the aging of the emissions. Agrawal et al. (2008) discovered that the PM emissions from a large two-stroke engine operating on the HFO were 80 % SO_4^{2-} and water (H_2O) bound with the SO_4^{2-}, the remainder being organic carbon (OC), and elemental carbon (EC) They also found that 3.7-5.0 % of the fuel sulfur is converted to the SO_4^{2-}. Different results were attained in a study made in China by Zhang et al. (2014). They measured that the SO_4^{2-}, organic matter (OM), NO_3, MMO, NH_4^+, and EC corresponded for 18.8 %, 16.5 %, 10.8 %, 9.4 %, 3.5 % and 3.3 % of the PM emissions, respectively. Wang et al. (2019) discovered that the composition of the PM emission is changing when the aerosol is aged. They stated that the freshly emitted PM emission is mostly composed of the SO_4^{2-}, EC and V and there is very little nitrate and in the aged emissions there is more nitrate but in other ways the chemical composition is mostly unchanged.

3.3 Particle size distribution in shipping exhaust emission

NSDs from diesel engines have fairly constant CMDs at about 55-65 nm (Ushakov, et al., 2013). When the HFO is used as a fuel in marine engines the NSD of the emission has a maximum around 70 nm and the geometric standard deviation (GSD) of 1.4-1.5. The maximum shifts to smaller particle sizes if the emission sample is dried with a thermodenuder (Ntziachristos et al., 2016). Kivekäs et al. (2014) found that the ship plumes transported in air have the fitted mode diameters of the plume peak concentrations on average at 39 nm, 10 % of the particles being smaller than 20 nm and 10 % being larger than 52 nm in diameter. The similar diameter of 40 nm for the maximum of the NSD of plumes has been reported also by Westerlund et al. (2015).

The NSDs of shipping emissions have been reported being dependent on the used engine loads and fuels (Anderson, et al., 2015; Kuittinen, 2016; Ntziachristos et al., 2016). Kuittinen (2016) found that the NSDs from direct emission measurements are fuel and engine load dependent. The HFO was found to have the largest size of the maximum of the NSD at 57 nm and then in descending order the IFO, the MDO and the mix of biofuel and marine diesel (BIO 30) that had the maximums of NSD at the diameters of 45 nm, 37 nm, and 28 nm, respectively. Anderson et al. (2015) measured the NSDs of shipping emissions being bimodal. Independent of the fuel, the NSDs had a smaller peak at 10 nm

and another larger peak at 45-50 nm for the distillate fuels and 100-110 nm for the HFO. Ntziachristos et al. (2016) found that the NSD of the ship emissions changes only a little as a function of engine load so that 25 % load leads to 23% higher particle numbers on average than 75 % load. Similar results of increased particle numbers for the lower engine load were also reported by Anderson et al. (2015). Ntziachristos et al. (2016) state that 75 % load resembles well the loading of ship engines at the open sea as the maximum efficiency of the ships is often achieved approximately at 75 % load. They also state that the lower loading point of 25 % resembles the load with what the ships usually operate in ports.

3.4 Emission restrictions

For the emission restrictions, the reader is referred to Buhaug et al. (2009). Many of the pollutants emitted in shipping have a negative effect on the human health. For example, the emissions of $PM_{2.5}$, SO_x and NO_x have been reported to lead to premature mortality and morbidity (Sofiev, et al., 2018). The sulfur emissions also contribute to the acidification of sea and land areas (Hassellöv, et al., 2013). Therefore, the restrictions on the shipping emissions are needed and they are done using multiple different approaches. The used means to reduce the emissions are redesigning superstructures, the optimization of propeller, engine energy recovery systems and after-body flow control systems, improvements in operational systems, hull coating, rerating, and upgrading of engines, propeller maintenance and using alternative fuels.

The emissions of NO_x, SO_x, PM, CH_4 and non-methane volatile organic compounds (NMVOCs) are affected by different factors and their emissions are reduced in different ways. The NO_x emissions originate in engines mainly as the result of reactions between nitrogen (N) and oxygen (O). The NO_x formation is highly dependent on a combustion temperature and residence time in the high temperature. The NO_x emissions are reduced mainly by reducing the peak temperatures of the engines, the time spent in the high temperatures of the engines, the O content in fuels and by using selective catalytic reduction (SCR). Using LNG as a fuel is also an effective way to reduce the NO_x emissions. The SO_x emissions originate from the sulfur in marine fuels. The most effective way to reduce the SO_x emissions is to reduce the sulfur content in the marine fuels. Another effective way to reduce the SO_x emissions is the seawater scrubbing. The PM emissions from the fuels with a high sulfur content can be reduced using scrubbers. The PM emissions from the low sulfur fuels can be reduced for example by optimizing the combustion process and minimizing the consumption of lubricant. The burning of fuel-water emulsion may also reduce the PM emissions from marine engines. Both the CH_4 and the NMVOC

emissions can be reduced by optimizing the combustion process. The NMVOC emissions can also be reduced by extra oxidation and the CH_4 by careful design and by replacing the premixed combustion with a high-pressure gas injection.

In International Maritime Organization, Sulphur oxides (SO_x) and Particulate Matter (PM) – Regulation 14 the sulfur restrictions are described as follows: In January 1st, 2012 the global limit for fuel sulfur content was changed from 4.50 % to 3.50 %. In January 1st, 2020 the restrictions are going to be tightened again to 0.50 %. For SECAs, the limits have already been set stricter being 1.50 % before July 1st, 2010, when the sulfur limit of 1.00 % was implemented. In January 1st, 2015 the limit was again tightened to 0.10 %. The Baltic Sea area concerned in this study has been a part of SECA since May 19th, 2006. The other areas part of the SECA are, the North Sea area, the North American region, and the United States Caribbean Sea areas (Chu Van, et al., 2019). Using cleaner marine fuels can reduce premature mortality and morbidity 34 % and 54 % respectively meanwhile reducing 80 % of the radiative cooling from the shipping emissions (Sofiev, et al., 2018).

3.5 AIS

This paragraph has been adapted from International Maritime Organization, AIS transponders (2019). The Automatic Identification System (AIS) is a system that automatically produces and transmits information about vessels to other vessels and coastal authorities. Regulations dictate which kind of information the AIS must provide. This information includes the identity, the type, the position, the course, the speed and the navigational status of the vessel and other safety related information. This information must be provided automatically to other ships equipped with AIS transponders, as well as appropriately equipped offshore stations and aircrafts. The AIS system must also receive AIS information from other vessels and exchange data with shore stations.

In this paragraph the information concerning IMO numbers has been adapted from International Maritime Organization, Identification number schemes, (2019) and the information concerning Maritime Mobile Service Identity (MMSI) numbers has been adapted from the U.S Department of Homeland Security, Maritime Mobile Service Identity, (2019). The IMO number is the permanent registration number of the ship. The IMO number remains unchanged when the ownership of the ship changes. The IMO number consists of first three letters “IMO” followed by seven numbers assigned to all ships by IHS Maritime upon construction. These seven-digit numbers are given to all propelled sea going merchant vessels over 100 gross tonnage (GT), exceptions being pleasure yachts, ships engaged on special service, hopper barges, hydrofoils, aircushion vehicles, floating

docks and other such structures, military vessels and wooden ship. The MMSI number is a nine-digit number that is used for identifying a vessel or a coastal radio station in the digital selective calling (DSC), the AIS or certain other equipment. The first three digits of the MMSI numbers denote the vessel to an administration or the geographical area of administration responsible for the vessels station so identified. The last six numbers are any numbers between 0-9 and identify the individual vessel. Unlike the IMO number the MMSI number may change during the lifetime of a vessel upon ownership changes.

This paragraph has been adapted from International Maritime Organization, AIS transponders (2019). The AIS regulation provides that the AIS transponders are mandatory for all the vessels of 300 GT or larger, that are engaged on international voyages and for all cargo ships over 500 GT even if they are not engaged on international voyages. All passenger ships must also be fitted with the AIS transponders irrespective of size. The regulation to fit the AIS transponders to ships applies to all ships build after July 1st, 2002. All ships build before July 1st, 2002 have had to be fitted with the AIS transponders by different dates before July 1st, 2004, depending on the ship type.

4. MEASUREMENTS

The measurement data used in this thesis was measured at the atmospheric research station of the FMI located on a small island Utö. Utö is located in the Finnish archipelago in the Baltic Sea. The coordinates of Utö are (59º 47N, 21º 23E). The measurement station is located 8 m above the sea-level and the distance to the closest city Turku is approximately 90 km (Hyvärinen et al., 2008). The measurements used in this study were made between 11.1.2007-31.12.2016. This measurement data was analyzed to produce the results in the thesis.

4.1 Measurement setup

The knowledge of the measurement setup at Utö during the measurements is based on a visit at Utö in 11.9.2019-13.9.2019 and measurement logs from the measurement station. The measurement setup varied slightly during the measurement period, as individual parts of the measurement setup needed repair or maintenance. The exact setup of the measurement devices also varied. Sometimes there were more instruments running, such as a nephelometer or extra condensation particle counters (CPCs). Some modifications and changes to the measurement setting itself were also made. Regarding to this work, the most important changes were the following. Between 24.1.2010 and 2.3.2010, the CPC was fitted with a temperature restrictor that turns a CPC off when temperature exceeds 35 °C. From 7.7.2011 onward, the bypass flow of the differential mobility particle analyzer (DMPS) was removed from the measurement setting. It was originally used for keeping a higher flow in the inlet than in the CPC to minimize particle losses in the inlet line but was later considered unnecessary. In the spring of 2015, the CPC used in the DMPS broke and was replaced in 20.8.2015 with a new CPC leading to a cap of several months in the measurement data. The measurement setting of the DMPS measurement line during the visit in Utö in September 2019 is presented in Figure 2.

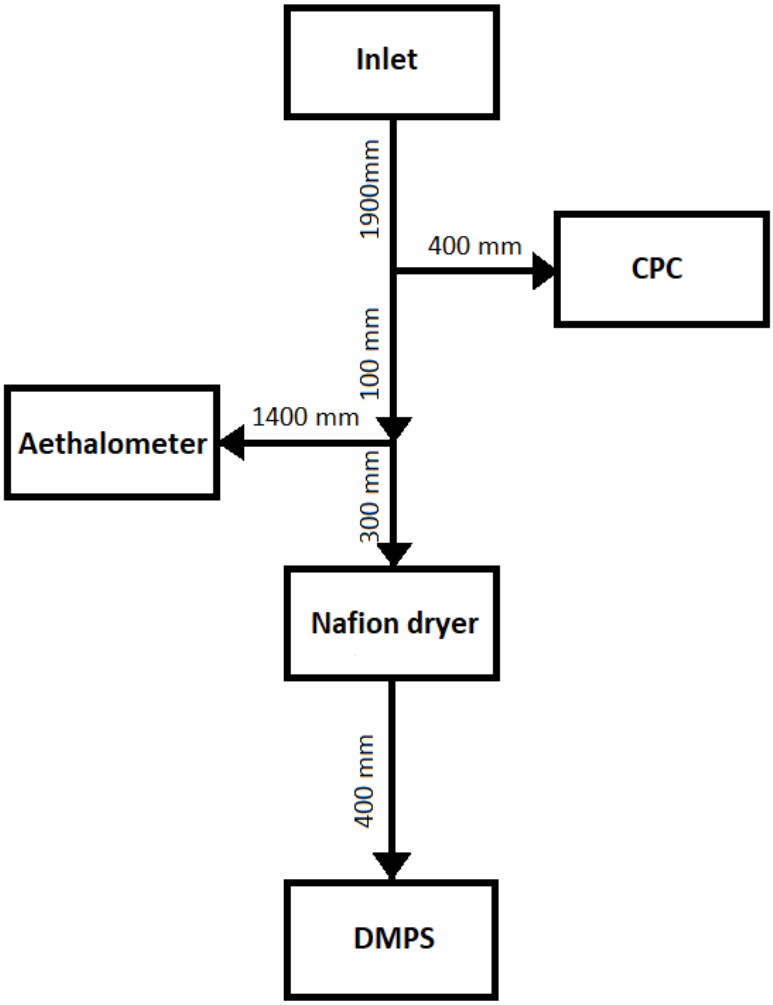

Figure 2 The measurement setup at the measurement station of Utö in September 2019.

The measurement setup used at Utö needs to be relatively simple, as it is meant to be operating alone with only occasional maintenance. Figure 2 of the measurement setup represents only the DMPS measurement line of the measurement station. The relevant parts in this study are the inlet, the nafion dryer and the DMPS that consist of a separate DMA and CPC. The data from the stand-alone CPC and the aethalometer are not included in this thesis and will not be discussed further. The sampling of ambient aerosol for the measurements was done using a $PM_{2.5}$ inlet. The $PM_{2.5}$ inlet removes particles larger than 2.5 µm (Solomon, et al., 2011). Before entering the DMPS, the aerosol is first dried with the nafion dryer to ensure a relative humidity less than 40 %. This is recommended in order to keep particle diameter changes below 5 % (Wiedensohler, et al., 2012). Welp et al. (2013) describe the structure and the working principle of the nafion dryer as follows: The nafion dryer is a tube of semi-permeable membrane separating the inner humid gas flow from the outer dried counterflow, contained in a stainless-steel

shell. If there is a difference in the partial water pressures between the airflows, the moisture will flow through the membrane drying the airflow. In Figure 3, the current measurement devises are presented as they were during the visit in Utö in September 2019.

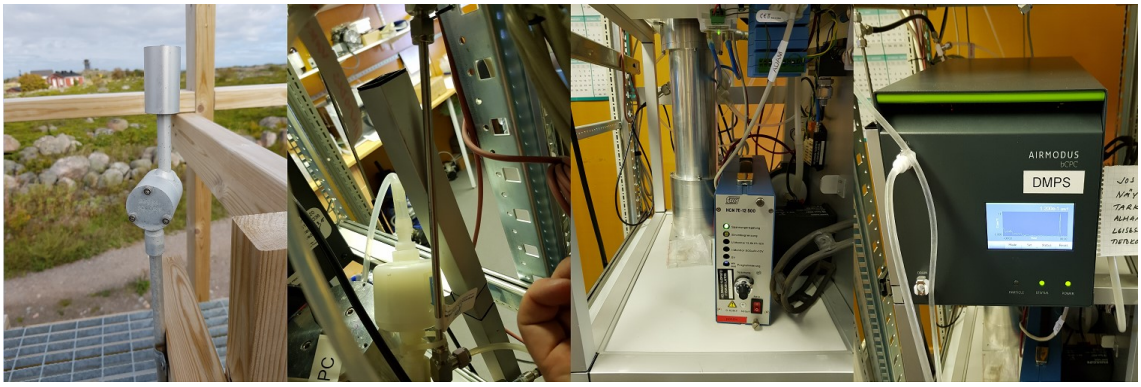

Figure 3 The pictures of the measurement setup at the atmospheric measurement station of Utö in September 2019. The instruments from left to right are: The $PM_{2.5}$ inlet, the nafion dryer, the DMA of the DMPS, and the CPC of the DMPS.

The $PM_{2.5}$ inlet (Figure 3, first on the left) is positioned approximately 50 cm over the roof of the measurement container. From the inlet, the sample flow is led to the nafion dryer (Figure 3, second on the left), that is positioned right behind the DMPS. After being dried, the sample flow enters the differential mobility analyzer (DMA) of the DMPS (Figure 3, second on the right). From the DMA the specified particle size range is lead to the CPC of the DMPS, Airmodus model A20 (Figure 3, first on the right), where the particle concentration is attained.

4.2 Instruments

For the CPC, the reader is referred to Cheng (2011) and for DMA and DMPS to Flagan (2011). The CPC is a measurement instrument that is used for counting the number of particles. The basic idea of the CPC is that the particles are introduced to a supersaturated vapor, that condenses onto the particles and grows them in the process. The particle growth in the CPC is needed as the actual detection of the particles is done by optical techniques which will not detect particles less than about 300 nm in size.

In the CPCs there are different techniques used for achieving supersaturation: condensation, adiabatic expansion, thermal diffusion and the mixing of hot and cold air streams. The CPCs used in this study are diffusion cooling type CPCs which use the thermal diffusion for creating the supersaturation. The schematic of the thermal diffusion type CPC is presented in Figure 4.

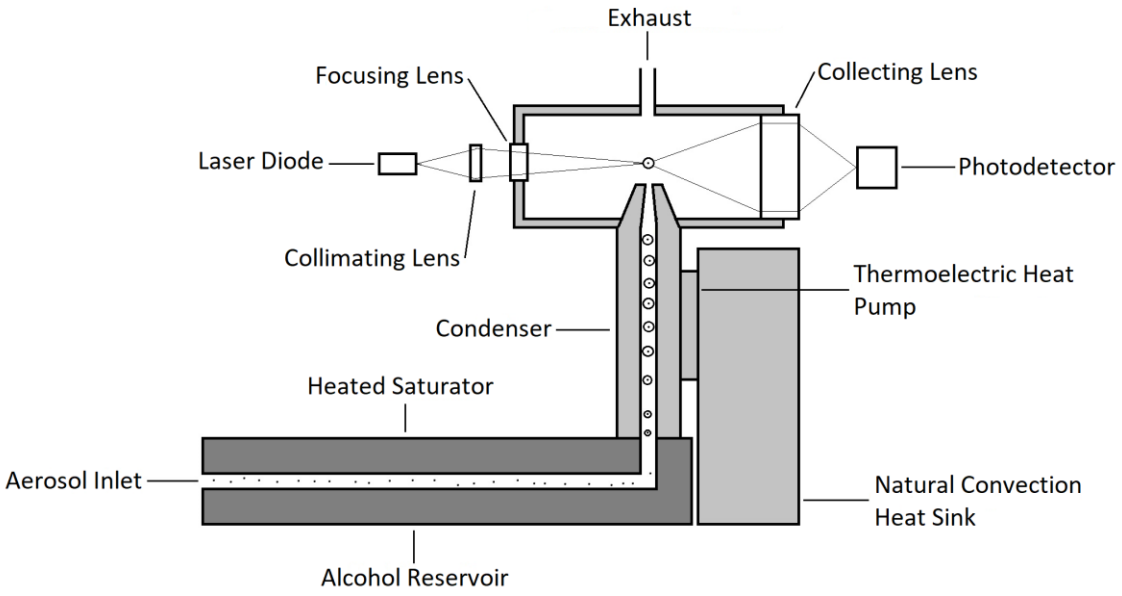

Figure 4 The schematic of the thermal diffusion type CPC adapted from TSI (2002).

The thermal diffusion type CPC uses diffusive cooling to induce the supersaturation of working fluid. In the CPC, the aerosol first passes through a saturator that is kept in an elevated temperature. In the saturator, the aerosol is saturated with the working fluid. From the saturator the saturated aerosol enters a condenser tube that is kept at a lower temperature than the saturator. In the condenser, heat transfers from the aerosol to cooled walls, and because the working fluid, for example n-butanol, has a high molecule mass, the heat transfers faster to the walls than the molecules. This creates an area of supersaturation in the middle of the condenser. This supersaturation causes particles to grow through condensation. After the condenser, the grown aerosol particles enter to an optical detector that measures the scattered light from the particles and so is able to count the total number of particles.

The largest problems with current commercial CPCs are the diffusion losses of small particles and the minimum detection limit. The diffusion losses in a CPC are related to the particle size. The diffusion losses increase when the particle size decreases. This together with the decreasing activation efficiency of the small particles significantly decreases the counting efficiency for the small particles. For positively charged particles extra problem is that they start growing at larger diameters than the negatively charged particles.

The DMA is an instrument that was first introduced by Knudson and Whitby in 1975 as a source of monodisperse sub-micrometer particles. The operation principle of a DMA is based on the different electrical mobilities of different sized charged particles. A typical design of the DMA is a coaxial flow condenser. In this condenser design, particles

charged to a known charge distribution enter the condenser through a narrow slot in an outer electrode. In the condenser the particle flow is separated from the high voltage inner electrode with a particle free sheet air flow. Inside the condenser, the charged aerosol particles are drawn toward the inner electrode by electrical force while at the same time moving along with the sheet air flow through the condenser. At the end of the inner electrode there is a narrow gap where a fraction of the aerosol particles is collected. The collected particles are selected according to their electrical mobilities. The particles with too large electrical mobilities migrate across the annulus too fast and deposit on the inner electrode too early. The particles with too low electrical mobilities take too long to migrate across the annulus and will not deposit on the inner electrode but are removed with the excess air flow. The schematic of the structure of the coaxial flow condenser DMA is presented in Figure 5.

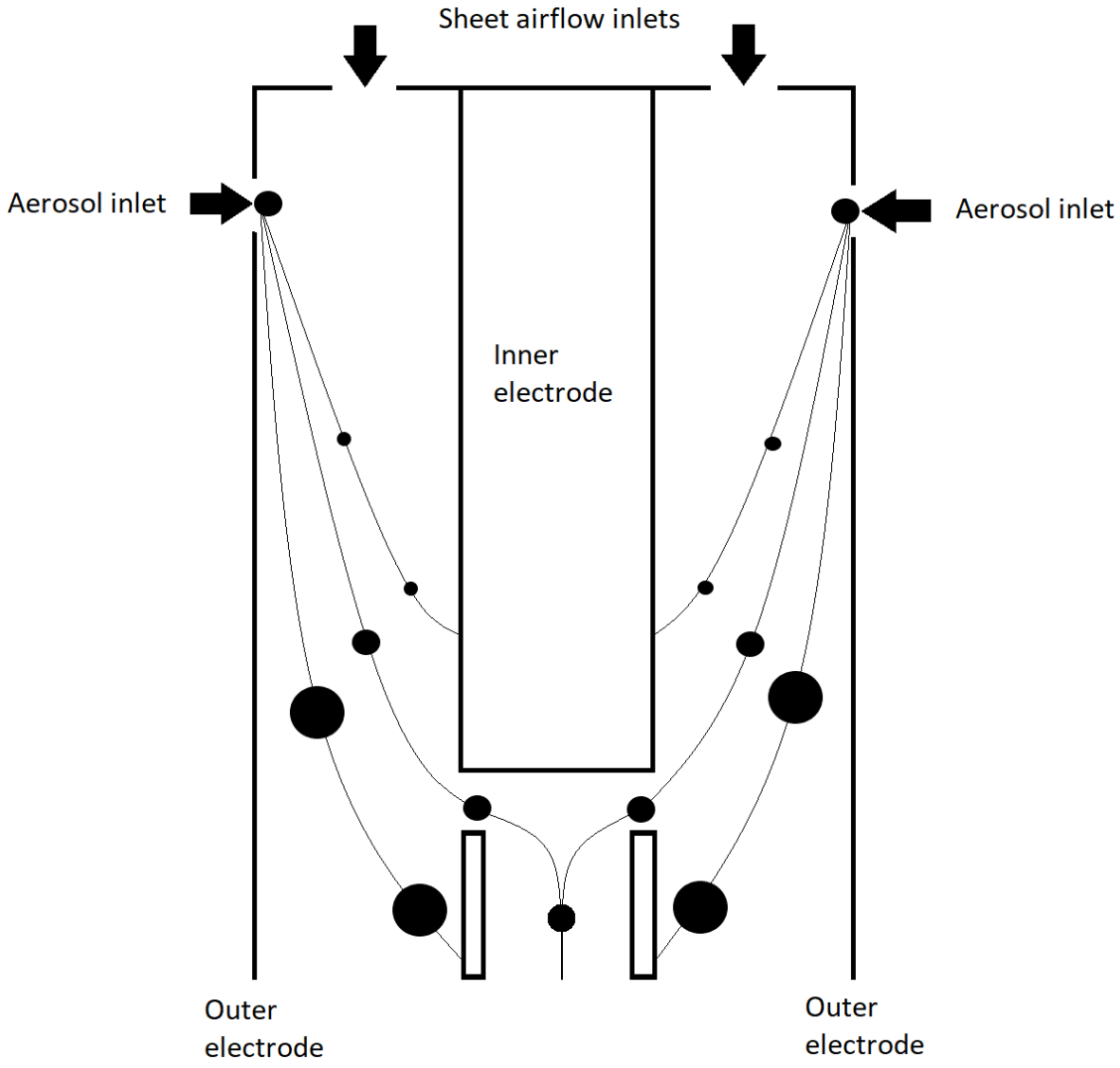

Figure 5 The schematic of the coaxial flow condenser design of the DMA adapted from Flagan (2011).

After the certain size range of the particles is collected, the airflow containing the particles is led to a CPC where the number concentration of the particles is attained. Repeating the measurement with different voltages between the electrodes the number concentration can be measured for different sized particles. If the voltage between the electrodes is increased as a step function the system is called a DMPS.

4.3 Particle losses

For the particle losses the reader is referred to Brockmann (2011). In every aerosol measurement system, there are particle losses that affect the particle concentrations. These particle losses happen through eight different mechanisms. These mechanisms are gravitational settling, diffusional deposition, turbulent inertial deposition, inertial deposition at a bend, inertial deposition at flow constrictions, electrostatic deposition, thermophoretic deposition and diffusiophoretic deposition.

Aerosol collection systems are usually designed to minimize the particle losses to have a minimal impact on the measured aerosol. The gravitational settling of the particles can be minimized by increasing a volumetric flow through a sampling line, decreasing the length of a sampling tube, and preferring vertical sampling tubes. The diffusion losses are a problem for small particles undergoing Brownian motion. They diffuse from a high concentration in the middle of the sampling tube to the outer edges of the sampling tube where the concentration is lower because the tube walls act as a sink for the particles. To minimize the diffusional losses the aerosol transport distance should be kept low and volume flow as large as possible while keeping the flow laminar. The turbulent flow increases particle losses that can be neglected if the flow is laminar. The inertial deposition happens because in bends, the inertial particles cannot perfectly follow the curved stream lines and hit and get deposited on the walls. When the sampling line must go through bends, the curvature ratio of the bend should be kept four or higher. The particle losses in this thesis were taken account in inversion codes used for converting the raw data from the DMPS to the final NSD.

5. DATA PROCESSING

For the data processing in this thesis, pieces of MATLAB code made earlier at the FMI were attained. Most of the codes had to be modified to be applicable for the data from the measurement station at Utö and the goals of this thesis. Most of the primary data handling was done using these modified codes. However, almost all the codes used for producing the end results and pictures were for the most part developed in this study.

In the data analysis three different sectors are used. These sectors are: 1) harbor, 2) nearby shipping lane and 3) distant shipping lanes sector. These sectors are characterized by angle starting from north to clockwise direction. The harbor (1) sector was angles 315°-350°, the nearby shipping lane sector (2) angles 225°-270° and the distant shipping lanes sector (3) angles 75°-165°. The reasoning of these angular limits is discussed in Chapter 5.5. Later in this thesis these sectors are referred according to their numbers.

5.1 AIS data

The AIS data consists of information about the shipping activity in different areas. In the AIS data, MMSI and IMO numbers of ships, the positions of ships as well as their speeds were listed at different times. For this thesis, HELCOM AIS data was available from the whole Baltic Sea area for the whole measurement period except January 2009. The AIS data was used for estimating shipping routes around Utö and to quantify the types of the ships passing by the island.

First, because of the limited calculation power available, the AIS data had to be reduced to a smaller area. For this, an area of 400 km^2 rectangular box centered around Utö was chosen. From the AIS data, the positions of vessels during the period of 01.01.2007-31.12.2016 were plotted on a map around Utö as dots (Figure 6). Every single position of the vessels recorded in AIS data is marked with an individual dot.

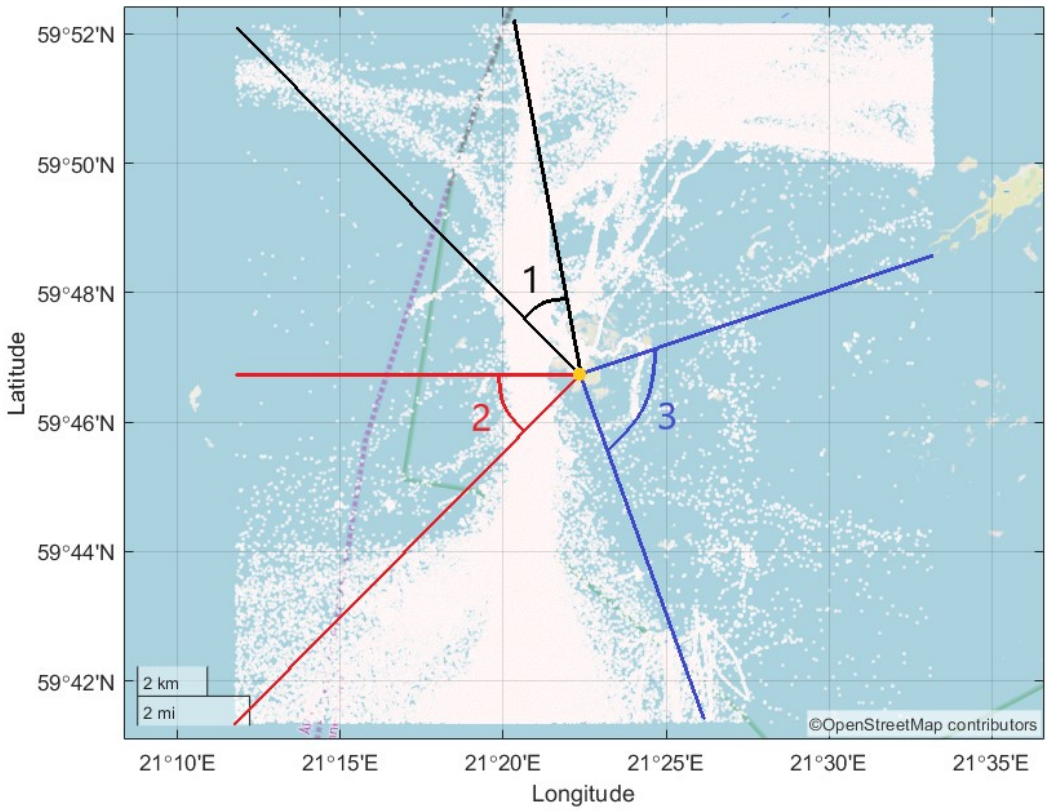

Figure 6 All AIS signals around Utö during the period of 2007-2016. The sector 1 is marked with black, the sector 2 with red, the sector 3 with blue and the measurement station with the yellow dot.

In Figure 6, all vessels around Utö with an AIS transponder have been plotted, showing vessel activity all around Utö. Most of the markings are on the western side of Utö while there are fewer signals on eastern side of the island. A significant vessel activity can also be seen in the northern and southern parts of the area.

Kivekäs et al. (2014) found in their study using the same plume detection method as in this thesis, that the number of the plumes never exceeded the number of the ships over 10 000 GT passing by the measurement site. They also found that when all the plumes considered as analyzable and unanalyzable were included, the detected plumes only counted for 30 % of all the ships and 59 % of the ships over 10 000 GT. Using extrapolated valid period detection efficiencies, the corresponding numbers were 27 % and 53 % respectively. They listed three possible reasons for this deficiency. The first reason was the fact that a substantial portion of the ships was small vessels, and their plumes may have been too weak to be detected by the used method. The second reason was the different distances to vessels resulting in different dilutions and dispersions of the plumes. The third reason was that the meteorological conditions such as the boundary layer height and the enhanced deposition for example the rain may have had an effect

on the PNCs of the air mass. The plume detection from the atmospheric air mass has been pointed to be sensitive to the meteorological conditions also by Pirjola et al. (2014). The IMO number is mandatory for the seagoing vessels over 100 GT with very few exceptions. (International Maritime Organization, Identification number schemes, 2019) As this number is much lower than the 10 000 GT used by Kivekäs et al. (2014), it may be assumed that almost no plumes from the vessels without the IMO number are detected in Utö. The distance in this study for the plumes to travel is in some cases shorter that might slightly increase the number of the detected plumes. Figure 7 shows the AIS signals only from the ships with the IMO number.

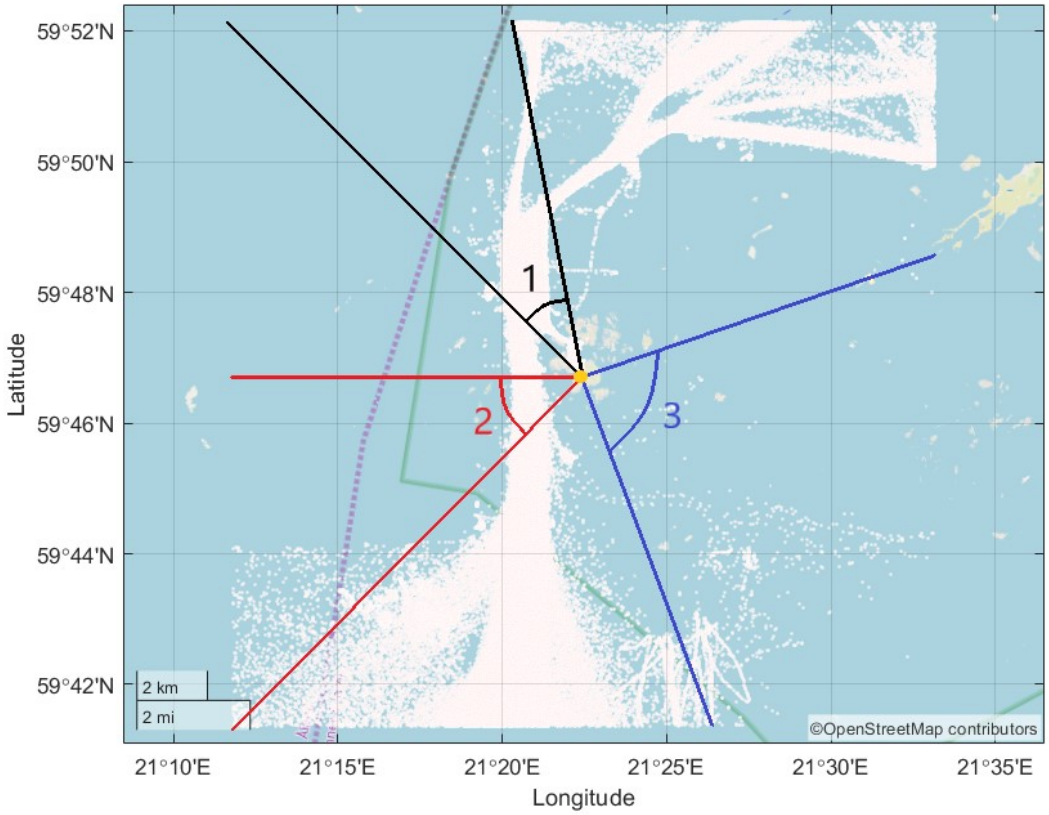

Figure 7 All AIS signals from vessels with the IMO numbers around Utö during the period of 2007-2016. The sector 1 is marked with black, the sector 2 with red, the sector 3 with blue and the measurement station with the yellow dot.

The disappearance of the AIS signals from the eastern side of Utö in Figure 7 indicates that the signals seen in Figure 6 on the eastern side of Utö were from smaller vessels. The busy shipping lane on the western side of the island approximately 1-2 km from the coastline is quite visible. There is very dense shipping activity on the narrow lane coming to the harbor of Utö. These markings are expected to be mostly of the regular ferries arriving in Utö. An important thing to notice is that in the sector 2 there is also significant background shipping activity behind the nearby shipping lane passing by the island.

From the data points shown in Figures 6 and 7, the data was sampled representative to the sectors 1 and 2. This was done to study which kind of vessels there were during the measurement period. Using the AIS data, the proportions of the different ship types for the different sectors were calculated. While there is no upper limit to the distance from which the plumes may be arriving to the measurement station, an arbitrary limit to sectors radius had to be set. This radius was set to be 5 km with origin on the measurement station. In Figure 8, the fractions of the vessels with and without the IMO numbers as well as the different vessel types with the IMO numbers are presented.

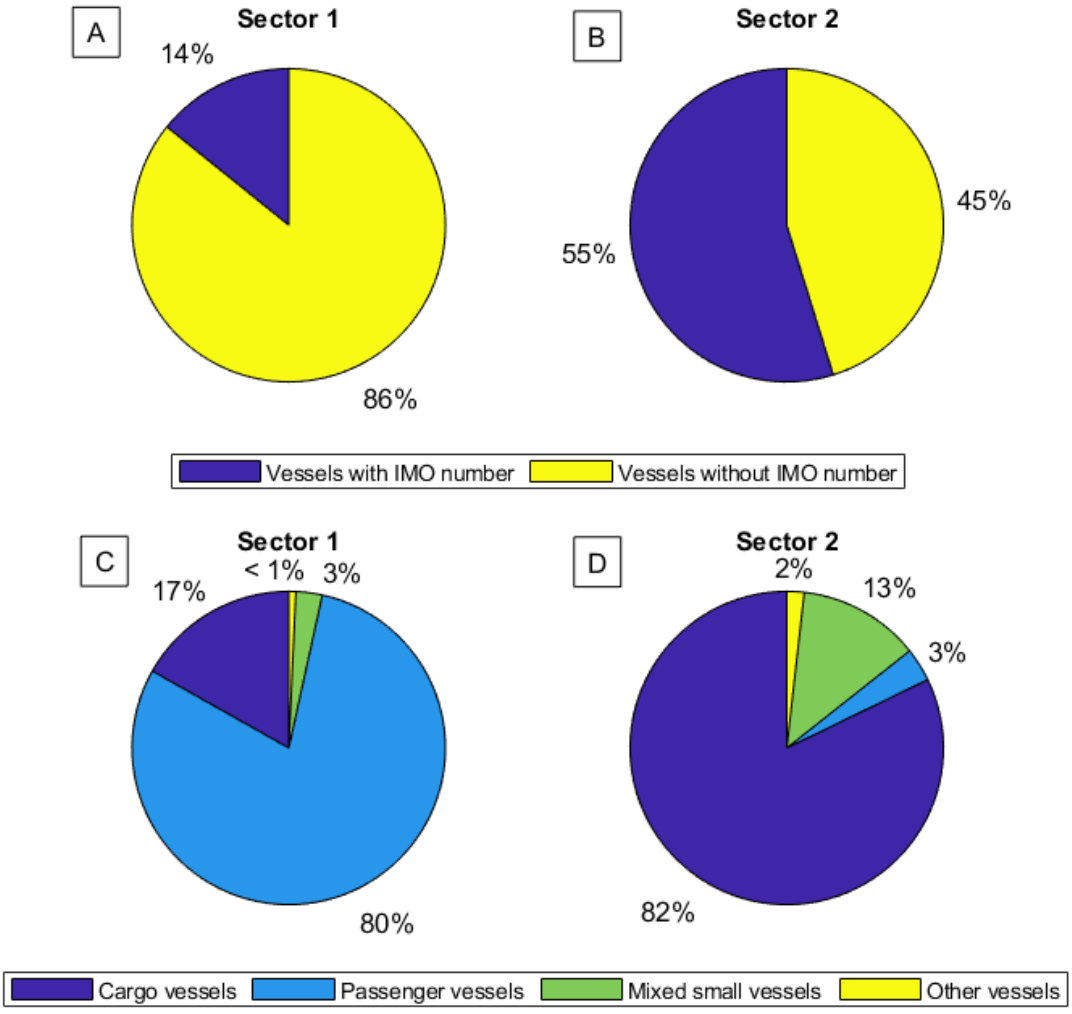

Figure 8 The A and B are the fractions of the vessels with and without IMO numbers in the sector 1 and the sector 2. The C and D are the fractions of the different types of vessels with IMO numbers in the sector 1 and the sector 2.

The share of the large vessels with the IMO numbers is vastly different between the sectors 1 and 2 as can be seen by comparing Figures 8 A and 8 B. In the sector 1, the majority of the AIS signals comes from the smaller vessels without the IMO numbers and

in sector 2 the larger vessels with the IMO numbers are responsible for over a half of the AIS signals. The plumes from the smaller vessels without IMO numbers are unlikely to be detected by the method used in this study.

Comparing Figures 8 C and 8 D, the ship traffic with IMO numbers in the sector 1 is seen to be mostly passenger vessels, and in the sector 2 mostly cargo vessels. In the sector 1, most of the AIS signals from the cargo vessels are from the vessels that went by the shipping lane behind the harbor but were still inside the sector. If this shipping lane is excluded from the data, 98% of the AIS markings with the IMO numbers were passenger vessels. This should not be done, however, as in the data analysis it is impossible to separate the plumes coming from the harbor bay and the shipping lane behind it. Many of the signals of the passenger vessels seem to be coming from ships that are at berth at the ferry harbor of Utö. The IMO number category mixed small vessels and other vessels, mostly included smaller vessels as tugboats and fishing boats, and so will not have any major effect on the upcoming plumes.

The different vessel types were also calculated for the sector 3, where there did not seem to be any significant vessel activity. The area from where the vessels were calculated was chosen similarly to the other two sectors. The area was a sector with the radius of 5 km, the origin being on the measurement site and sides limited by the limits of the sector 3. The exact numbers of the AIS signals from the different vessel types in different sectors are presented in Table 2. In Table 2 the ships of which IMO numbers were marked falsely, or which could not be found from the data base, were marked as small/unidentified.

Table 2 The numbers of the AIS signals from the different vessel types with the IMO numbers.

Type	Vessel type	Sector 1	Sector 2	Sector 3
Cargo vessels	General cargo	25084	9744	0
	Containership	1265	774	0
	Oil product tanker	387	125	0
	Crude oil tanker	2014	955	0
	Bulk cargo	2482	980	0
	Vehicle carrier	251	127	0
	RoRo cargo	17691	7400	0
	LPG tanker	126	17	0
	Chemical tanker	18915	7797	0
	Refrigerated cargo	2967	36	0
Passenger vessels	Passenger cruiser	6356	227	0
	RoRo passenger	235932	920	0
	Passenger	110	23	0
	Ferryboat	94911	8	0
Mixed small vessels	Tugboat	9230	3706	0
	Police, law, military	36	15	0
	Fishing	629	146	8
	Pleasure yacht	763	61	0
	Search and rescue	42	8	0
	Supply ship	68	26	0
	Icebreaker	722	311	0
	Other	2725	465	63
	Oilrig	4	3	0
	Sailboat	289	116	0
	Small/unidentified	46	23	0
Total		423045	34013	71

In the Table 2 the small number of 71 AIS signals from the vessels with IMO number in sector 3 can be seen. All these signals are also from the smaller vessels and may be assumed to have almost no effect in theplume detection. This ensures that the plumes measured from the sector 3 have been carried at least 5 km with the wind before being measured.

It is important to note that the number of the AIS signals from the sector 1 is very high compared to the other sectors. The total number of the AIS signals from vessels with the IMO numbers in the sector 1 is approximately 12 times as large as in the sector 2 and approximately 6000 times as large as in the sector 3. If also the different widths of the sectors would be taken into consideration, this difference would only increase, as the sector 1 with the highest number of the AIS signals is also the narrowest and the sector 3 with the lowest number of the AIS signals is the widest. The high number of the AIS signals from the sector 1 might be due to the excessive number of the AIS signals from passenger ships at berth in Utö harbor. This may add some uncertainty to the results, as the ships that were at berth might have been using ground electricity some time to power the AIS transponder instead of electricity produced by auxiliary engine and may not have acted as plume sources. However, López-Aparicio, et al. (2017) reported in a study made in the harbor of Oslo that approximately 50 % of the emissions of ocean-going vessels occur at berth. This indicates that many of the plumes from sector 1 are still likely to be coming from the ferries at berth. Goldsworthy and Goldsworthy (2019) also speculated that in portal areas the shipping emissions can be dominated by the berthed activity. Another factor that increases the number of the AIS signals especially from cargo ships in the sector 1 is the fact that the sector 1 is partly lined up with the shipping lane behind the Utö harbor as seen in Figures 6 and 7. This results to the prolonged residence time of the ships in the sector 1 and the individual ships have time to cause a higher number of the AIS signals while passing by Utö.

To further examine the sector 3, another AIS signal plot was made where the shipping lanes behind the low shipping activity area in sector 3 could be seen. The plot was made from larger area on the eastern side of Utö and is presented in Figure 9.

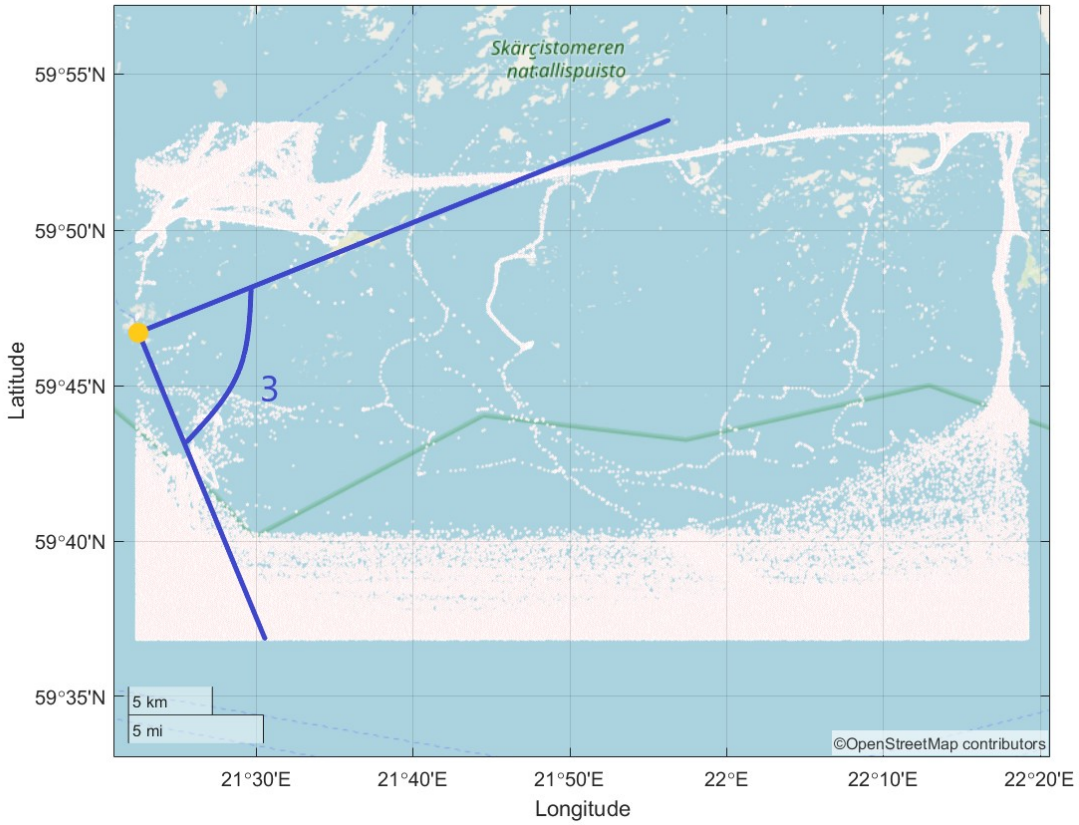

Figure 9 The shipping lanes behind the area of low shipping activity in the sector 3. The sector 3 is marked with blue and the measurement station is marked with the yellow dot.

From Figure 9 the distance to the nearest shipping lanes in the sector 3 can be seen to vary between approximately 8-50 km. Therefore, the distance to the nearest shipping lanes in this sector is approximately four times the maximum distance of 2 km to the shipping lane in the sector 2. Notable is also that the shipping lanes are wide especially in southern and southeaster directions. This increases the possible distance to ships sailing on the shipping lanes to more than 50 km. It can be seen that some ships have been sailing between the measurement station and the shipping lanes, but the number of these ships is relatively low and the number of detected plumes from these ships is likely to be very low.

5.2 DMPS data cleaning

The initial DMPS data inversion and cleaning in this thesis was based on the codes made by Niku Kivekäs. The codes used for data inversion and for removing the corrupted and unwanted data were originally made for ambient measurement data from the atmospheric measurement site of FMI at Sammaltunturi in Muonio. The other codes used in the data analysis were based on the codes that were used and evaluated in article by

Kivekäs et al. (2014). The data used by Kivekäs et al. (2014) was obtained with a scanning mobility particle sizer (SMPS) whereas the data used in this thesis was obtained with a DMPS. The codes were applicable despite of the different measurement instruments. The data from the SMPS must be averaged over the measurement cycle and therefore the data produced by the SMPS is in the same form as the data from the DMPS. The different measurement mechanism of the SMPS and the DMPS might still cause some differences between the two instruments.

To analyze the results from the DMPS, the data had to be first converted from raw data to a meaningful form. The data produced by the DMPS instrument is an electrical mobility spectrum. This spectrum was converted to a format where the normalized particle number concentration was given for 30 distinct size bins ranging from 7 nm to 538 nm. In this conversion, the size dependent tube losses, the bipolar charging function of the particles and multiply charged larger particles in each size bin were considered and corrected.

After the inversion, the data was cleaned from obvious bad data. This was done visually. The daily raw data was plotted and the corrupted data and the data which seemed to be from unwanted sources such as a tractor passing by measurement site were flagged. The flagged data was removed from further analysis. In Figure 10, an example of a day with an obvious bad data is presented. The picture consists of the timeseries of total NSD and total PNC.

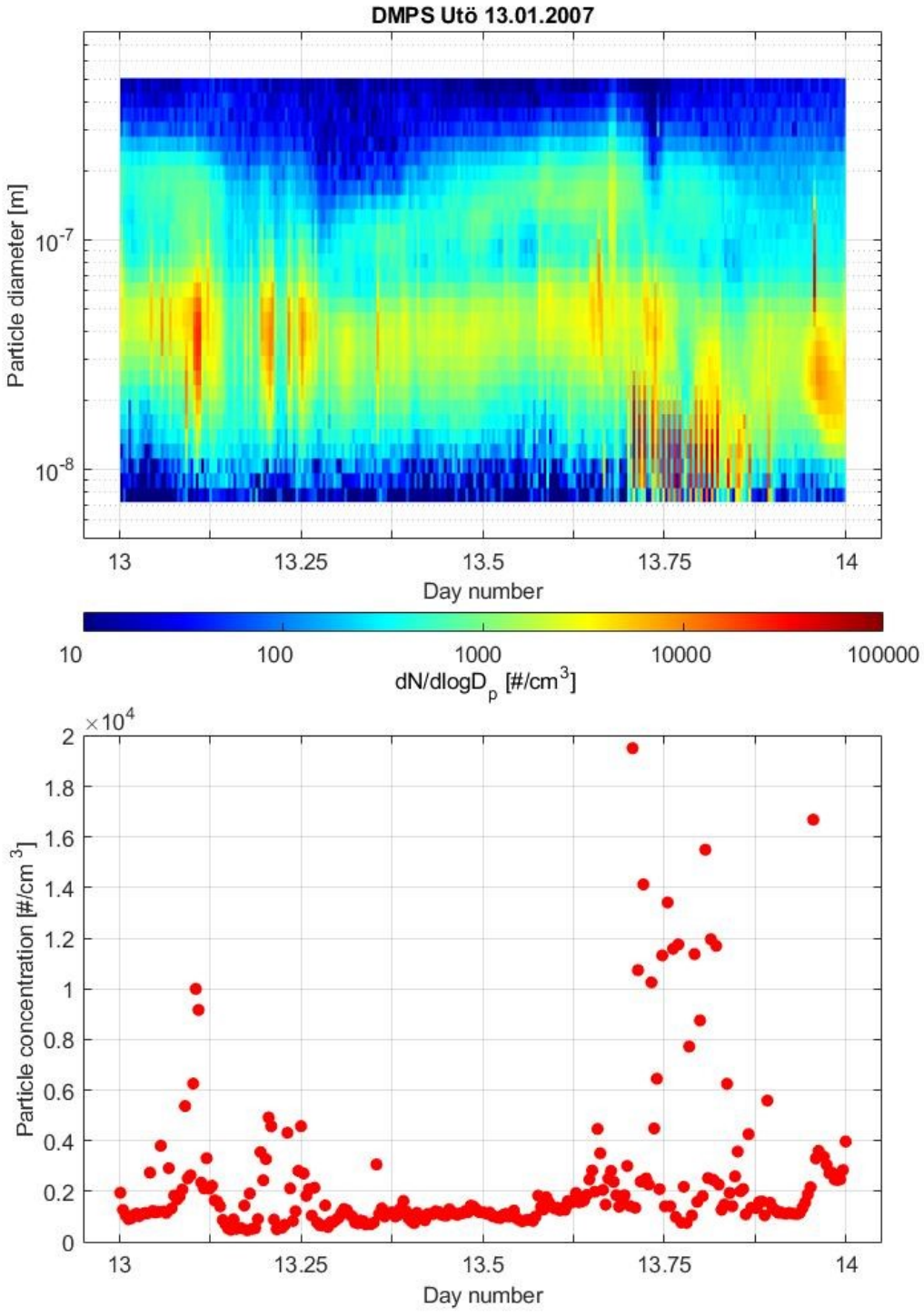

Figure 10 An example of bad data in the data cleaning phase. In the upper picture the total NSD is plotted as the function of time. In the lower picture the total PNC is plotted as the function of time.

In Figure 10 it can be seen that from 4 pm to 9 pm there is a noticeable periodical variation in the concentration data. This kind of variation is likely to be from a local source or malfunction of the measurement system. Since this study discusses only the atmospheric background aerosol and the ship plumes, this kind of data is considered as bad. All this kind of phenomena that were likely to be from unwanted sources were removed from the data.

After the initial cleaning of the data, the remaining data was further automatically scanned for outlier values in the total concentration. The found outlier values were flagged as bad data and removed from further analysis. The code calculated the total concentration of the measurement point and four measurement points before and after that and formatted two vectors out of them. The first vector included the current measurement point and the four measurement points before and the four measurement points after it. The second vector included only the four measurement points before and the four measurement points after the current measurement point. The standard deviations of these two vectors were compared and if the standard deviation of the first vector was more than 5.5 times the standard deviation of the second vector the current measurement point was flagged as an outlier value. In addition to the original code all the days with four or less good measurement cycles were also removed from the further analysis.

5.3 Plume detection from cleaned DMPS data

The plume detection in this thesis was based on the codes used and evaluated in Kivekäs et al. (2014). In the codes, the plumes were found by extracting the particle number concentration of the background (PNC_{bg}) from the total PNC. The remaining data was considered as excess particle number concentration (PNC_e). Maximums of the PNC_e were found, and if these fulfilled the criteria set for the plume detection, they were assumed being the peaks of the plumes. The criteria for the maximum of the PNC_e being the peak of a plume, were the following: 1) The PNC_e had to be at least 500 #/cm^3 or 2) the ratio of the total PNC to the PNC_{bg} (R_e) had to be at least 1.5. These requirements were the same as used by Kivekäs et al. (2014) and are compromises between including all clear plumes and excluding peaks caused by other variability in the data. The two criteria were needed to count all the plumes. In some meteorological conditions, the total PNC in air may be lower and the PNC_e would not exceed 500 #/cm^3 over the PNC_{bg} but the R_e would still be over 1.5 and be the sign of the existence of a ship plume. If there were several peaks in a continuous time period fulfilling the criteria for the PNC_e or the R_e, all the peaks were defined as separate plumes. These plumes were separated by the measurement point with the lowest PNC_e or R_e between them.

In the article Kivekäs et al. (2014) the plume detection was done manually, and the maximums of the PNC_e were found visually from MATLAB plots. For this thesis, the code was automated. This was needed, as in this thesis there were continuous data from 10 years of measurements when in comparison the measurement period in the article by Kivekäs et al. (2014) was less than four months.

The PNC_{bg} data was defined and extracted from the total PNC as 25^{th} percentile values of a sliding window with the width of 40 consecutive measurements. The duration of this window in this thesis was slightly longer (3 h 33 min 20 s) compared to the window used in the article by Kivekäs et al. (2014) (3 h 20 min). This was because the measurement cycle used in the DMPS at the measurement station at Utö was 20 s longer than the averaging time of 5 min used in the SMPS by Kivekäs et al. (2014). The percentile and length of the time window were chosen in the article based on testing with different values. Higher percentiles led to some of the plumes being counted in PNC_{bg} if the plumes were very frequent. Lower percentiles did not follow changes in the PNC_{bg}, but the minimum points of the total PNC. The shorter time window included plumes in PNC_{bg} when the plumes were long or frequent. As the time window was a bit longer in this thesis, we can assume that the code was slightly more sensitive to finding plumes than in the original article.

Figure 11 represents a typical day with clear plumes exceeding both the PNC_e and the R_e limits. In the uppermost sub figure, the number size distribution the of the PNC_e (NSD_e) is presented as a function of time. In the lower two sub figures, the PNC_e and the R_e are presented as functions of time. The black lines in the two lower plots represent the limits set for the PNC_e and R_e for detecting a plume. The time periods when the red dotted line exceeds these lines are considered being the plumes. The parts of the PNC_e exceeding the plume detection limits during the plumes are considered being particle number concentrations of the plumes (PNC_{pl}).

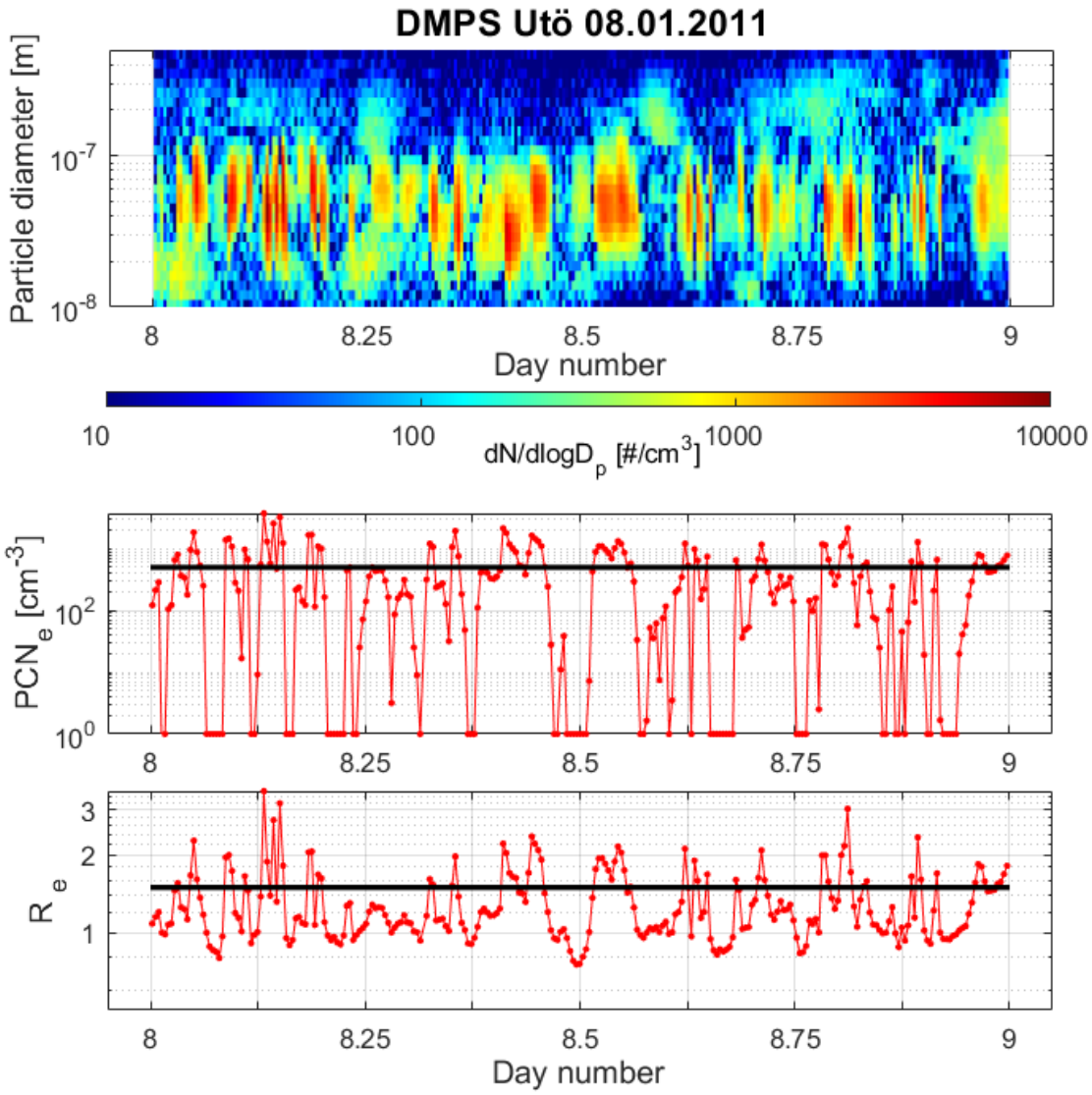

Figure 11 From top to bottom: The NSD_e, PNC_e and R_e plotted as the functions of the day number for a day with clear cases of plumes exceeding both, limits set for the PNC_e and R_e.

From the detected plumes, using the codes from Kivekäs et al. (2014) we were able to calculate for each plume several different quantities. For example, the starting and ending times and the durations of the plumes, the highest PNC_{pl} and R_e during the plume, the particle diameter at the maximum of the PNC_{pl} and the total number of particles during the plume. Also, the NSD_{pl}s and the NSD_{bg}s were calculated.

5.4 Plume validation

For the data, a validity check was made to ensure the reliability of plume detection at different times. The data was divided to valid and invalid time periods according to the analyzability of the plumes during that time. If the plumes could be analyzed reliably from the current time period, the time period was considered as valid and if not, the time period was considered as invalid. This validation of the time periods was done as in Kivekäs et al. (2014). The code scanned the PNC_{bg}s for rapid and significant changes. The scanning was done by counting both the absolute and the relative change rates in the PNC_{bg} and smoothing them by taking the smoothed sliding average of six consecutive measurement points. When changes in these smoothed values were greater than ± 53 #/cm^{-3} in the absolute change or ± 5 % in the relative change, the data was marked as invalid. These values were set so that they corresponded for 67 % of what was needed to define a plume. The changes in the PNC_{bg}s were checked because, if there were large and fast changes, those would have caused an error to analysis of the plumes detected during those times. The error occurs as the sliding 25^{th} percentiles that were used to define the PNC_{bg} reacted to decreasing concentrations roughly 10 measurement points too early and roughly 10 measurement points too late to the increasing concentrations. That is why also 10 measurement points before and after every invalid point had to be marked as invalid. The code marked every detected plume with one or more invalid measurement points as invalid.

The original code needed to be modified as it failed to invalidate the plumes in some special cases. Firstly, the code failed to take in account the day changes during the plumes as data used by the code was divided to separate data files for each of the measurement days. If the last or the first measurement point of the plume was on another date and therefore on another data file as the rest of the plume, the code ended up to on error. This was corrected so that the code stops the seeking of the plume end and start positions if the measurement point was the first or last of the day and marks these plumes as invalid. This was done as it is uncertain whether the plume continues in the other date and data file or not. The second problem with the original code was that it counted plumes that were limited by missing data as valid plumes. This needed to be fixed because when the plume ends to the missing data, we cannot be sure if the plume really ends to the last existing measurement point or somewhere during the missing data. This was corrected by invalidating these plumes. The third problem with the original code was that it did not function properly when data was missing somewhere between the ending and starting point of the plume. The code just assumed the plume continuing over the missing

data. This led to some of the plumes lasting many hours. All these plumes were also marked as invalid.

The yearly coverages of the cleaned and the valid periods of the data are presented in Figure 12. The cleaned data included the data that was left after the obvious bad data and the outlier values were removed from the original DMPS data in the data cleaning phase. The valid data included the parts of the cleaned data that had been validated in the data validation phase.

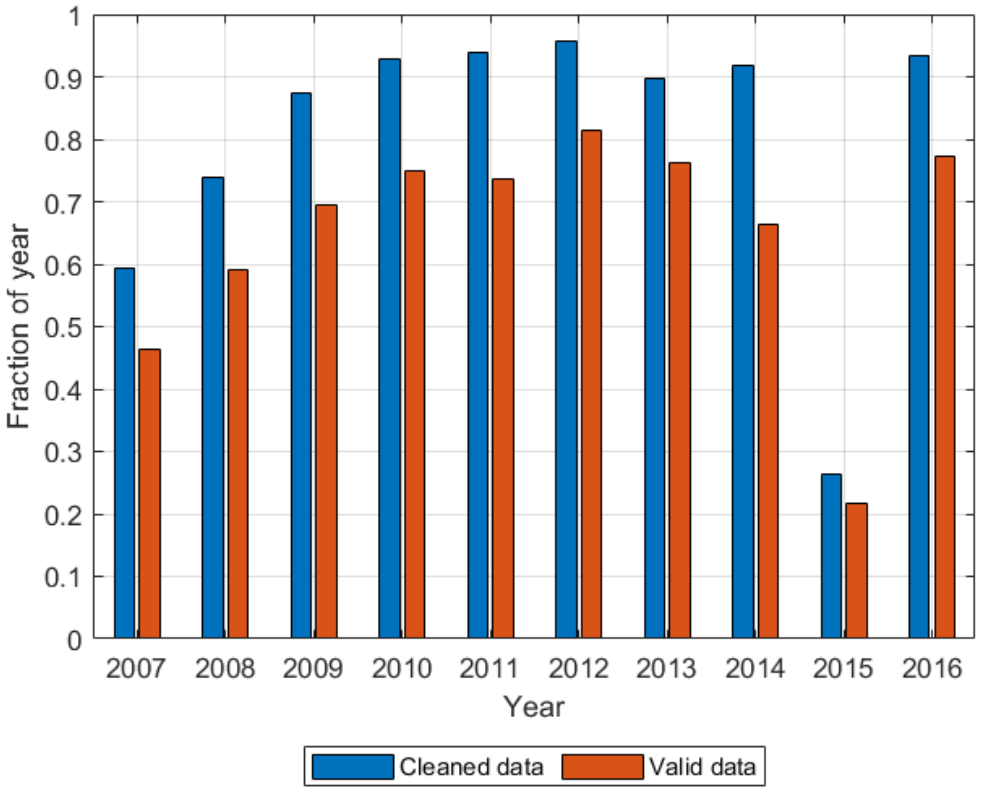

Figure 12 The yearly cleaned and valid fractions of the data. The blue bars represent the cleaned fractions of the data and the orange bars the valid fractions of the data.

The blue bars in Figure 12 represent the amount of the cleaned data, the fraction of the year that was left for analysis after the bad data was removed. In the bad data all the missing periods of the data, the days with four or less measurement points and data that was likely to be from unwanted sources such as a passing by tractor were included. The outlier values found by the code were also considered as bad data. The orange bars represent the fractions of the year of the valid data. From the cleaned data all the invalid periods of the data were removed, and the remaining part was characterized as the valid data. An important thing to notice is that as there were extended periods of the data

missing from year 2015. There was just approximately 26 % coverage of the cleaned data and approximately 22 % coverage of the valid data. This increases the uncertainty of results because the data may not resemble the entire year. Most of the missing data in 2015 were between 17th of January and 19th of August meaning that the whole spring and almost all of the winter and summertime from 2015 are missing. This might cause an error because of the possible effect of the different season having different concentrations and larger fractions of some seasons being presented in data than others.

In this thesis wind directions were attached to the plumes and every individual measurement point of the DMPS data for later analysis. The wind direction data was attained from the weather service of the FMI with a 10 min time resolution. The wind directions were given as angles starting from the north in the clockwise order. For the plumes, the wind directions were calculated as the averages during the plumes. The first and the last values of the plumes were set to be the values at the nearest wind direction data points. A plume was marked to miss the wind direction if the distance to the nearest point of wind direction data point at the start or end of the plume was longer than 5 min. The plume was marked to miss the wind direction also when at least one data point of the wind direction was missing inside the plume. For the individual measurement points the values of the nearest wind direction data points were given. If the distance to nearest wind direction data point was longer than 5 min or value from the nearest data point was missing, the DMPS measurement point was marked to miss the wind direction.

For evaluating the difference of the aged and the fresh plumes, total radiation data was attached to the plumes. The radiation data used was 1 min resolution data produced by the FMI. The radiations were attached to the plumes using similar method as in case of the wind directions. The data points at the end and the start times of the plumes were picked from the total radiation data. The radiations between these points were averaged and set as the radiation values for the plumes. If the distance to nearest radiation data point was over 30 s or even on radiation data point inside of the plume was missing, the plume was marked to miss the radiation data.

5.5 Dividing data to sectors

The wind direction data was used for classifying the plumes in three different sectors: 1) plumes from the Utö harbor, 2) plumes straight over the nearby shipping lane, and 3) plumes from the distant shipping lanes. These sectors are referred in this work according to their numbers 1, 2 and 3. The angles 315°-350° were classified as plumes from the sector 1, the angles 225°-270° were classified as plumes from the sector 2 and the angles 75°-165° were classified as plumes from the sector 3. These sectors did not include

all the measured plumes at Utö but are considered to be representative samples for different types of plumes.

The classifications for plume sectors were made using the AIS data plots shown in Figures 6 and 7. The angles for the sector 1 were chosen so that all the plumes measured had to come through the harbor bay of Utö. The upper angle limit for the sector 2 was chosen so that plumes would not cross any land areas. The lower limit for the sector 2 was chosen so that the maximum distance to the shipping lane would not get too large. The larger maximum distance to the shipping lane would have introduced more variability to the distances that the plumes had to be carried by the wind to the measurement site. In case of the sector 3 the lower angle limit was chosen so that the plumes would not cross the island of Jurmo seen in the upper right corner of Figures 6 and 7. The upper limit for the sector 3 was chosen so that the plumes would not come from the shipping lane on the western side of Utö and the distance that the plumes had to be carried by the wind to the measurement site would be recognizably larger than in the sector 2. Using back trajectories for classifying the plumes was also considered. Since in this study the shipping plumes are expected to be arriving from short distances on average, the back trajectories were almost linear and the wind directions were expected being good enough approximations. In Figure 13 the different sectors are presented as photographs from the roof of the measurement station.

Figure 13 The pictures of each of the sectors used in the data analysis, taken from the top of the measurement station at Utö. The pictures from top to bottom: the sector 1 (315-350°), the sector 2 (225-270°) and the sector 3 (75-165°).

As seen from Figure 13, in the sectors 2 and 3 there are no significant aerosol sources on the island itself. Therefore, most of the peaks identified as plumes are likely to be from marine sources as wanted. Since the plumes from the sector 1 must pass by few local houses with chimneys, they might occasionally include some particles from biomass burning. However, when there are only few houses and the firewood must be transported to Utö from the mainland of Finland, the number of the particles included in the plumes from the domestic biomass combustion is likely to be very low.

6. RESULTS

In this part of the thesis the produced results are presented and discussed. The discussed results are the total number of the ship plumes, their distribution according to the wind directions, the effects of sulfur restrictions in the marine fuel content on the measured plumes and the effects of the sulfur restrictions in the marine fuel content on the air quality in the area. The properties of the plumes that are discussed are NSD_{pl}s, PNC_{pl}s, PSC_{pl} and aging. The properties of the atmospheric air quality that are discussed are the contribution of PNC_{pl}s to total PNCs, the total PNCs and NSD_{bg}s. In the end of this chapter the attained NSD_{pl}s are compared to the NSDs of the direct emission measurements produced by Kuittinen (2016).

The sulfur emission restrictions have been found to be strictly complied in SECAs. Kattner et al. (2015) found that more than 99 % of all the measured ships in the Hamburg harbor in SECA complied the 1.00 % marine fuel sulfur content restriction in autumn 2014 and in January 2015 already 95.4 % of the measured ships complied the new restriction of 0.10 % sulfur in fuel. Similar high compliance percentages have also been reported by Pirjola et al. (2014). They found that all the measured ships in Helsinki and Turku in the Baltic Sea SECA followed the 1.00 % sulfur limit in the measurements made during 2010 and 2011, even though some of the measurements of 2010 were made during the sulfur restriction period of 1.50 %. They also found that none of the measured ships used fuel that would have fulfilled the next sulfur restriction of 0.10 % implemented in the beginning of January 2015. As the compliance of the restrictions is high, the results during the sulfur restrictions of 1.00 % and 0.10 % can be assumed to give a good expression of real sulfur contents in the marine fuel. As seen in Pirjola et al. (2014), there is however uncertainty how much the sulfur concentrations changed after the change of the sulfur restriction from 1.50 % to 1.00 %, as at least some of the ships seemed to use fuel with less than 1.00 % sulfur even before the change of the restriction.

6.1 Ship plumes

The total number of the ship plumes was counted and plotted according to the wind directions from which the plumes arrived to Utö. The total number of the detected plumes in the measurement period of 11.1.2007-31.12.2016 was 71811. A considerable number of 43503 valid plumes was observed. The high number of the valid plumes decreases the uncertainty in the results caused by the uncertainties concerning the detection of he individual plumes. The wind directions could be attached for 42322 of the valid plumes.

In Figure 14 the numbers of the plumes with wind directions have been plotted according to the wind directions.

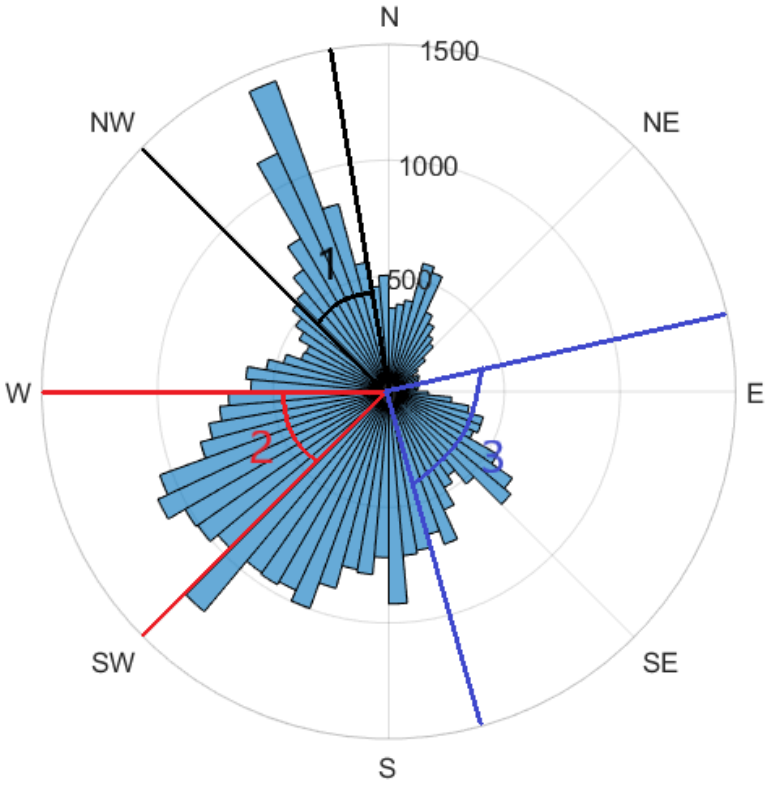

Figure 14 The total number of the valid plumes from the whole measurement period of 11.1.2007-31.12.2016, divided into 5° bins. The sector 1 is marked with blue, the sector 2 is marked with red and the sector 3 with black.

In total 21960 plumes were found to be arriving from inside the predetermined sectors and ended up being analyzed further. In Figure 14, most of the plumes are seen to be arriving from SSW, WSW, and NNW directions, those being the relative directions of the harbor of Utö and the nearest shipping lanes. Almost no plumes were arriving from the ENE direction, which is expected as there is little to no shipping activity as seen in the Figure 7. Interestingly, very few plumes seemed to be arriving from WNW direction even though the distance to the nearby shipping lane in this direction is similar to the plumes coming from WSW direction and even smaller than the distance of the plumes coming from the SSW direction. This can be because of two factors: 1) either the amount of wind originating from this direction is lower or 2) there is significant background activity of shipping in WSW and SSW sectors.

The number of the plumes coming from the different wind directions is heavily influenced by the amount of time that the wind plows from each direction. To study this effect, the total time of wind blowing from the different angles is plotted in 5° bins in Figure 15.

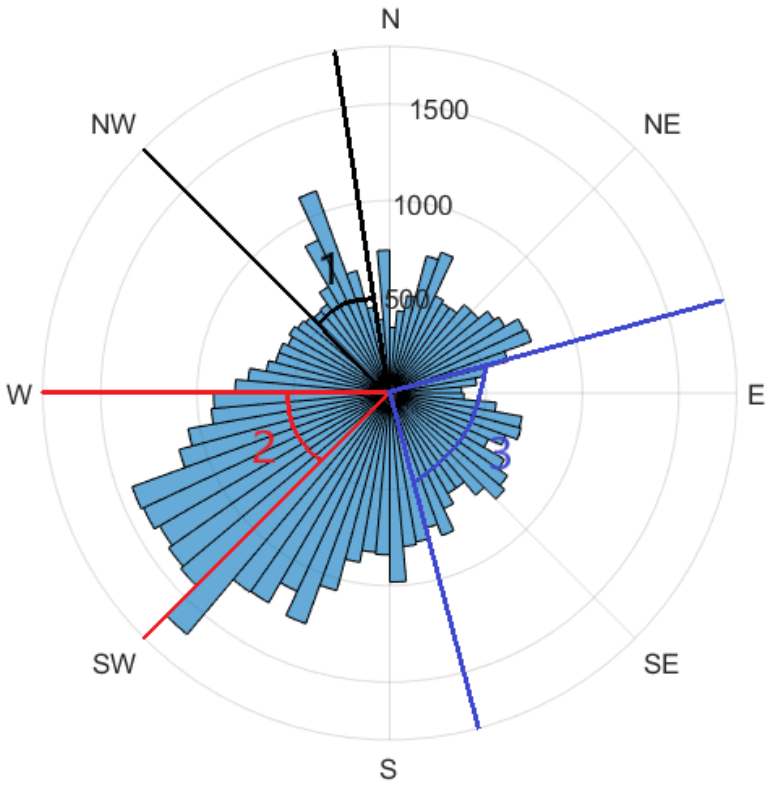

Figure 15 The total number of the hours of wind during the valid time periods from the whole measurement period of 11.1.2007-31.12.2016, divided into 5° bins. The sector 1 is marked with blue, the sector 2 is marked with red and the sector 3 with black.

Southwestern winds are typical for Utö during winter and fall and north to southwestern winds during spring and summer times (Hyvärinen, et al., 2008). The Figure 15 is in good accordance to this showing majority of wind coming from southwestern directions. Interestingly, winds from angles 330°-340° seem to be more common than the other northern winds which will magnify the number of the plumes arriving from the sector 1 to the measurement site. Now it can also be seen that at least some of the reduced plume numbers in WNW direction is because of the lower amounts of wind than in WSW and SSW directions.

When the number of the plumes is divided by the time of wind blowing from the different directions, the plume density in time per different wind directions is attained. This is presented in Figure 16.

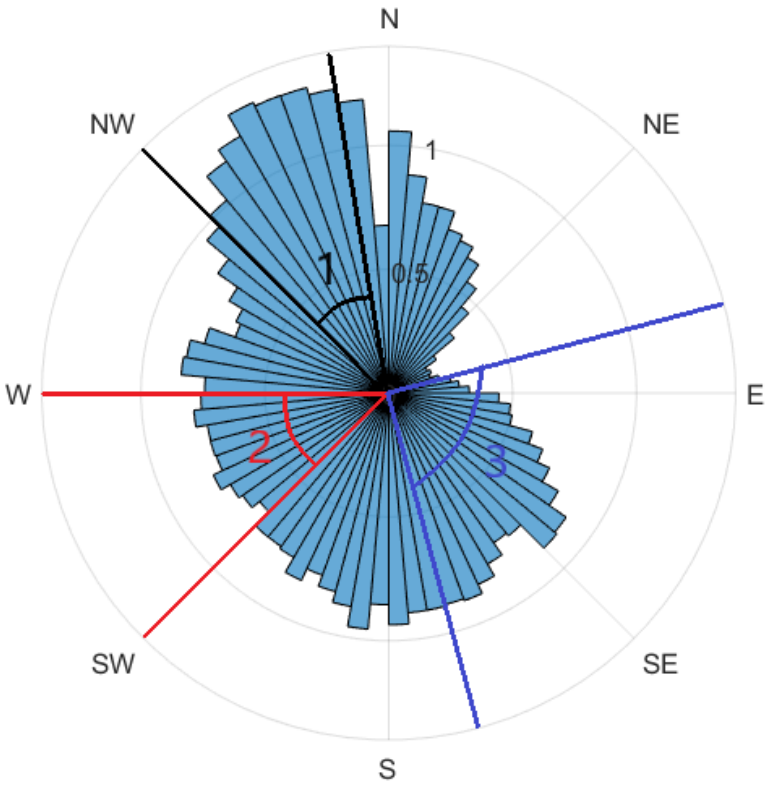

Figure 16 The total number of the valid plumes divided by the total number of the hours of wind during the valid time periods from the whole measurement period of 11.1.2007-31.12.2016, divided into 5° bins. The sector 1 is marked with blue, the sector 2 is marked with red and the sector 3 with black. The Value on the R-axis is the number of the plumes per hour of wind.

From Figure 16 it can be seen that the small number of the plumes coming from WNW direction is mostly because the wind is blowing to Utö more often from WSW and SSW directions than from the WNW direction. When the amounts of wind are considered, the number of the arriving plumes per time is more similar for all the directions SSW, WSW, and WNW. However, the effect of existing background shipping activity can still be seen especially in SSW direction as the increased plume density in time. It can also be seen that, even when the amounts of wind from the different directions are considered, there are still almost no plumes coming from ENE direction. Interestingly, the density of the plumes from ESE and SSE directions are approximately same as the density of the plumes from the WSW, SSW and WNW directions. This is important as there are no nearby shipping lanes in the EES and the SSE directions and therefore the plumes can be expected being carried from the distant shipping lanes. This makes sure that the statistics of the detected plumes are comparable between the plumes from the different sectors used in the analysis.

6.2 Total particle number concentrations

In this chapter the overall effects of the plumes to the PNCs in Utö are discussed. Dividing data to sectors is not used in this chapter, but all the data irrespective of the wind direction has been included. The total PNCs presented here are the total PNCs of only the particles in the size range of 7-538 nm. In counting the yearly averages for Figures 17,19 and 20, every measurement point was weighted equally. Averages for the whole sulfur restriction periods were counted as averages of the different yearly averages so that each yearly average was weighted equally. The exception to this was the year 2010 where the sulfur restriction changed in the middle of the year in 1st July. The averages for the half-year periods before and after the July 1st, 2010 were calculated separately. They were then weighted with 0.5 compared to 1 used for the whole years. The weighting was done in this manner to neglect the effect of the different data coverages for each year. The different data coverages have been presented in Figure 12.

The yearly averages of the total PNC as well as the averages of the total PNCs over the different sulfur restriction periods were calculated and are presented in Figure 17. The total PNCs were calculated over all cleaned periods of the data, not only for the valid time periods. This is a valid procedure as the validity of the time periods is only relevant for the plume detection and the invalidity of the data does not cause error on total PNCs.

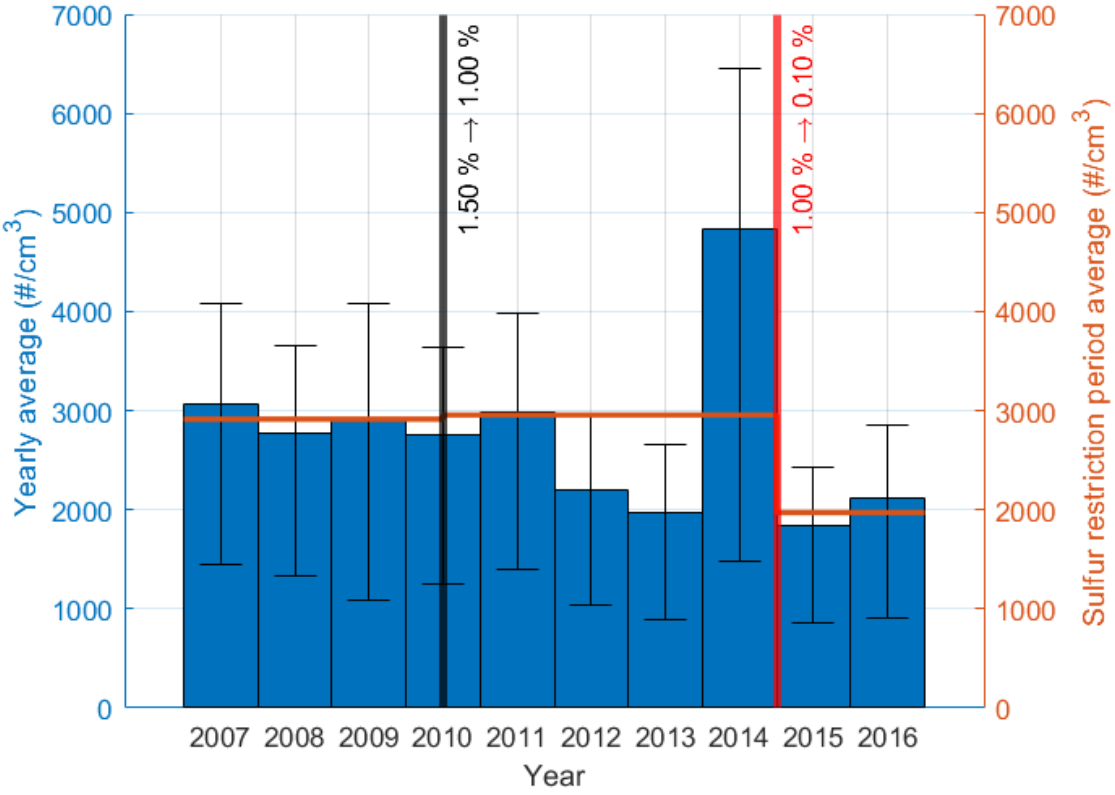

Figure 17 The yearly averages and the sulfur restriction period averages of the total PNCs for the particles in the size range of 7-538 nm in Utö during years 2007-2016. The blue bars are the yearly averages. The orange lines are the averages over the different sulfur restriction periods. For each of the yearly averages 25th and 75th percentiles have been marked with the black error bars. The black vertical line marks the change of the sulfur restriction of the marine fuels from 1.50 % to 1.00 % in June 1st, 2010 and the red vertical line marks the change of the sulfur restriction from 1.00 % to 0.10 % in January 1st, 2015.

In Figure 17 the yearly averages of total PNCs at Utö are seen to vary between approximately 2000-3000 #/cm^3 with the exception of year 2014. Similar total PNCs have been measured earlier in the Baltic Sea. For example, Plauškaitė et al. (2017) measured in southern and southeastern regions of the Baltic Sea the total PNCs of 3000-4000 #/cm^3 in the open sea and 2000-3000 #/cm^3 in the coastal site during years 2005-2006 and 2008-2010. These measurements excluding the measurements in 2005 were made during the sulfur restriction period of 1.50 %. The average PNC during this sulfur restriction period measured in this thesis was just under 3000 #/cm^3, that is between the PNCs measured by Plauškaitė et al (2017). This is to be expected as the location of the measurement station at Utö is a mix of open sea and coastal area. It is a small island in relatively open sea area.

The effect of the first change in the sulfur content restrictions of marine fuels from 1.50 % to 1.00 % seems to have had a minimal to no effect on the total PNCs. The PNCs are even slightly higher for the 1.00 % restriction period, because the high total PNCs of 2014 raise the total PNC average for the whole period. After the second change in the restrictions of the fuel sulfur content from 1.00 % to 0.10 % in beginning of 2015 the total PNC is seen to decrease drastically. However, the drop is likely to be smaller in reality because of the high PNCs of 2014. The PNCs for years 2012-2013 are approximately at the same level as during the time period after January 1st, 2015. The high PNCs of 2014 were found likely to be because of many long and intense nucleation events during the year. One example of the nucleation events is shown in Figure 18.

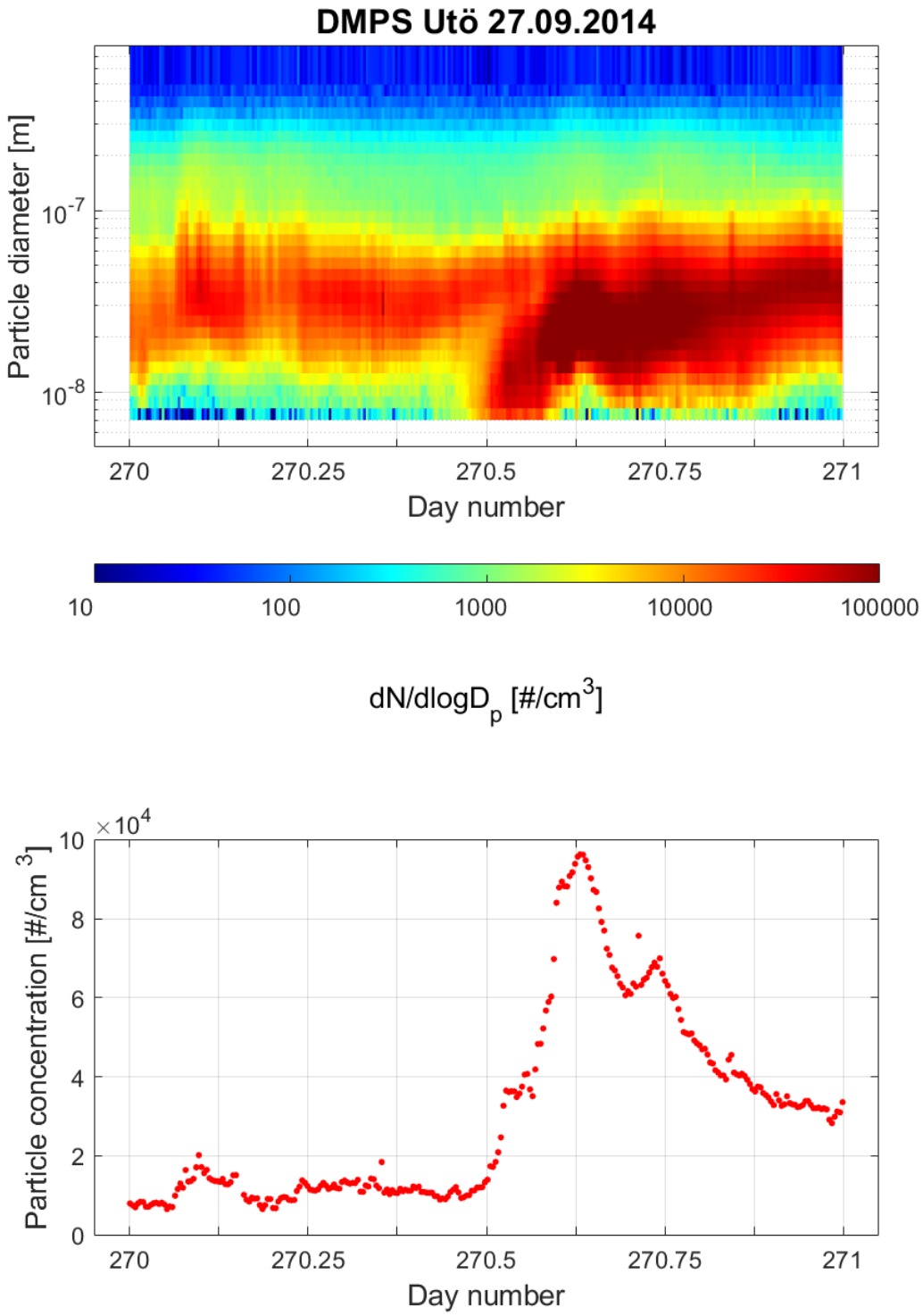

Figure 18 The example of an intense nucleation event in cleaned data of year 2014.

In Figure 18, the total NSD has been plotted as a function of time in the upper sub figure and in the lower sub figure the total PNC has been plotted as a function of time. In this

case the nucleation event raises the total PNC for more than 80 000 #/cm^3 which is eight times the total PNC before the nucleation event. The total PNC stayed elevated to at least three times the original PNC for half a day.

After further inspection, 14 strong and clear nucleation events and numerous possible weaker nucleation events were observed during year 2014. Of the 14 strong and clear nucleation events 9 happened in the spring, 1 in the summer, 3 in the autumn and 1 in the winter. The winds during these events were mostly from the northern directions, 57 % between west and northeast and only few from the southern directions. This is in accordance with the previous study made in the area by Hyvärinen et al. (2008), where they found that approximately 49 % of the events came between west and northeast with only very few coming from the southern and eastern directions. Differing from the previous study, even 29 % of the nucleation events came from the easterly directions while in the previous the study only very few nucleation events were observed from the easterly directions.

The average yearly PNC_{pl}s were also calculated and are presented in Figure 19. The PNC_{pl}s represented in the following figure are the average total PNCs over the PNC_{bg} during the plume. Only the valid plumes have been considered in plotting the figure.

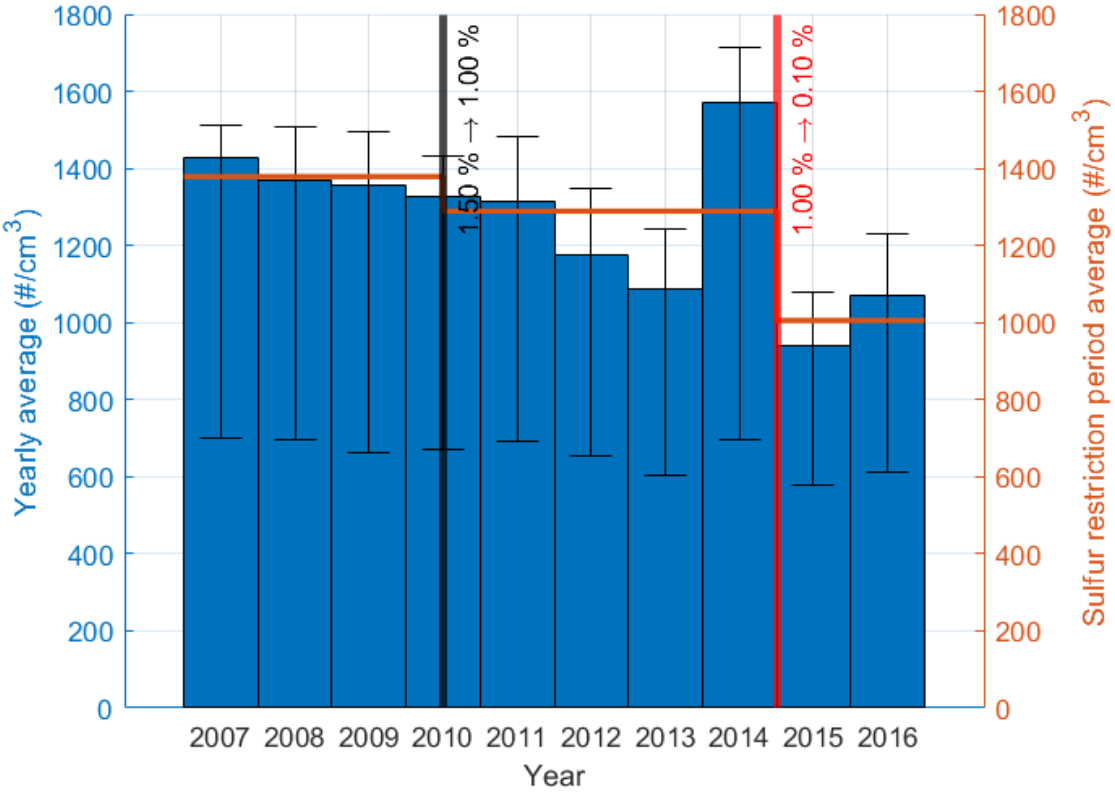

Figure 19 The yearly averages of the PNC_{pl}s in Utö for years 2007-2016 and the different sulfur restriction periods. The blue bars represent the yearly averages. The orange lines represent the averages during the different sulfur restriction periods. For each yearly average 25th and 75th percentiles have been marked with black error bars. The black vertical line represents the change of the sulfur content restriction in the marine fuels from 1.50 % to 1.00 % and the red vertical line represents the change of the marine fuel sulfur content restriction from 1.00 % to 0.10 %.

In Figure 19 a decreasing trend of PNC_{pl}s can be seen. With the exception of year 2014, all the yearly averages during the sulfur restriction periods of 1.00 % and 0.10 % are lower than the averages during the sulfur restriction of 1.50 %. The yearly averages during the sulfur restriction of 0.10 % are also lower than the yearly averages during the sulfur restriction of 1.00 %. The average value of the PNC_{pl} for year 2014 seems to be affected by some systematical error in the plume detection method caused by the nucleation events of 2014. This raises the question; how much the plume concentrations detected by this method from Kivekäs et al. (2014) are affected by natural phenomena that raise the PNC_{bg}?

After the second change of sulfur restriction from 1.00 % to 0.10 % in January 1st, 2015 the PNC_{pl}s decreased more than after the first change of the sulfur restrictions from 1.50 % to 1.00 %. This decrease may be portrayed larger than it really is as the average PNC_{pl} for the period of the sulfur restriction of 1.00 % seems to be raised because of

high concentrations of 2014. The effect of the sulfur restrictions on shipping emissions was studied by Zetterdahl et al. (2016). They found that the number of particles emitted stayed constant even though PM emissions reduction was 67 %. This implies that the usage of other PM removal mechanisms in the area might also have increased as in this thesis also the particle number was found to decrease. For example, open loop wet scrubber reduced 92 % of the total particle number and 48 % of the fraction of solid particles in ship emission in on-board measurements made by Lehtoranta et al. (2019).

Direct contributions of the valid plumes to the total PNCs in Utö were also calculated for every year and the different sulfur restriction periods. These contributions are presented in Figure 20.

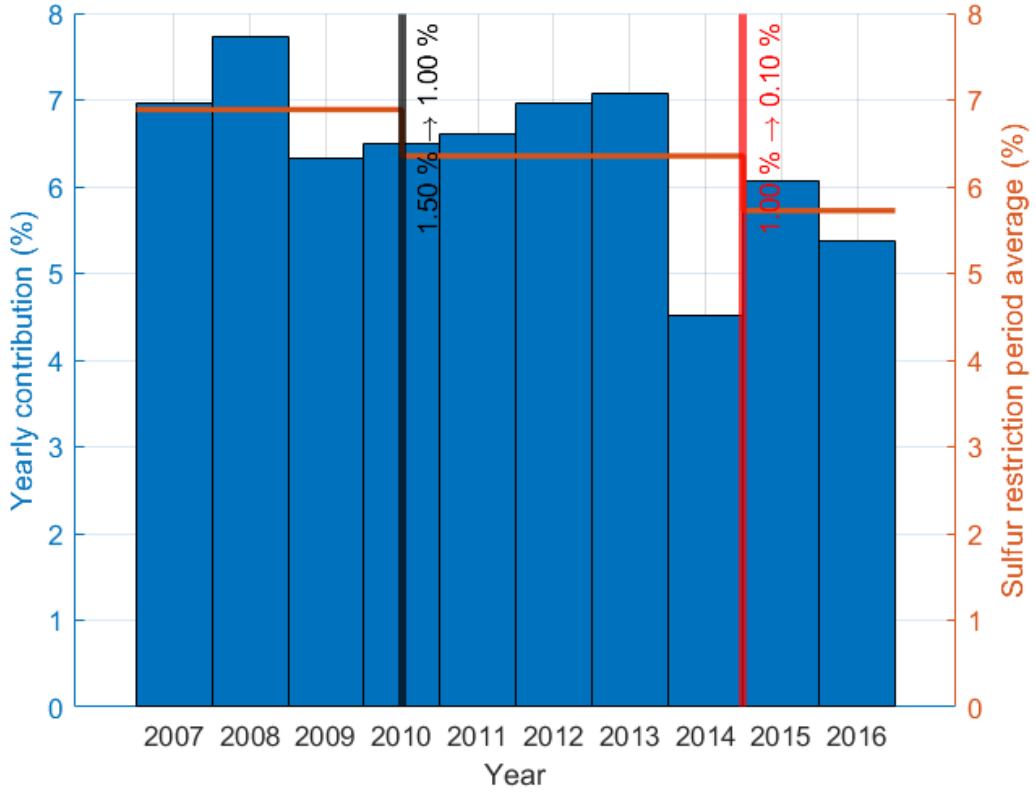

Figure 20 The direct contributions of the PNC_{pl}s to the total PNCs in Utö for each year of 2007 - 2016 and for the periods of the different the sulfur content restrictions in the marine fuels. The blue bars represent the yearly average values. The orange lines represent the average concentrations during the different sulfur restriction periods. The black vertical line represents the change of the sulfur content restriction in the marine fuels from 1.50 % to 1.00 % and the red vertical line represents the change of the marine fuel sulfur content restriction from 1.00 % to 0.10 %.

From Figure 20 the yearly direct contributions of the plumes to the total PNC in Utö can be seen to have been 4-8 % which is approximately the same level as the 5-8 % observed earlier by Kivekäs et al. (2014), using this same method in similar conditions. As

only the valid plumes were considered, the real values are likely to be slightly higher as some of the invalid plumes might have been real plumes. Supporting this Ausmeel et al. (2019) have reported contributions of 10-18 % in the Baltic Sea SECA during the sulfur restriction of 0.10 %. Although in the study by Ausmeel et al. the shipping line might have been more densely trafficked.

The decreasing trend of the direct contributions of the PNC_{pl}s to the total PNCs is seen in Figure 20. Notable is that the majority of the decrease after the first change in the sulfur restriction from 1.50 % to 1.00 % is caused by the low contribution value of 2014. This low value is likely to be result of elevated PNC_{bg}s, as mentioned earlier. The second change in the sulfur restriction from 1.00 % to 0.10 % in the beginning of 2015 still seems to have a clear effect by decreasing the contributions of the plumes. This decrease might be even downplayed because of the decreased contribution in 2014.

In Table 3 the averages of the total PNC, the PNC_{pl} and the direct contribution of the PNC_{pl} to the total PNC during the different sulfur restrictions are presented. The relative changes of the quantities after the changes of the sulfur restriction have also been calculated.

Table 3 The averages of the total PNC, the PNC_{pl} and the direct contribution of the PNC_{pl} to the total PNC during the different sulfur restriction periods and their relative changes during the changes of the sulfur restrictions.

	Sulfur restriction period			Relative change		
	<1.50 %	<1.00 %	<0.10 %	Change 1	Change 2	Total change
Total PNC	2914#/cm^3	2956 #/cm^3	1971 #/cm^3	+1 %	-33 %	-32 %
PNC_{pl}	1379 #/cm^3	1289 #/cm^3	1005 #/cm^3	-7 %	-22 %	-27 %
Contribution	6.9 %	6.4 %	5.7 %	-8 %	-10 %	-17 %

The effect of the second change in the sulfur restrictions is seen to be larger in all the three measured quantities. The difference of the changes 1 and 2 is especially large in the case of the total PNC. Notable is also that as the direct contribution of the PNC_{pl} to the total PNC is approximately 6 % and the total decrease of the PNC_{pl} is 27 %, the decrease caused to the total PNC by the decrease of PNC_{pl} is only about 2 %. However, the decrease of the total PNC is 32 % implicating that the indirect contribution of the shipping on the atmospheric aerosol might be far greater than the direct effect. There might also be other factors on top of the sulfur restriction changes reducing the total PNC

in the Utö. This is to be suspected as the decrease of the PNC_{pl} is smaller than the change of the total PNC, which should not be possible when the SOA production has not been taken into account, even if all the PNC_{bg}s would be caused by the PNC_{pl}s.

6.3 Number size distribution of plumes

In this this chapter the properties of the NSD_{pl}s are studied. The NSD_{pl}s are plotted separately for the sectors 1, 2 and 3 during all the three different sulfur restriction periods. The used sectors are described in Chapter 5.5 of this thesis. All the individual NSD_{pl}s that are used in calculating the average NSD_{pl}s are normalized to the total concentration of 1000 #/cm^3. This is done to cancel out the different PNC_{pl}s of the different plumes caused by the different dilutions of the plumes. Only the valid plumes are taken into account in plotting the figures.

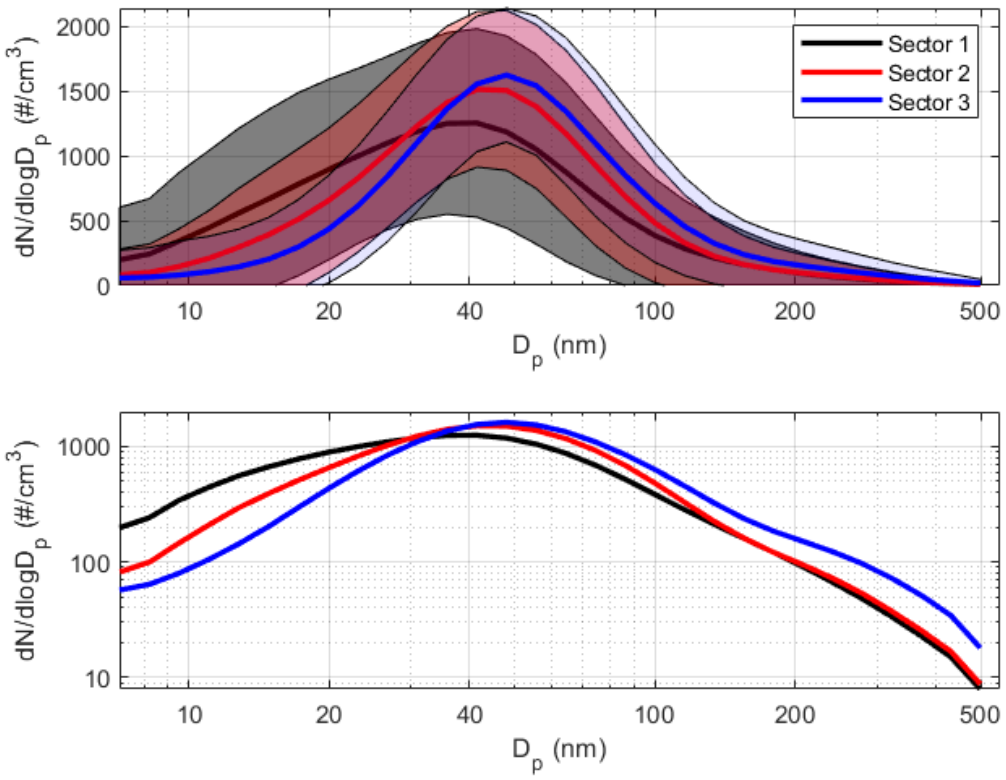

Figure 21 The average normalized NSD_{pl}s of the observed plumes during the measurement period of 11.1.2007-31.12.2016 with geometric standard deviations for the sectors 1, 2 and 3.

In Figure 23 the NSD_{pl}s with their standard deviations have been presented for all the sectors 1, 2 and 3 during the whole measurement period. From the three sectors, the average NSD_{pl} from the sector 3 has a maximum at largest particle size and the smallest standard deviation. The plumes from the sector 3 also have relatively the largest number

of large particles in them. This is to be expected as all the plumes from the sector 3 have to travel at least 8 km in air from a ship to the measurement site and most of the plumes seem to be coming from even longer distances as seen from Figures 7 and 9. As the transportation time in the air is longer, the smaller particles have time to grow to larger sizes through condensation or coagulation. As a reference, particle growth during nucleation events from 10-15 nm to sizes of approximately 50 nm takes several hours (Dall'Osto, et al., 2012). Similar growth rate of 3 nm/h^{-1} for particles in the marine environment has been presented also by Ehn et al. (2010). In case of the shipping emissions, the maximum of NSD from direct emission measurements has been observed to be anything between 28 nm and 70 nm, depending on used fuel and engine load (Kuittinen, 2016; Ntziachristos, et al., 2016). This decreases the needed growth of the plume particles to reach the measured particle diameters.

When the average NSD_{pl} from the sector 2 is compared to the average NSD_{pl} from the sector 3, the standard deviation increases, the NSD_{pl} broadens and the maximum shifts to a smaller particle size. The broadening of the NSD_{pl} and the increasing standard deviation may be because in this sector, the shipping lane lies 1-3 km to west from the measurement site and many of the plumes are coming from there, but many also come from longer distances. The existence of this shipping lane and background shipping activity can be seen from Figure 7. The smaller particle size of the maximum of the NSD_{pl} is the result of many of the plumes coming from the nearby shipping lane and not having time to grow. The relative number of the small particles in this sector is also higher. The fact that the broadening of the NSD_{pl} happens to the smaller particle sizes supports the assumption about the reason of the broadening.

The average NSD_{pl} from the sector 1 is the widest and it has the largest standard deviation. In the sector 1, the maximum of the NSD_{pl} being at the smallest particle size follows the same pattern as the sector 2. When more of the plumes are coming from shorter distances, the plumes do not have time to grow and the particle diameter at the maximum of the NSD_{pl} is smaller. The standard deviation is the largest and the NSD_{pl} the broadest in the sector 1 as many of the plumes can be expected to be coming from the nearby harbor of Utö, where there is a lot of passenger vessel traffic. The same western shipping lane that crosses the sector 2 also crosses the sector 1 behind the harbor bay and many off the plumes are coming from there. Some of the plumes may also be coming from even longer distances leading to the large variability of the ages of the plumes in this sector.

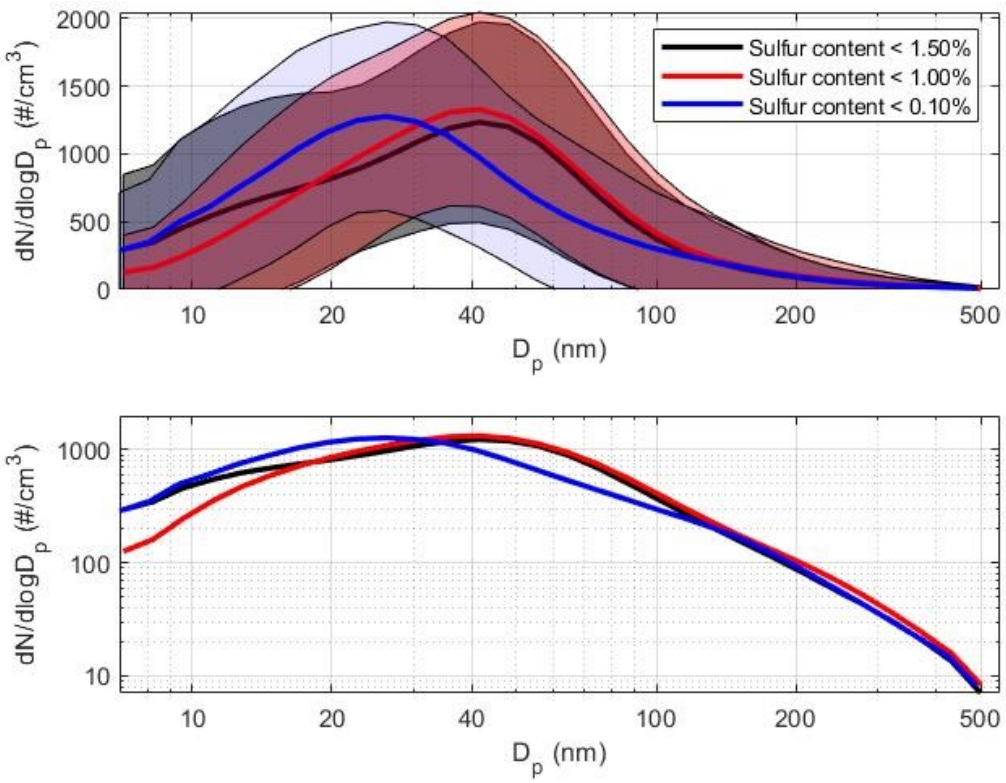

Figure 22 The average normalized NSD_{pl}s of the observed plumes from the sector 1 during the different sulfur restrictions.

In Figure 22 the effect of the change in the sulfur restriction on the size distributions with their standard deviations are presented for the observed plumes from the sector 1. From Figure 22 the effect of the first change in the sulfur restriction from 1.50 % to 1.00 % is seen to have been smaller than the effect of the second change in the sulfur restriction from 1.00 % to 0.10 %. The first change of the sulfur restriction did not affect the maximum of the NSD_{pl} and only decreased the relative number of particles smaller than 18 nm, meanwhile slightly increasing the relative particle numbers with diameters larger than 18 nm. After the second change of the sulfur restriction, the changes in the shape and maximum of the NSD_{pl} were larger. The maximum of the NSD_{pl} shifted to a noticeably smaller particle diameter, the relative particle numbers smaller than 31 nm in diameter increased and the particle numbers in the size range of 31-150 nm decreased. In the sizes larger than 150 nm there was no significant difference in the relative particle concentrations between the three restriction time periods. These changes in the NSD_{pl} seem to implicate that the higher percentages of sulfur in marine fuels grow small particles to larger particle sizes.

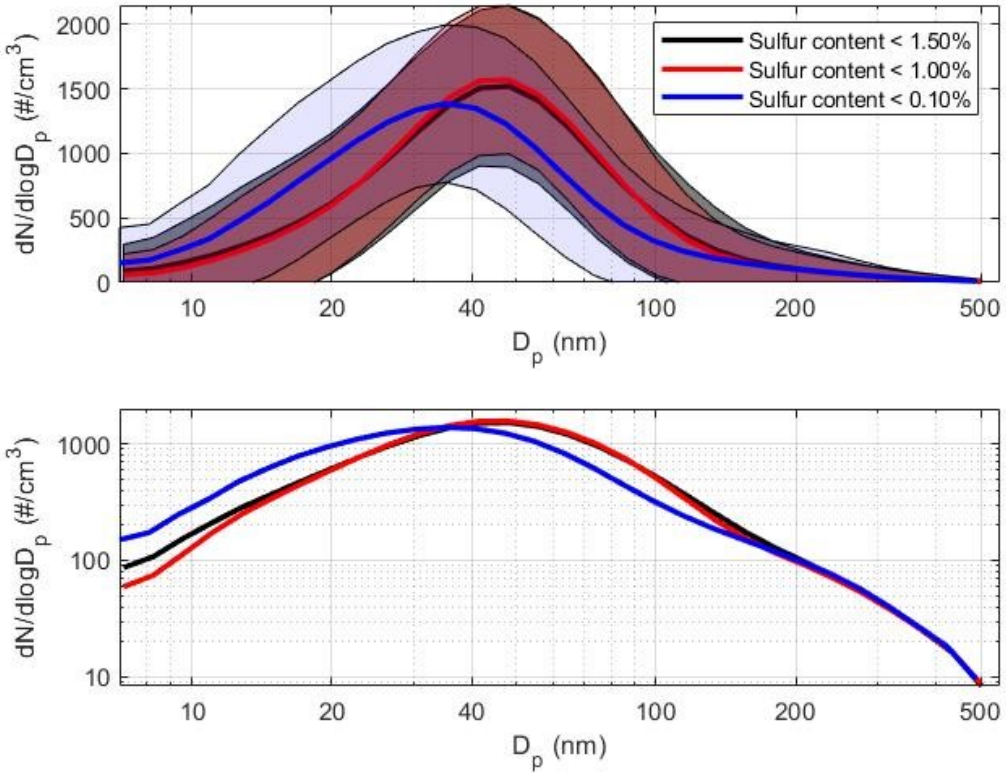

Figure 23 The average normalized NSD_{pl}s of the observed plumes from the sector 2 during the different sulfur restrictions.

In the Figure 23 the NSD_{pl}s for the three sulfur restriction periods with standard deviations from the plumes observed from the sector 2 are presented. From Figure 23 the effect of restricting sulfur content in marine fuels from 1.50 % to 1.00 % is observed being almost nonexistent in the sector 2. Both of the NSD_{pl}s have the same maximums and almost identical shapes. The second change of the sulfur restriction from 1.00 % to 0.10 % caused clear changes in the shape and the maximum of the NSD_{pl}. These changes were similar to the changes in the sector 1. The maximum of the NSD_{pl} shifted to a smaller particle diameter and the relative particle numbers increased in sizes smaller than 35 nm and decreased in sizes 35-150 nm. As in the sector 1, all the different restriction periods had relatively the same number of particles in the sizes larger than 150 nm. The effects seen in the sector 2 after the changes of the sulfur restrictions of the marine fuels seem to support the assumption of the higher sulfur content in fuels leading to the small particles growing to the larger particle sizes.

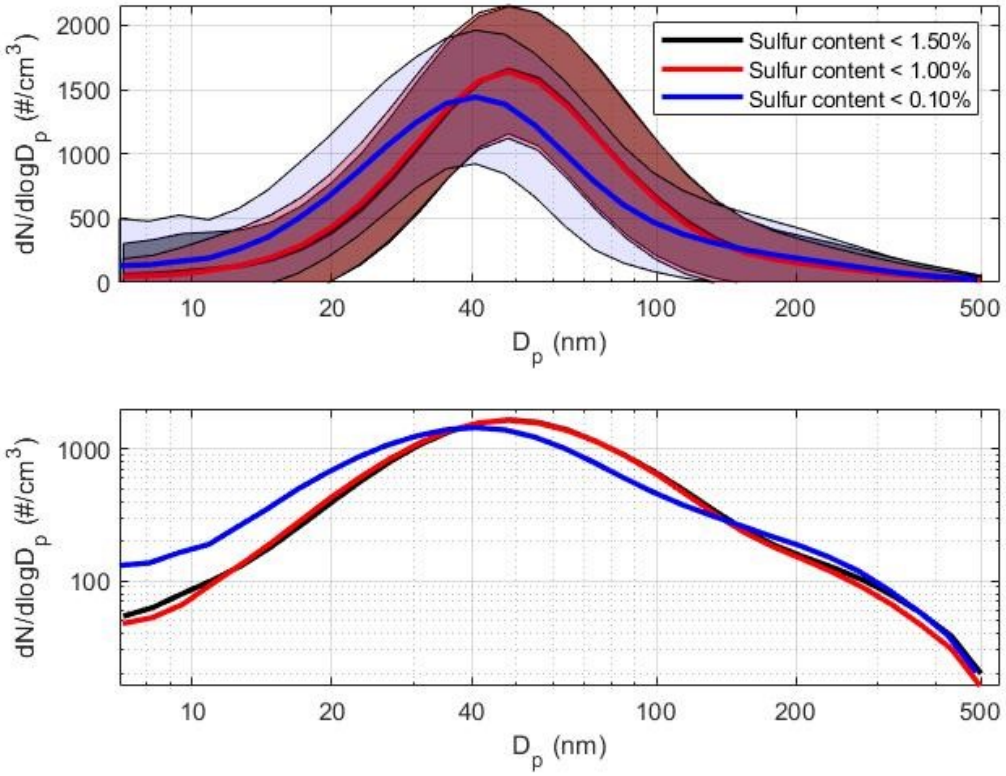

Figure 24 The average normalized NSD_{pl}s of the observed plumes from the sector 3 during the different sulfur restrictions.

In Figure 24 the averaged NSD_{pl}s of the plumes observed from the sector 3 during the three different sulfur restriction periods are presented. In the sector 3, the effects of the first change of the sulfur restriction from 1.50 % to 1.00 % were even smaller than in the case of the sectors 1 and 2. The maximums of the both NSD_{pl}s were the same and the shapes were almost identical. The second change of the sulfur restriction from 1.00 % to 0.10 % still had a clear effect on the NSD_{pl}. The maximum of the NSD_{pl} shifted to a smaller particle size, the relative particle concentrations with diameters smaller than 35 nm increased and the relative number concentrations of particles in the size range of 35-150 nm decreased. In the sector 3, similar to the sectors 1 and 2, the relative number of the particles larger than 150 nm was similar for the different sulfur restrictions. The results from the sector 3 are in line with the results from the sectors 1 and 2 supporting the assumption of the larger sulfur contents in the marine fuels allowing the growth of the small particles to the larger sizes.

Table 4 The diameters of the maximums of the NSD_{pl}s and their relative changes upon the sulfur restriction changes.

	Sector average	Sulfur restrictions			Relative change		
		<1.50 %	<1.00 %	<0.10 %	Change 1	Change 2	Total change
Units	nm	nm	nm	nm	%	%	%
Sector 1	41	42	42	26	0	-38	-38
Sector 2	42	48	48	35	0	-27	-27
Sector 3	48	48	48	41	0	-15	-15

In Table 4 the maximums of the NSD_{pl}s from the different sectors during the different sulfur restriction and their relative changes upon the sulfur restriction changes are presented. The smaller effect of the first change of the sulfur restriction from 1.50 % to 1.00 % compared to the second change from 1.00 % to 0.10 % can be clearly seen. The diameters of the maximums of the NSD_{pl}s did not change in any of the sectors after the first change but the second change caused considerable reductions to all of the maximums of the NSD_{pl}s. This change is seen to be the largest in the sector 1 where the average distance to the ships is the shortest, and the smallest in the sector 3 where the distance to the ships is the longest. This indicates that the reductions of the sizes of the fresh emission particles may be larger than the reductions of the sizes of the aged emission particles. Considering the changes of the maximums of the NSD_{pl}s, an important thing to consider is that the diameter resolution of the DMPS in these particle sizes was over 5 nm and therefore the minor changes of the diameter are not seen in Table 4.

Because there were no plumes coming from near the measurement site in the sector 3, the NSD_{pl}s during the 1.00 % sulfur restriction should be comparable to the NSD_{pl}s that Kivekäs et al. (2014) measured using the same method of plume detection. The NSD_{pl}s should be similar because the both measurements were made in the SECA during the same sulfur restriction period. The major differences were the different distance to the shipping lanes, the possibly different ship base and the different measurement instruments. The distance from the shipping lanes in the article by Kivekäs et al. (2014) was from 25 km to 60 km and in this thesis 8 km and upwards. Kivekäs et al. found that the maximum of NSD_{pl} was 41 nm which is slightly smaller than 48 nm found in this study. However, in this study, the number of the analyzed ship plumes was many times higher and the measurements were made at the different stations. The similar NSD_{pl} of 40 nm

in the Baltic Sea SECA area during the sulfur restriction period of 1.00 % has also been observed by Westerlund et al. (2015).

6.4 General plume properties

In this chapter the maximums of the NSD_{pl}s, PSC_{pl}s and PNC_{pl}s were calculated and are presented here as boxplots separately for all the sectors 1, 2 and 3 during all the three different sulfur restriction periods. In the end of this chapter also the size class averages for the plumes from the different sectors during the different sulfur restriction periods have been calculated. The different quantities have been calculated for only the valid plumes. The maximums of the NSD_{pl}s from the different sectors during the different sulfur restriction periods are presented as boxplots in Figure 25.

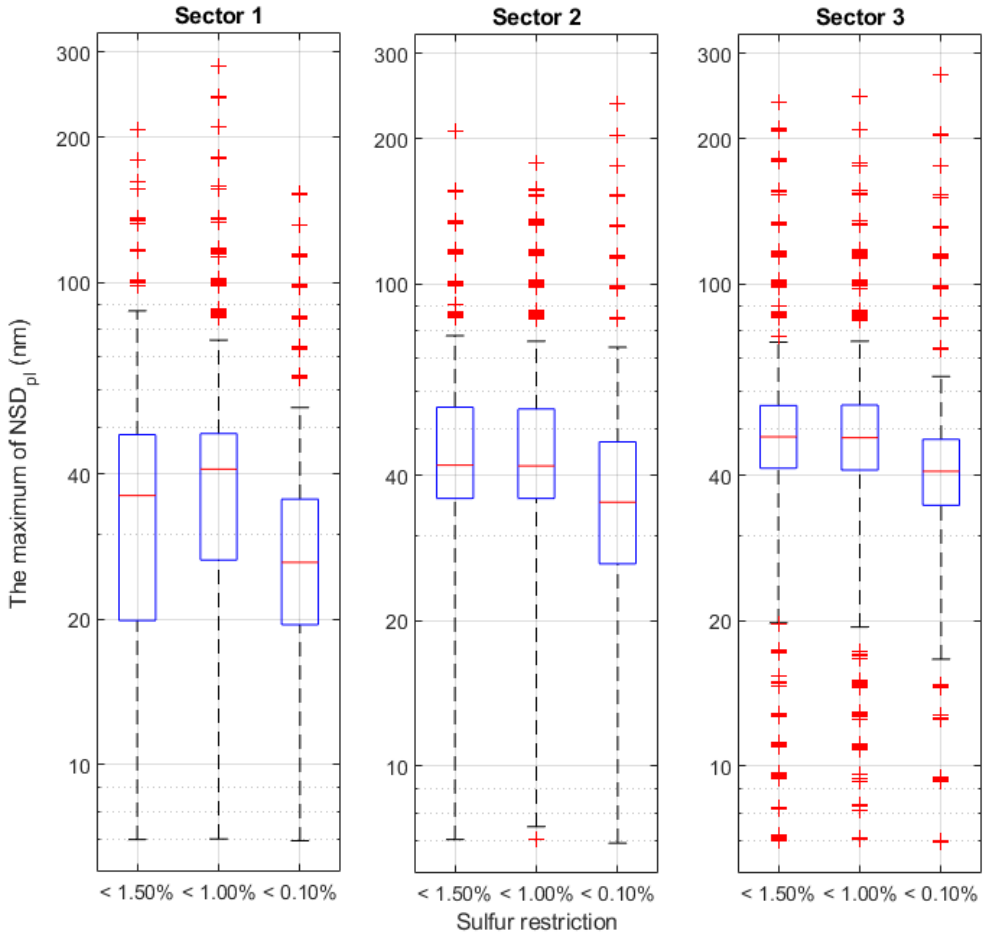

Figure 25 The boxplots of the maximums of the NSD_{pl}s of the individual plumes from the different sectors during the different sulfur restriction periods. The red lines represent the medians, the blue boxes the 25th and 75^{rh} percentiles and the red plus mark (+) the outlier values of the maximums of the NSD_{pl}s.

In all the sectors the overall change of the sulfur restriction from 1.50 % 0.10 %, led to reduced median diameters of the NSD_{pl}, the change being for the sectors 1, 2 and 3 10 nm (27%), 7 nm (16 %) and 7 nm (15%), respectively. Notable is that these changes in median diameters of the maximums of the NSD_{pl}s were smaller than the changes of the average diameters of the NSD_{pl} maximums listed in Table 4 in the cases of sectors 1 and 2. This implicates that especially the number of the plumes with the largest diameters of the maximums of the NSD_{pl}s decrease as the sulfur content in the marine fuels decreases.

The effect of the later, larger change in the sulfur restriction of marine fuels from 1.00 % to 0.10 % was significant in all the sectors. The first change of the sulfur restriction from 1.50 % to 1.00 % did not have as clear of an effect. The medians and percentiles in the sectors 2 and 3 remained almost unchanged and in the sector 2 the median diameter of the maximums of the NSD_{pl}s even increased. Two possible reasons why the effect of the first sulfur restriction was smaller are suggested. 1) The relative change in the sulfur content of the marine fuels was larger after the restriction change from 1.00 % to 0.10 %, 90 % compared to the 33 % of the sulfur restriction change from 1.50 % to 1.00 %. 2) The uncertainty of the real sulfur content change in the marine fuels during the change of the sulfur restriction from 1.50 % to 1.00 %. This uncertainty seen in the study by Pirjola el al. (2014) is discussed on the first page of the chapter 6 of this thesis.

Notable in Figure 25 is also the high number of the maximums of the NSD_{pl}s at the small particle diameters in the sector 1 during the sulfur restriction of 1.50 %. This is seen as the low 25^{th} percentile. This same phenomenon is not seen in any of the other sectors or during the other sulfur restriction periods. The high numbers of the small particles in the sector 1 during the sulfur restriction of 1.50 % is seen also in Figure 22.

PSC_{pl}s for the plumes from the three different sectors during the three different sulfur restriction periods are presented in Figure 26. The presented PSC_{pl}s are only the PCS_{pl}s of the particles in the measurement range of the DMPS (7-538 nm). The real PCS_{pl}s are likely to be considerably larger as the largest particles with large surface area are not measured.

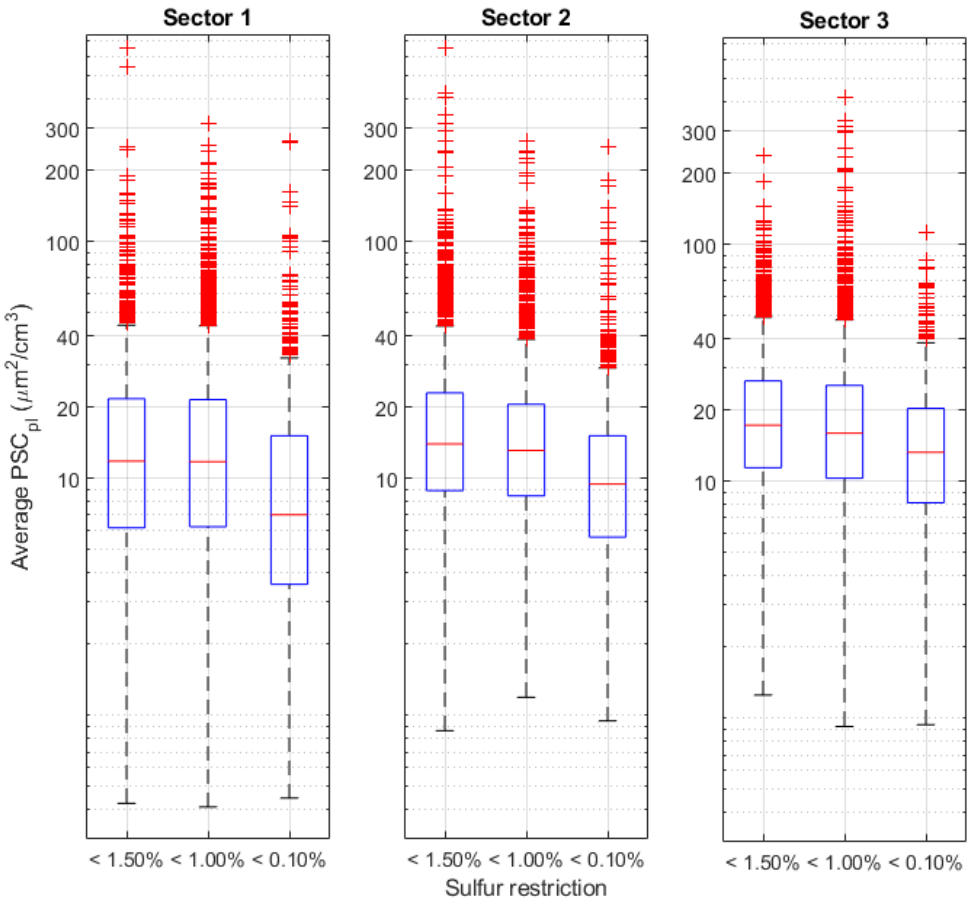

Figure 26 The boxplots of the average PSC$_{pl}$s of the individual plumes from the different sectors during the different sulfur restriction periods. The red lines represent the medians, the blue boxes the 25th and 75th percentiles and the red plus marks (+) the outlier values of the PSC$_{pl}$s.

In Figure 26 the average PSC$_{pl}$s can be seen to be lower when the particles are coming from shorter distances. Both changes of the sulfur restriction of the marine fuels can also be seen to decrease the PSC$_{pl}$s in the sectors 2 and 3. In the sector 1 only the later change of the sulfur restriction from 1.00 % to 0.10 % seems to have influenced the PSC$_{pl}$s.

In the sector 1 the total effect of the change in sulfur restrictions is larger than in sectors 1 or 2. In the sector 1, the median PSC$_{pl}$ decreases for 4.8 µm^2/cm^3, in the sector 2 for 4.5 µm^2/cm^3 and in the sector 3 for 4.0 µm^2/cm^3. These correspond for 41 %, 32 % and 23 % of the PNC$_{pl}$s during sulfur restriction period of 1.50 %, respectively. The same phenomenon as in the case of the maximums of the NSD$_{pl}$s is seen. The measured reductions are smaller when the plumes are arriving from longer distances. The surface

area of the particles has been related to toxicity and bioactivity of inhaled aerosol particles (Sager and Castranova, 2009). Therefore, the reductions of PSC_{pl}s are likely to improve the human health in marine and coastal areas.

The average PNC_{pl}s during the plumes from the different sectors during the different sulfur restriction periods were plotted and are presented in the Figure 27.

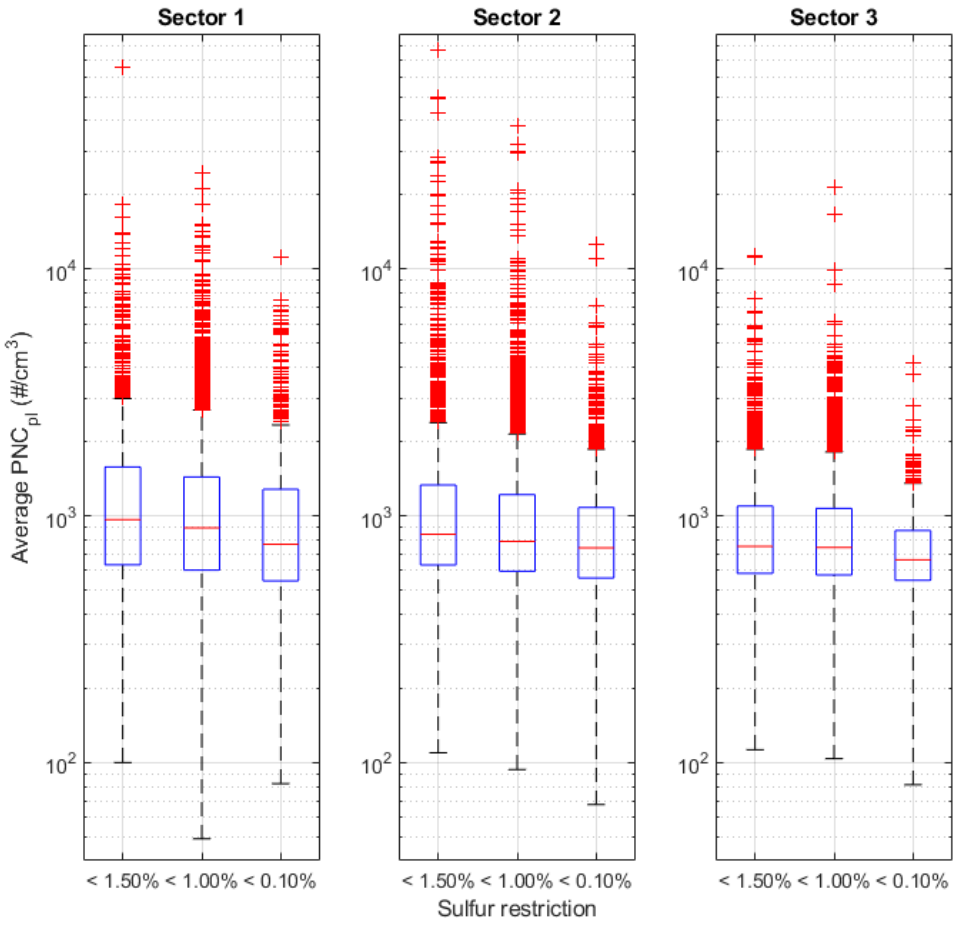

Figure 27 The boxplots of the average PNC_{pl}s of the individual plumes from the different sectors during the different sulfur restriction periods. The red lines represent the medians, the blue boxes the 25th and 75th percentiles and the red plus marks (+) the outlier values of the PNC_{pl}s.

The average PNC_{pl}s during the plumes from the different sectors during the different sulfur restriction periods were plotted and are presented in Figure 27. All the sulfur changes in the sulfur restriction are seen to have reduced the PNC_{pl}s in all the sectors. Also, the increasing distances between the emission sources and measurement station are seen to have decreased PNC_{pl}s. The decreases were larger after the second change in sulfur restriction from 1.00 % to 0.10 %. In all the sectors this change of the sulfur restrictions also reduced the maximum outlier values, indicating that the highest average

PNC_{pl}s during the plumes were related to the high sulfur contents in the fuels. Also, the variability in the PNC_{pl}s was reduced after the implementation of every new sulfur restriction. This effect is especially visible in the sector 3 and the second change of the sulfur restriction from 1.00 % to 0.10 %.

The PNC_{pl}s measured from the sector 1 are higher than from the two other sectors. This is to be expected as low engine loads have been shown to lead to higher particle number concentrations by Anderson et al. (2015) and many of these plumes are assumed coming from the ships using the low engine loads in the harbor area. The second factor increasing the concentrations in the sectors 1 and 2 in is the lower dilution of the plumes compared to the plumes measured from the sector 3 that are coming from longer distances.

Ausmeel et al. (2019) measured during the sulfur restriction of 0.10 % in the Baltic Sea SECA the PNC_{pl}s of 700-750 #/cm^3 during the winter and 860-1470 #/cm^3 during the summer depending on the used measurement instrument. This is in good accordance with 663 #/cm^3 seen in Figure 27 in the sector 3 during the same sulfur restriction of 0.10 %. The slightly higher concentrations may be related to the shorter distance to the shipping line, the much lower number of the observed plumes and the slightly different particle size range of the used instruments in the study by Ausmeel et al. (2019).

The average PNC_{pl} during plumes were also calculated for different size classes. These PNC_{pl}s were calculated for all the sectors and the sulfur restriction periods and are presented in Table 5. Similar values as presented in Table 5 were also calculated for all plumes with removed first and last measurement cycles to test the error caused by the plume starting and ending inside the measurement cycles on the PNC_{pl}. The attained PNC_{pl}s were on average higher, but the trend of changes was similar as in Table 5. These values are listed in Table 2 in the Appendix A.

Table 5 The average PNC_{pl}s from the sectors 1, 2 and 3 during the different sulfur restrictions divided into three distinct size classes.

	Particle size	Sulfur restriction			Relative change		
		<1.50 %	<1.00 %	<0.10 %	Change 1	Change 2	Total change
Units	nm	#/cm^3	#/cm^3	#/cm^3	%	%	%
Sector 1	7-33	760	641	767	-16	+20	+1
	33-108	820	743	418	-9	-44	-49
	108-537	87	82	76	-6	-6	-12
	Total	1667	1466	1261	-12	-14	-24
Sector 2	7-33	509	437	530	-14	+21	+4
	33-108	941	789	505	-16	-36	-46
	108-538	88	72	63	-18	-12	-28
	Total	1538	1298	1098	-16	-15	-29
Sector 3	7-33	273	271	298	-1	+10	+9
	33-108	681	675	462	-1	-31	-32
	108-538	106	104	85	-1	-18	-19
	Total	1060	1050	846	-1	-19	-20

In Table 5 the reductions of the sulfur content in the marine fuels are seen to lead in all sectors to reduced total PNC_{pl}s. Only in the case of the sector 3 and the first change in the sulfur restriction from 1.50 % to 1.00 % the effect is small with the concentrations decreasing only 1 %. The total PNC_{pl}s changes in all the sectors after each of the sulfur restriction changes are negative for the particle sizes larger than 33 nm. However, for the particles in the size class of 7-33 nm the PNC_{pl}s increase after the implementation of the sulfur restriction of 0.10 %. This leads to overall increased concentrations in this size class. The effect of the first sulfur restriction change from 1.50 % to 1.00 % is quite even in all the size classes and sectors. The change of the sulfur restriction from 1.00 % to 0.10 % decreased the PNC_{pl}s only in size classes of 33-108 nm and 108-538 nm. The effect is largest in size range of 33-108 nm. The particle numbers increased in the size range of 7 - 33 nm indicating that while there is a reduction in the total particle numbers, some produced particles are smaller than before and are seen in the smallest size class

instead of the larger size classes. The increase of the average PNC_{pl}s is relatively largest when the average distance of the source vessels is the largest.

In the sectors 1 and 2 the effects of the both sulfur restrictions changes on the average PNC_{pl}s of largest particles are quite even, but in the sector 3 the effect of the second sulfur restriction change is almost 20 times as large as the effect of the first change of sulfur restriction. This implicates that the low sulfur content of 0.10 % in the marine fuels restricts the growth of the particles while the 1.00 % sulfur content in fuel does not have any significant effect on the particle growth.

Kivekäs et al. (2014) found in their study that average the PNC_{pl} in similar conditions during the sulfur restriction of 1.00 % was 790 #/cm^3. This is in the same order as 1050 #/cm3 observed from the sector 3 during the same sulfur restriction period in this study. The slightly higher value obtained by Kivekäs et al. might be because the average distance to the shipping lanes in the article was longer than in this thesis, and the ship plumes had more time to dilute. The measured particle diameter range of 12.2 nm to 496 nm in Kivekäs et al. (2014) was also slightly narrower than 7-538 nm used in this study, leading to lower concentrations overall.

The decreased total PNC_{pl}s seen in Table 5 and Figure 27 together with the reduced particle sizes seen in Figures 22, 23, 24 and 25 implicate that the sulfur reductions lead to reduced PM emissions. Similar results have been reported by López-Aparicio et al. (2017). They found that reducing sulfur content of the marine fuels from 1.00 % to 0.10 % reduces the SO_2 and PM_{10} emissions by 90 % and 10 %, respectively.

6.5 Aging of plumes

Emission restrictions have been shown to reduce formation of secondary organic carbon (SOC) in atmosphere (Ji et al., 2018). This raises the interest of exploring if similar effects are seen in the total SOA production. The oxidation of gaseous emissions produces SOA by forming low volatility compounds that either nucleate or partition on the existing aerosol particles (Kang, et al., 2007). This oxidation is caused by O_3, OH and hydroperoxyl (HO_2) that are produced by UV-light (Kang, et al., 2007). For example, the formation of SO_4^{2-} has been shown to be highly related to photochemical reactions during daytime (Ji et al., 2018). Also, the oxidation of anthropogenic emissions has been observed to happen mainly during daytime by Warneke et al. (2004) Because of this it is convenient to separate plumes to day- and nighttime in order to study the plume aging in the atmosphere.

In this thesis the division of the plumes to the day- and nighttime plumes is done according to the solar radiations during the measurement times of the plumes. The used solar radiation is the total solar radiation measured on a black horizontal plane. The valid plumes during the solar radiation of 0 W/m^2 were considered as the nighttime plumes and the valid plumes during the solar radiation of 200 W/m^2 or more were considered as the daytime plumes. The NSD_{pl}s and the size class averages were calculated for the both types of the plumes. In counting the average NSD_{pl}s, all the individual plumes were normalized to the total PNC_{pl} of 1000 $\#/cm^3$ to even the effect of different plumes to average NSD_{pl}s. The plumes during the different sulfur restrictions and sectors were studied separately.

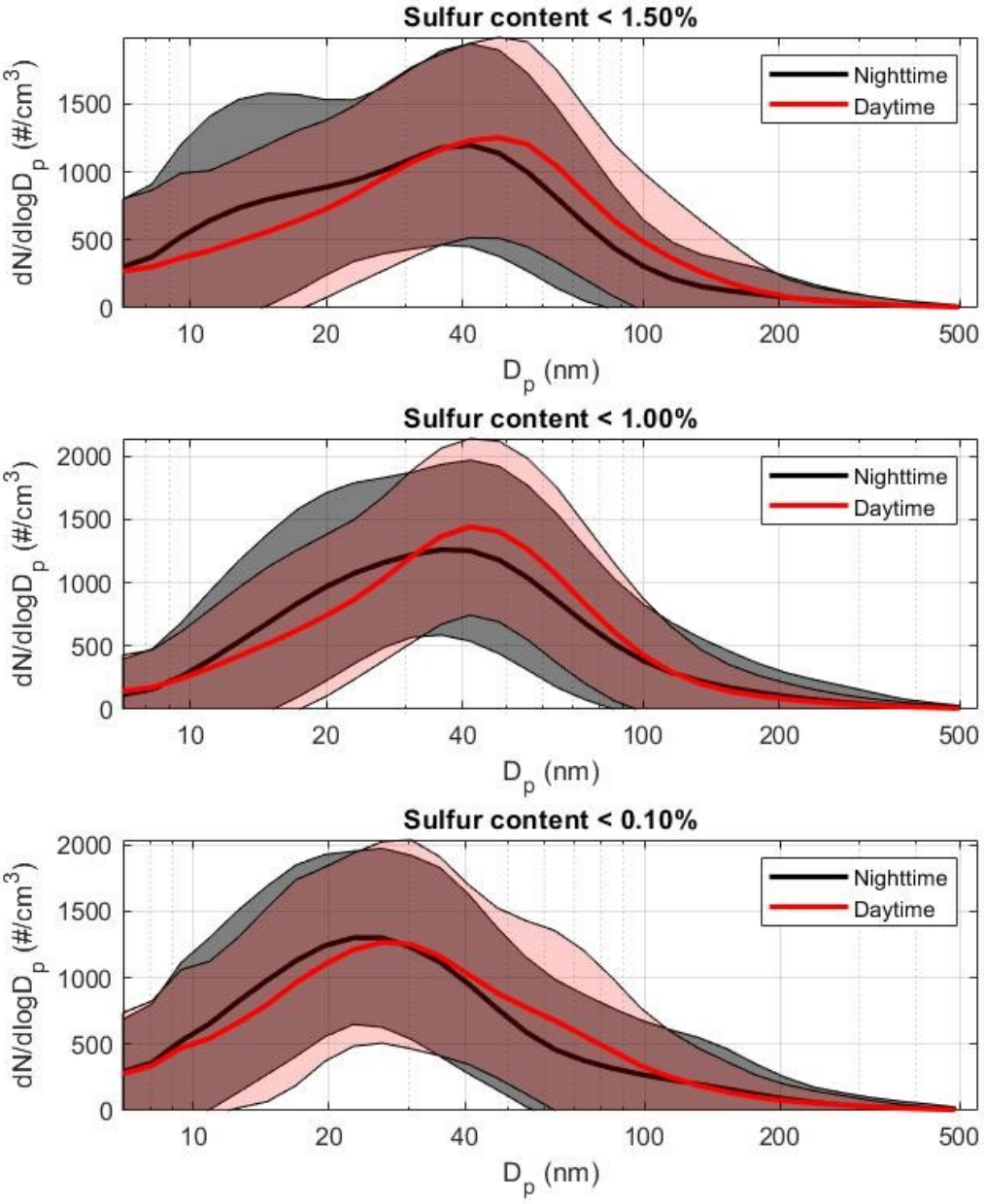

Figure 28 The average normalized NSD_{pl}s of the observed plumes from the sector 1 during the nighttime (total solar radiation intensity ~0 W/m^2) and the daytime (total solar radiation intensity >200 W/m^2).

In Figure 28, the NSD_{pl}s have been drawn for the both intensities from the sector 1 during the different sulfur restriction periods. The NSD_{pl}s from the daytime plumes are seen to have relatively lower PNC_{pl}s in sizes approximately smaller than 30 nm and increased PNC_{pl}s in mid-size particles, approximately from 30 nm to 120 nm. The relative PNC_{pl}s stay almost unchanged in particle sizes larger than 120 nm. In Figure 28 the particle

diameters of maximums of the both daytime and the nighttime NSD_{pl}s are seen to decrease as the sulfur content in the marine fuels decreased. Especially the effect of the sulfur restriction change from 1.00 % to 0.10 % is clearly visible.

During the sulfur restriction period of 1.50 % there is a clear nucleation mode visible as a shoulder in the nighttime NSD_{pl}. As the sulfur content decreased this shoulder disappeared. This mode was not visible in any of the NSD_{pl}s during the daytime or any of the NSD_{pl}s from the sectors 2 or 3. Therefore, this shoulder can be expected to be fresh sulfur related emissions that have not yet grown to larger sizes. The similar bimodality of fresh emissions has been observed by Anderson et al. (2015).

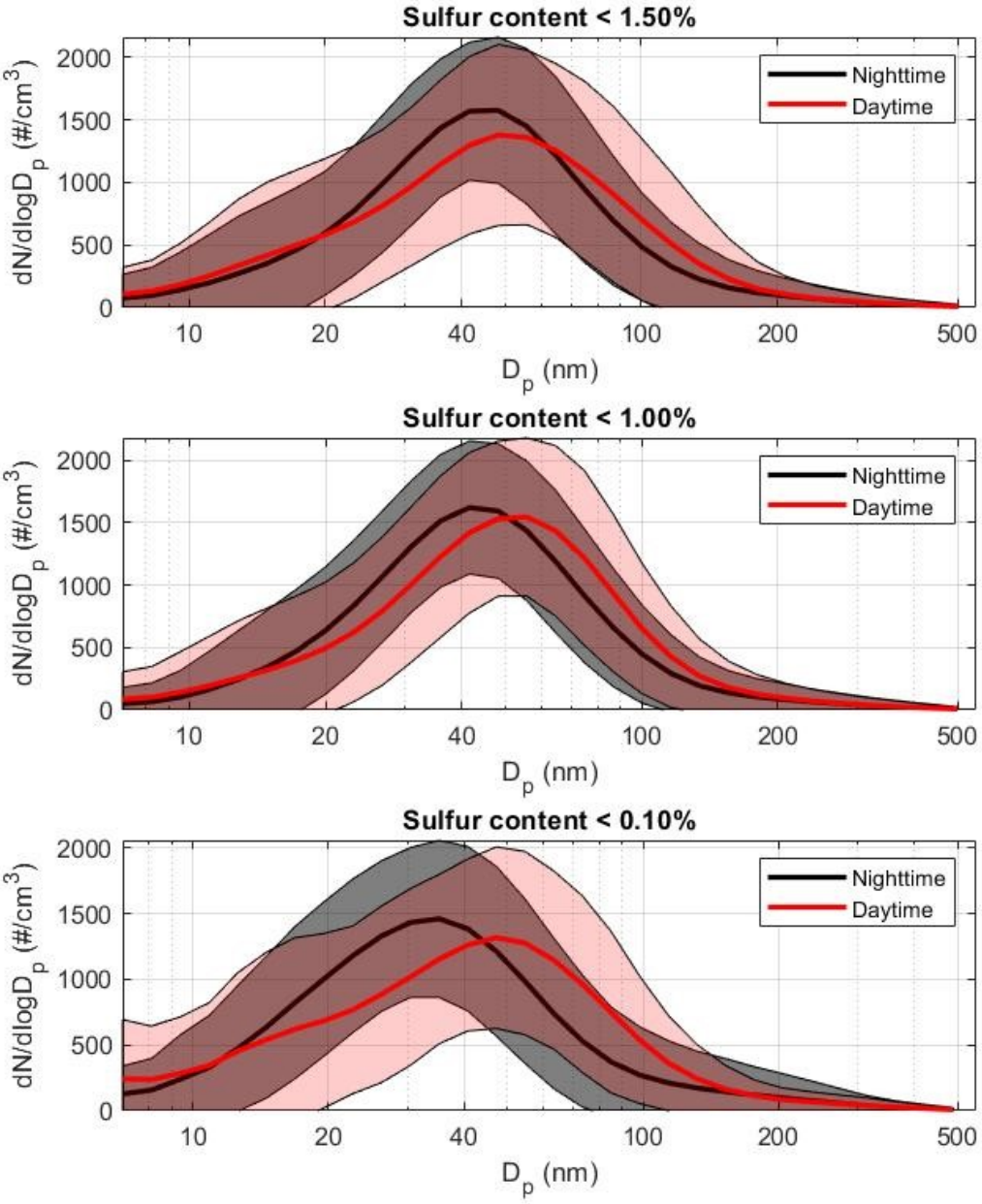

Figure 29 The average normalized NSD_{pl}s of the observed plumes from the sector 2 during the nighttime (total solar radiation intensity ~0 W/m^2) and the daytime (total solar radiation intensity >200 W/m^2).

In Figure 29 the NSD_{pl}s of plumes during the nighttime and the daytime are presented for the sector 2 during the different sulfur restriction periods. The same phenomenon as in Figure 28 is seen. The diameter of the maximum of the NSD_{pl} during the nighttime decreases as the sulfur content in the marine fuels decreases. The same phenomenon cannot be seen in the plumes during the daytime where the maximum of the NSD_{pl} remains almost unchanged during different sulfur restriction periods. The diameter of the

maximum of the NSD_{pl} was even highest during the sulfur restriction period of 1.00 %. Also, the diameters of the maximums of the NSD_{pl} can be seen to have increased during every sulfur restriction period, when the NSD_{pl} from plumes during the nighttime are compared to the NSD_{pl}s from plumes during the daytime.

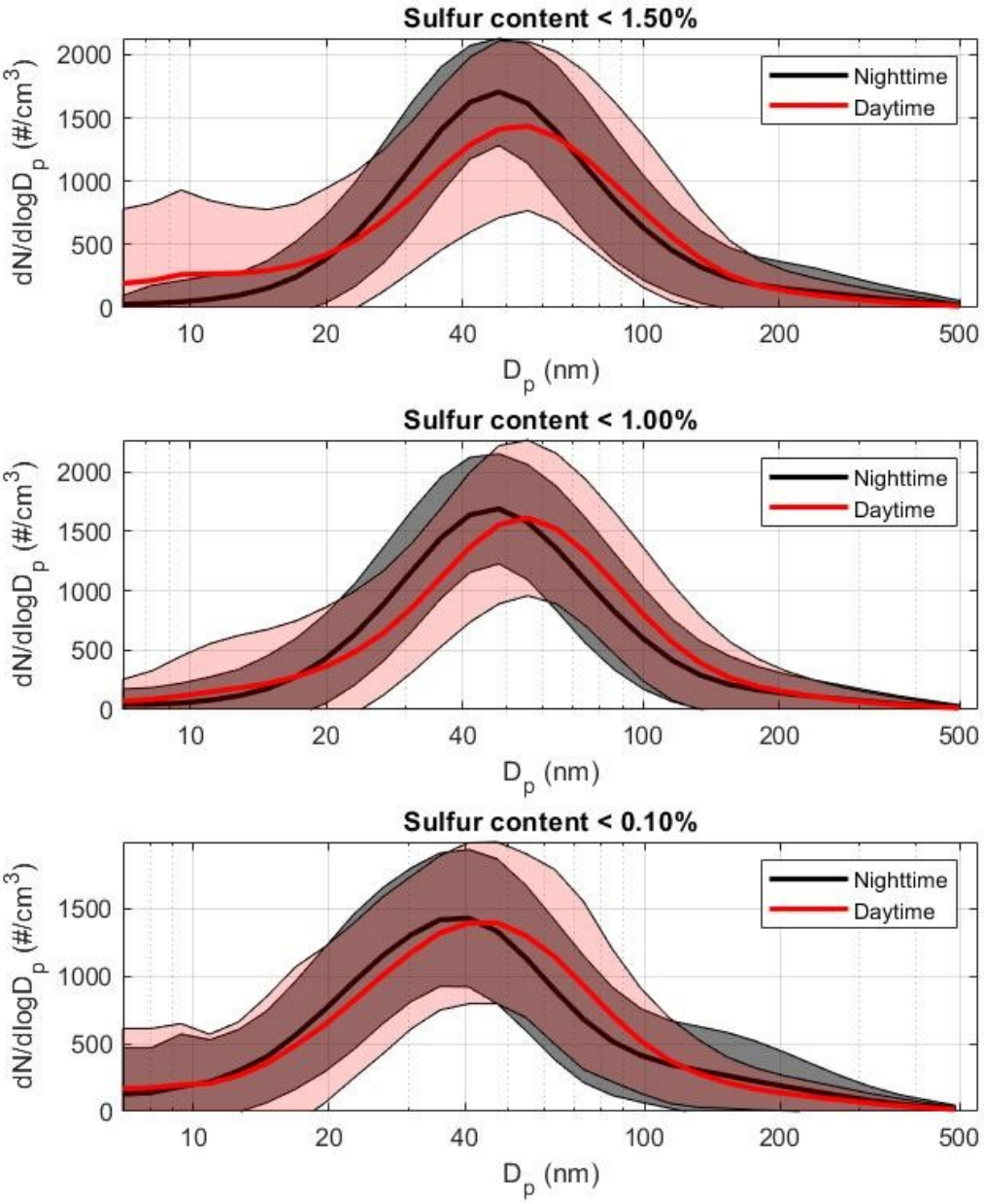

Figure 30 The average normalized NSD_{pl}s of the observed plumes from the sector 3 during the nighttime (total solar radiation intensity ~0 W/m^2) and the daytime (total solar radiation intensity >200 W/m^2).

In Figure 30, the NSD_{pl}s of the plumes during the nighttime and the daytime are presented for the sector 3 during the different the sulfur restriction periods. In Figure 30 in

the sector 3 the maximum of the NSD_{pl} from the nighttime plumes did not seem to decrease after the implementation of sulfur restriction of 1.00 % differing from the sectors 1 and 2 seen in Figures 28 and 29. The restriction of 0.10 % still decreased the maximum of the NSD_{pl}. The same phenomenon could be seen in the NSD_{pl}s during the daytime. The maximums of the NSD_{pl}s are the same between the two restriction periods but decreased during the second change of the sulfur restriction from 1.00 % to 0.10 %.

In sector 3 the maximums of the NSD_{pl}s during daytime are seen being larger than NSD_{pl}s during nighttime. This difference is however smaller than in the sectors 1 and 2. To further study these changes the exact diameters of the maximums of the NSD_{pl}s as well as their relative changes have been calculated separately for the night- and daytime plumes, sectors 1, 2 and 3 and the different sulfur restriction periods. These values are presented in Table 6.

Table 6 The diameters of the maximums of the NSD_{pl}s of the plumes during the daytime and the nighttime with the relative changes after the changes of the sulfur restriction.

	Day /night	Sulfur restrictions			Relative change		
		<1.50 %	<1.00 %	<0.10 %	Change 1	Change 2	Total Change
Units		nm	nm	nm	%	%	%
Sector 1	Night	42	36	23	-14	-36	-45
	Day	48	42	26	-13	-38	-46
Sector 2	Night	48	42	35	-13	-15	-27
	Day	48	56	47	+17	-16	-2
Sector 3	Night	48	48	41	0	-15	-15
	Day	56	56	47	0	-16	-16

In Table 6 the reductions during the both sulfur restriction changes both in the daytime and the nighttime plumes are seen to be the largest in the sector 1. The reductions of the diameters of the NSD_{pl} maximums are also seen to be similar between the day- and nighttime plumes in the sectors 1 and 3. The changes are however different in the sector 2, where the diameter of the maximum of the daytime NSD_{pl}s increases after the first sulfur restriction. This increase might however be only an error caused by the diameter resolution of the DMSP in these particle sizes being over 5 nm.

The effects of the sulfur restriction changes on the changes the PNC_{pl}s in plume aging were also studied. The increases of the PNC_{pl}s in plume aging during the three different sulfur restrictions, and in the sectors 1, 2 and 3 and the relative changes of the PNC_{pl}s increases are presented in the three different size classes in Table 7

Table 7 The difference of the PNC_{pl}s in three different size classes, between the plumes during the sunlight intensity of 200 W/m2 (Daytime) and ~0 W/m2 (Nighttime). The differences have been presented separately for each size class, sector, and sulfur restriction period. Both the absolute and relative changes have been presented.

	Particle size	**Sulfur restriction**					
		Change in average PNC_{pl}			Relative change		
		<1.50 %	<1.00 %	<0.10 %	<1.50 %	<1.00 %	<0.10 %
Units	nm	#/cm^3	#/cm^3	#/cm^3	%	%	%
Sector 1	7-33 nm	+84	+45	+281	+12	+7	+42
	33-108	+308	+248	+250	+47	+37	+77
	108-537	+78	+17	+18	+135	+23	+27
	Total	+471	+309	+550	+33	+22	+52
Sector 2	7-33	-122	-85	-129	-22	-18	-22
	33-108	-361	-39	+49	-32	-5	+10
	108-538	+33	+21	+11	+40	+33	+18
	Total	-450	-103	-68	-26	-7	-6
Sector 3	7-33	+242	+69	+44	+98	+27	+14
	33-108	+38	+106	+121	+5	+26	+29
	108-538	+32	+43	+12	+31	+46	+16
	Total	+312	+216	+178	+30	+21	+22

From Table 7 the exposure to light can be seen to have grown the PNC_{pl}s during all sulfur restriction periods in all size classes in the sectors 1 and 3. In the sector 2 the effects were different with the PNC_{pl}s decreasing in the plume aging during every sulfur restriction period in the smallest particle size class (7-33 nm) and also in the middle size class (33-108 nm) during the first two sulfur restrictions. This might be because of on

average larger vessels acting as sources of the plumes measured during the nighttime compared to vessels during the daytime in the sector 2.

The clearest effect of the plumes exposure to the sunlight is that during all the time periods and in all the sectors the PNC_{pl} in the largest particle size class (108-538 nm) increases. This increase is the smallest for the sector 2, where the total change in the PNC_{pl} was negative. The relative growth of the PNC_{pl}s in this size class seems to be decreasing while the sulfur content in the fuels decreases. This effect is especially visible in the sector 1. This indicates that the particle growth potential by aging seems to be limited by the low sulfur content in the fuels.

In the sectors 1 and 3 there are clear increases in PNC_{pl}s in the size class of 7-33 nm during the plume aging. This indicates that at least one of the following effects is happening: 1) Smaller than 7 nm particles grow to the size class of 7-33 nm or 2) homogenous new particle formation is happening and the newly produced particles grow to 7-33 nm size class. When the sulfur content decreases, the increase of the PNC_{pl}s in aging moves to the smaller particle size classes. This indicates that the lower sulfur contents in the marine fuels decrease the amount of particle growth in aging compared to the new particle formation. Although this effect cannot be seen in sector 2.

6.6 Comparison to direct emission data

From the direct emission data (Kuittinen, 2016) MDO emissions measured were chosen for the comparison. In the MDO used by Kuittinen (2016) there was less than 0.10 % sulfur which best resembled the regulations after the implementation of the sulfur restrictions of 0.10 % in January 1st, 2015. In Figure 31 the NSDs of the emissions from the engine loads of 25 % and 75 % have been plotted in the same figure with the average NSD_{pl} of the nighttime plumes from the sector 1 during the latest sulfur restriction of sulfur content less than 0.10 %.The maximums of the NSDs have been normalized to the concentration of 1. The nighttime plumes were chosen as they are expected to be composed mostly from unaged emissions as discussed in the chapter 6.5 of this thesis. The sector 1 was chosen because the distance to ships is on average the shortest.

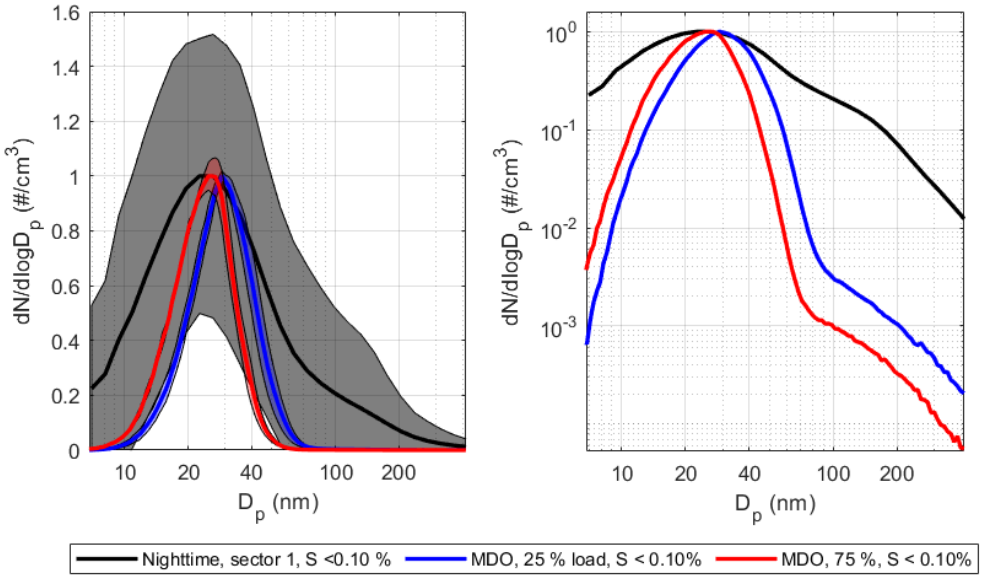

Figure 31 The comparison of the average NSD_{pl} of the plumes from the sector 1 during the nighttime and the sulfur restriction of 0.10 % to the NSDs from the direct emission measurements from Kuittinen (2016). The NSDs for the direct emission measurements have been drawn for the engine loads of 25 % and 75 %. The maximums of the NSDs are normalized to 1.

The load of 25 % is expected to resemble ship engines load conditions in maneuvering and nearing the harbor and the load of 75 % is expected to resemble the load conditions of the ship engines in open waters. The maximum of the NSD_{pl} of the nighttime plumes of the sector 1 is found to be slightly smaller than either of these two load conditions. In the plot on the right, where the both axes are set as logarithmic, all the NSDs can be seen to have two distinct modes, one at the maximum of particle sizes of 20-40 nm and another in larger particle sizes. This mode is seen as a shoulder in all the three size distributions and is expected to be composed of soot.

Notable in Figure 31 is that the shapes of the NSDs are almost identical in particle sizes larger than 100 nm. These particles can be assumed to be composed mostly from soot. Anderson et al. (2015) stated that particles with a diameter over 50 nm from the combustion of marine fuels are solid primary particles and are associated with the quality of the fuel and not the sulfur content. They also stated that the nanoparticles smaller than 50 nm can be related to both sulfur content and the other properties of the fuels and consist both primary and secondary particles. They also found that the volatile particles were in the size class of the nanoparticles. If the NSDs are normalized according to the concentrations of the particles larger than 100 nm the NSDs are assumed having approximately the same shapes as they have the same sulfur fuel content. To further study

this, another normalization for the NSDs was made. In Figure 32 the NSDs from the direct emission measurements of Kuittinen (2016) and the nighttime sector 1 NSD_{pl} have been normalized to have equal particle concentrations of 100 #/cm^3 in particle sizes of approximately 18-402 nm.

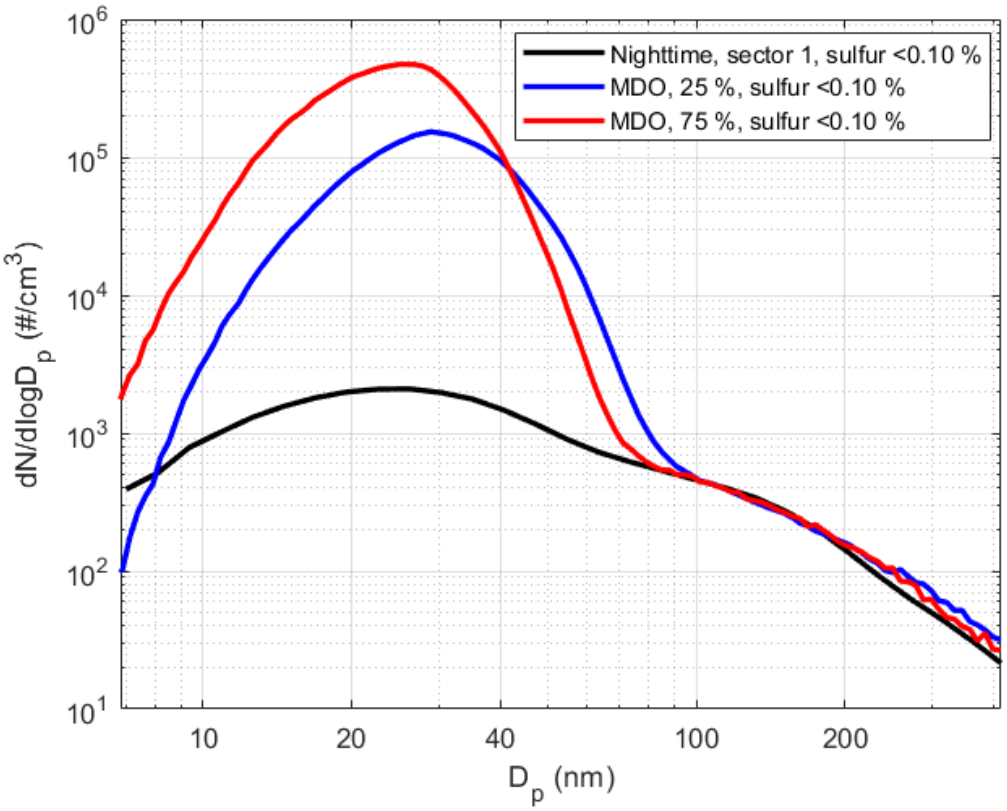

Figure 32 The comparison of the average NSD_{pl} of the plumes from the sector 1 during the nighttime and the sulfur restriction of 0.10 % and the NSDs from the direct emission measured by Kuittinen, (2016). The NSDs of the direct emission measurements have been drawn for the engine loads of 25 % and 75 %. The NSDs have been normalized to have the same number of particles in the particle sizes of 108-402 nm.

From Figure 32 it is clearly visible that the NSDs in particle the sizes larger than 100 nm have almost identical shapes. In the NSDs from the direct emission measurements the mode in smaller particle sizes is seen to have many orders of magnitude higher concentrations than the mode in larger particle sizes. In the case of NSD_{pl} the difference of the concentrations is much smaller.

When the large soot modes of the three NSDs are normalized to the same concentrations, the normalized concentrations for the smaller mode are found to be approximately two orders of magnitude lower for the NSD_{pl} in comparison to the NSDs of the direct emission measurements. The difference in the NSDs might be partly caused by the different shapes of the emission NSDs form the different kind of engines producing the

emissions. This means that that the NSDs from Kuittinen (2016) and the average NSD_{pl} of the harbor nighttime plumes might have had different shapes from the start. However, it is unlikely that this alone would explain the difference of the two orders of magnitude in the concentrations. Robinson et al. (2007) found that primary emissions evaporate substantially upon dilution to ambient conditions. They stated that up to 75 % of the POA might evaporate in the atmospheric conditions. This is well in line with the results attained in this study. As the nanoparticles smaller than 50 nm are assumed being partly volatile (Anderson et al., 2015) and the concentrations in this study are reduced in particle sizes of less than 70 nm.

6.7 Background number size distributions

NSD_{bg}s were drawn for each of the sectors during all the three different sulfur restriction periods to examine if the changes of the sulfur restrictions had influenced the PNC_{bg}s. Differing from the NSD_{pl}s of the plumes, the NSD_{bg}s were drawn from unnormalized distributions. The NSD_{bg}s have been calculated only for the valid time periods as during the invalid time periods the PNC_{pl}s and the PNC_{bg}s get mixed to some degree because of the plume detection method used. In Figure 33 the NSD_{bg}s from the sector 1 have been plotted during all three sulfur restriction periods.

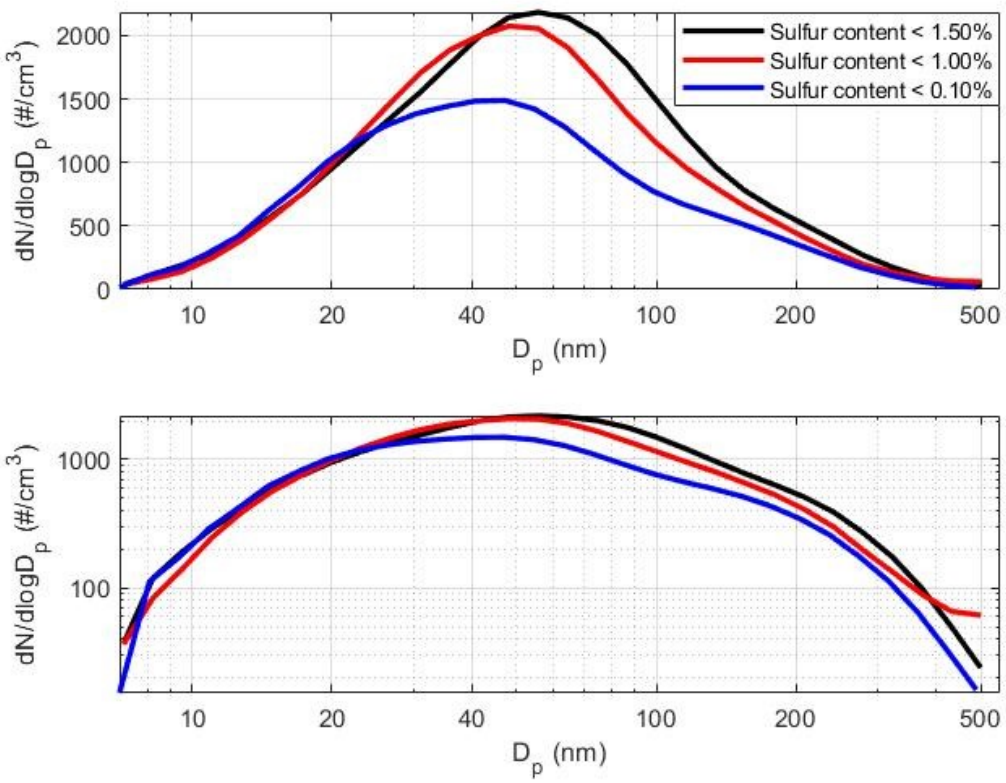

Figure 33 The NSD_{bg}s from the sector 1 during the different sulfur restrictions.

A clear difference in the NSD_{bg}s between different sulfur restriction periods can be seen in Figure 33. As the sulfur content in the marine fuel decreases the maximum of NSD_{bg} shifts to smaller particle sizes and the total PNC_{bg} decreases. During the sulfur restriction period of 1.50 % the maximum of the NSD_{bg} was 56 nm decreasing to 48 nm during the sulfur restriction of 1.00 % and to 47 nm during the sulfur restriction of 0.10 %. These diameters are slightly larger than the maximums of the NSD_{pl}s measured in sector 1 during the same sulfur restrictions. These diameters of the maximum of the NSD_{pl}s are presented in Table 4.

Notable is that the shape and height of NSD_{bgs} during different sulfur restriction periods are remarkably similar in particle sizes smaller than of approximately 22 nm. This is expected as the shipping plumes have effect on the PNC_{bg} when they are diluted to point that they are undetectable as individual plumes. This dilution takes time and the particles have time to grow during this time.

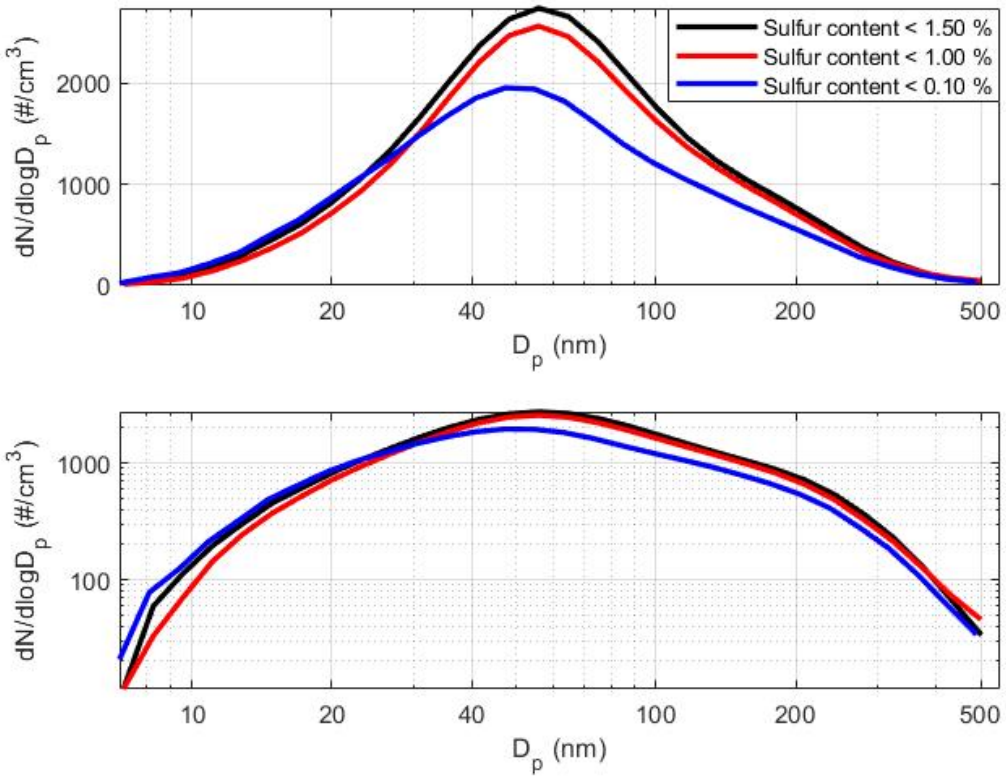

Figure 34 The NSD_{bg}s from the sector 2 during the different sulfur restrictions.

In Figure 34 the NSD_{bg}s have been presented for the sector 2. Restricting the sulfur content in the marine fuels seems to have effect on $NSD_{bg}{}^{s}$ also in the sector 2. The decreased sulfur contents decrease the total PNC_{bg}s and shift the maximum of the NSD_{bg} to smaller particle sizes. The maximum of the NSD_{bg} during the first sulfur restriction is 56 nm as in case of the sector 1, but the shape of the peak is sharper, and the peak is higher. During the second sulfur restriction period the diameter of the NSD_{bg} maximum stays unchanged, but the concentration overall is lower. During the third sulfur restriction period the diameter of the NSD_{bg} drops to 47 nm, which again is same as in the sector 1. The similarity of the maximums of the NSD_{bg}s during the different sulfur restriction periods with the sector 1 is expected as the nearby shipping activity should not have any major effect directly on the NSD_{bg}s. The effect of shipping can still be seen in NSD_{bg} because when plumes are coming from very long distances, they have much time to dilute and will not be identified as individual plumes anymore but are just added to PNC_{bg}s and NSD_{bgs}. This effect might be a reason the total PNC_{bg}s seem to be decreasing as the sulfur content in the marine fuels decreases.

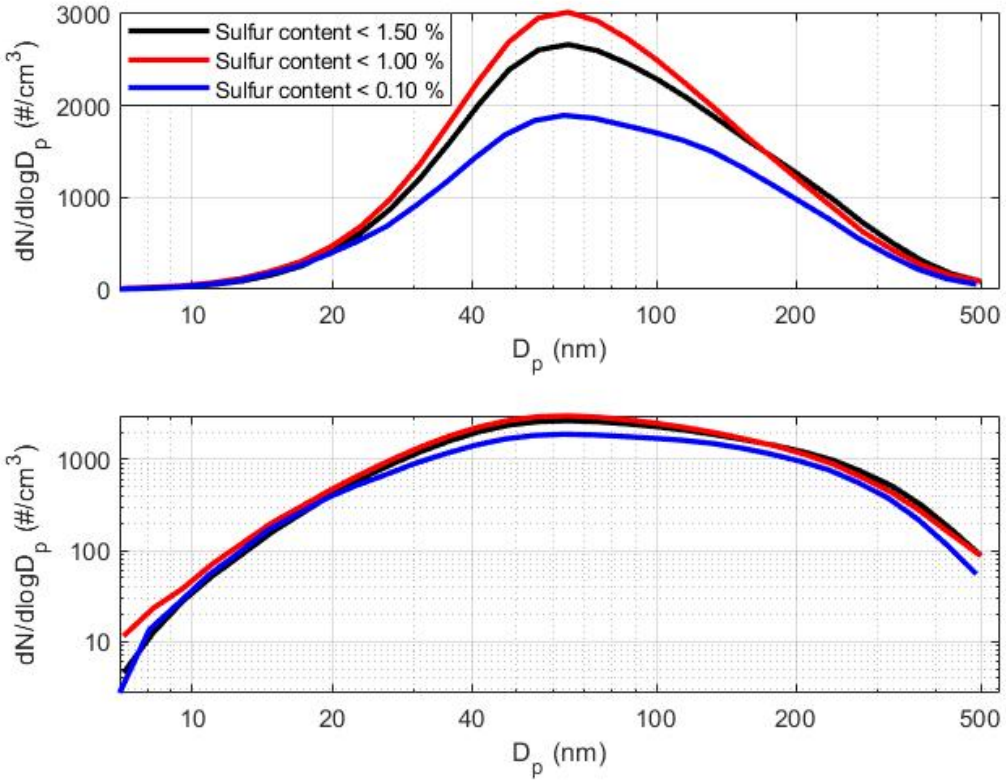

Figure 35 The NSD$_{bg}$s from the sector 3 during the different sulfur restrictions.

In Figure 35 the NSD$_{bg}$s have been presented for the sector 3. In the sector 3 the different amounts of sulfur in the marine fuels also seem to influence the NSD$_{bg}$s. Now only the PNC$_{bg}$s rise after the first change of the sulfur restrictions from 1.50 % to 1.00 % and decrease after the second change from 1.00 % to 0.10 %. Notable is that in this sector the sulfur restrictions do not have an effect on the diameters of the maximums of the NSD$_{bg}$s and all these maximums are larger than in the other two sectors. The maximums of the NSD$_{bg}$s being 65 nm during the first, 64 nm during the second and 63 nm during the third sulfur restriction period. The number of large particles in total is also larger for this sector. In this sector there was a significant shipping activity behind the closest shipping lanes and many, if not all, the plumes arriving from these very long distances will be distillated to the point of being undetectable as individual plumes. Therefore, they only contribute to the PNC$_{bg}$s as the increasing concentrations. The maximum of the NSD$_{bg}$ is in good accordance with this as the maximum is at the larger particle size than in the other two sectors where the plumes are coming from shorter distances. In this sector there is also a visible decrease in the PNC$_{bg}$s after the implementation of sulfur limit of 0.10 % in the marine fuels.

The NSD_{bg}s were plotted also for all the measured background data during the valid time periods. To this plot all the NSD_{bg}s with and without wind direction were included. These NSD_{bg}s are presented in Figure 36.

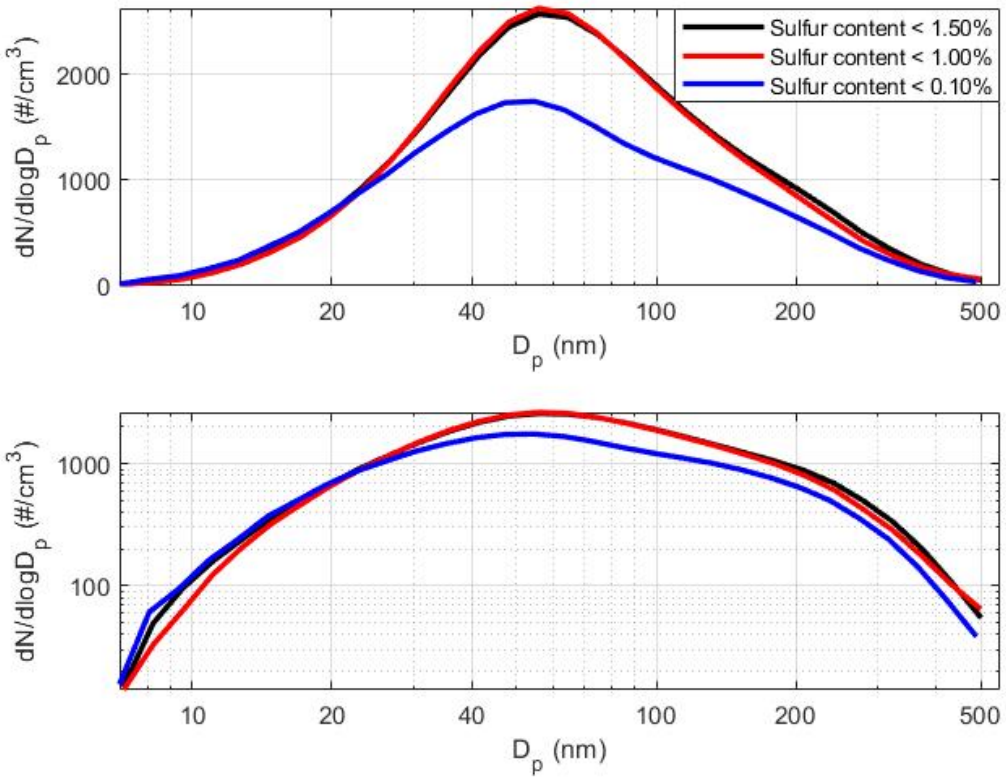

Figure 36 The NSD_{bg}s from all wind directions including undetermined wind directions, during the three different sulfur restriction periods.

In Figure 36 the NSD_{bg}s during the sulfur restriction periods of 1.50 % and 1.00 % are seen to be almost identical. There are only minor differences in the largest and the smallest particle sizes. The NSD_{bg} during sulfur restriction period of 0.10 % is different. The maximum of the NSD_{bg} has shifted to the slightly smaller particle size of 55 nm from the previous 56 nm and the average PNC_{bg} has decreased. This is in line with Figures 33-35. After the first change of sulfur restrictions from 1.50 % to 1.00 %, the background aerosol changes very little and almost all of the change happens after the second change of restrictions from 1.00 % to 0.10 %. This might be related to the uncertainty concerning the real sulfur content change of the marine fuels after the change of 1.50 % to 1.00 % in sulfur restriction seen in Pirjola et al (2014).

6.8 Error sources

The largest possible causes of errors in this study are the quality of the data cleaning, long measurement cycle of the DMPS, functioning of the plume detection method, the

uncertainty concerning the functioning and the composition of the measurement setup and the different data coverages for the different years.

The initial cleaning of the data was done manually by visual evaluation of the data. This might have produced an error as some errors in data might have been considered to be normal phenomenon for some days and errors for others. Also, some corrupted data might have been left in the data or some real phenomenon might be considered as bad data and falsely removed from the data. The automatic data correction might have caused similar errors to the data when the code from Kivekäs et al. (2014) removed the data with too fast changes in the total PNC data. Some of these removed fast changes might have been real phenomenon like ship plumes and not necessarily bad data. Because of this, the number of the plumes and the total PNC caused by the plumes may be portrayed to be lower than they are in the reality.

The relatively long measurement cycle of the DMPS (5 min 20 s) might have caused an error in the plume analysis. The error is caused because every plume starts during the first and ends during the last measurement cycle of the DMPS. This leads to the periods of time right before and after the plume being included in the detected plume. This reduces the average PNC_{pl}s as parts of the time considered as plume are really only periods with PNC_{bg}. The plume starting and ending inside the measurement cycle also causes an error in the PNC through inversion code when the multiple charge particles are corrected. However, depending on if the plume starts or ends inside the measurement cycle the effects are opposite and counteract each other. These errors could be avoided if the first and the last measurement cycle would be removed from every plume. This would lead to large data loss as all measured plumes lasting at maximum two measurement cycles (10 min 40 s) would be removed. This corresponds to large part of the measured plumes as 63.8 % plumes were at maximum two measurement cycles and 36.4 % were even shorter than one measurement cycle (5 min 20 s) of the DMPS. To examine the errors caused by the long measurement cycle of the DMPS the normalized NSD_{pl}s were calculated and plotted for all the plumes, the plumes lasting longer than one measurement cycle and the plumes lasting longer than two measurement cycles. These NSD_{pl}s are presented in Figure 37.

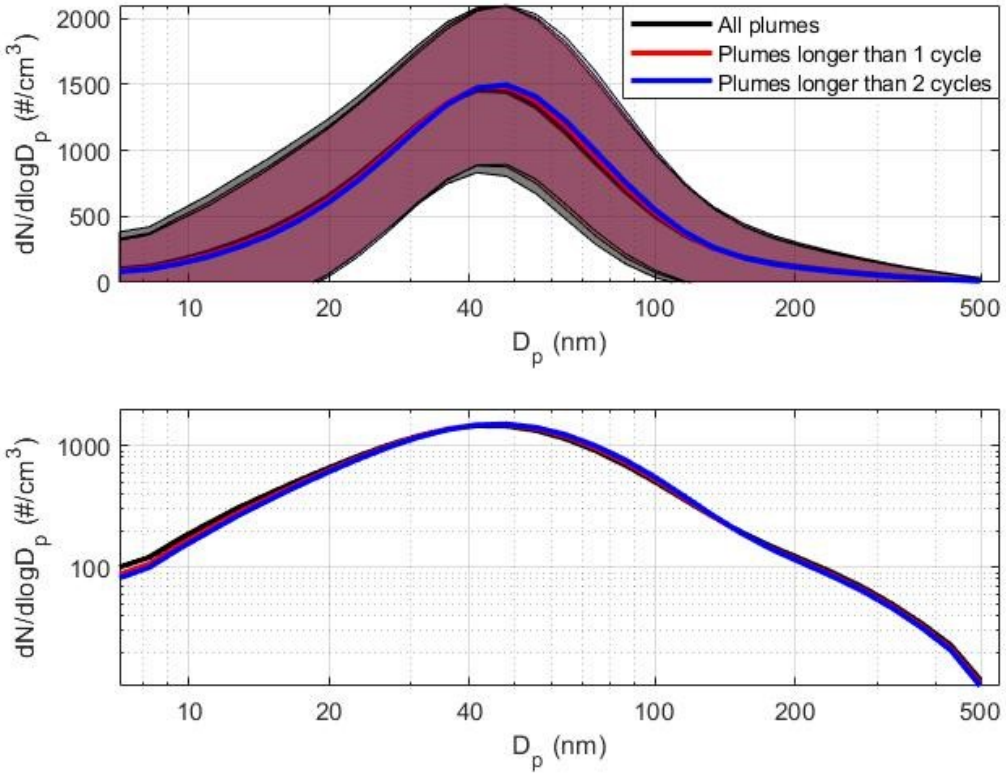

Figure 37 The normalized average NSD_{pl}s of all plumes, the plumes lasting longer than one measurement cycle and the plumes lasting longer than two measurement cycles of the DMPS.

From figure 37 all NSD_{pl}s and their standard deviations are seen to be practically identical. Therefore, there is no need to leave the short plumes out of the analysis. To further study the error caused by the first and the last measurement cycles of the DMPS, NSD_{pl}s were plotted for plumes the with removed first and last measurement cycles. The attained NDS_{pl}s had very similar shapes as NSD_{pl}s presented in this thesis. These reduced NSD_{pl}s have been presented in the Appendix B in Figures 1-3. The similarity of the NSD_{pl}s indicates that the negative error at beginning of the plume and the positive error in the end of the plume correct for each other because of the large number of analyzed plumes and there is no need to remove the short plumes from the data.

The plume detection method created by Kivekäs et al. (2014) is highly dependent on the values of the background percentile and limits for the PNC_e and the R_e used for identifying the plumes. These values used in this study were the same as in the original article Kivekäs et al. (2014). The reasoning behind these values is presented in Kivekäs et al. (2014) and effect of changing these initial values on the results was not further examined in this work. Another error caused by the plume detection method is that the data validation used by the code also removed all the plumes measured during the fast changes in

the PNC_{bg} and the plumes from which data was missing. These reduce the total number of the plumes compared to the real situation. Also, the added feature to invalidate all the plumes going over the day changes slightly reduces the number of the detected plumes and the effect of the PNC_{pl}s on the total PNCs.

The measurement setting used in this study was most of the time operating alone without continuous manual supervision and the measurement logs were partially incomplete. These together lead to certain uncertainty concerning the quality and reliability of the measurement data. These errors were corrected in the initial data cleaning removing all suspicious periods of the data. As data containing possible errors was exquisitely removed, the coverage of the cleaned data was relatively low for some years ranging between approximately 25-95 %. This coverage has been presented in Figure 12. The low coverages of the cleaned data for some years may have led to some seasons being underrepresented and others overrepresented in the data.

7. CONCLUSIONS

The PM emissions from shipping have a considerable effect on the climate and the human health. The ship emissions have a net cooling effect on the climate, as the increased reflection of sunlight back to the space from the particles outweighs the warming effects of the GHGs emitted in shipping. The effect that the PM and the gaseous emissions produced by the shipping have on human health is negative. The emissions produced by shipping have been related to numerous respiratory diseases and increased premature mortality and morbidity.

In this thesis the effect of changing the sulfur limit of the marine fuels on particle properties in atmospheric environment was studied. The atmospheric measurement data measured at the measurement site of the FMI at Utö in the Baltic Sea between 11.1.2007-31.12.2016 was used for this thesis. The used data was the DMPS data combined with the AIS and the weather data. From the DMPS data, ship plumes were found using the modified version of the plume detection method developed by Kivekäs et al. (2014). The AIS data was used for evaluating the amount of the ship traffic and the ship types in the area around Utö. The wind directions were attached to the observed plumes in order to divide them into three representative sectors with the plumes arriving from different distances on average. Also, the effects of the sulfur restrictions on total PNCs and plumes direct contribution to the total PNC in the area as well as the effect on the plume aging and the comparability of the measured plumes to the direct emission measurements from Kuittinen (2016) were discussed.

The statistically significant number of 42322 plumes with available wind data was found from the DMPS data. The significant portion (21960) of these arrived from the predetermined sectors 1, 2 and 3, and ended up being analyzed further. Notable is that 63.8 % of the plumes were at maximum two measurement cycles long and 36.4 % of the plumes were even shorter than one measurement cycle of the DMPS. This did not seem to produce any significant error in the results. Still in future, an instrument with a shorter time resolution would be better for detecting and analyzing the plumes.

Especially the later change in sulfur restriction from 1.00 % to 0.10 % was found to have been effective. After the reduction the total PNC, PNC_{pl} and the contribution of PNC_{pl} to the total PNC in the area all decreased. The total decreases were 32 % for the total PNC in the area, 27 % for PNC_{pl} and 18 % for the contribution of the PNC_{pl} to the total PNC.

The effect of the sulfur restriction change from 1.50 % to 1.00 % was small and most of the reductions happened during the change of sulfur restriction from 1.00 % to 0.10 %.

The low concentrations of sulfur in the marine fuels seemed to limit the particle growth to larger particle sizes in combustion process. This was observed as the both restrictions decreased the diameters of the maximums of the NSD_{pl}s also the relative normalized PNC_{pl}s increased in small particle sizes approximately smaller than 35 nm and decreased in particle sizes of 35-150 nm while the concentrations in particle sizes larger than 150 nm stayed almost unchanged. Also, when the unnormalized PNC_{pl}s were divided into three size bins of 7-33 nm, 34-108 nm and 108-538 nm, the total PNC_{pl}s concentrations were decreasing in all sectors after the implementation of the both sulfur restrictions of 1.00 % and 0.10 %. After the implementation of the sulfur restriction of 0.10 % the PNC_{pl}s slightly increased in the smallest particle size class of 7-33 nm and decreased in larger size classes, indicating that while there is reduction in total particle numbers, some produced particles are smaller than during periods with the higher concentrations of sulfur in the fuels and are seen in the smallest size class instead of the larger size classes. The reduction of the PNC_{pl}s was largest in the size class of 34-108 nm which most closely resembles the expected maximum of the NSD of the shipping emissions.

In all sectors the implementation of the sulfur restrictions of 0.10 % reduced the maximum values of PNC_{pl}s, indicating that the highest average values of PNC_{pl}s were related to the high sulfur contents in the fuels. Also, overall reductions of the PNC_{pl}s after the changes in the sulfur restriction were observed. The reduction of the PNC_{pl} was especially large in plumes with the largest maximums of the NSD_{pl}. This was observed as the reduction in the average of the NSD_{pl} maximums was larger than in the medians of the NSD_{pl} maximums even as the largest diameters of the NSD_{pl} maximums stayed almost unchanged during the different sulfur restriction periods.

There did not seem to be any clear correlation between the fuel sulfur content and the increase of the total PNC_{pl} during aging. However, the relative increase of PNC_{pl}s sifted towards the smaller particle sizes in all the sectors as the sulfur content decreased. This indicates that while the amount of new particle formation seems to be unaffected by the sulfur content restrictions in marine fuels, the growth potential of the particles is reduced as the sulfur content in fuels decreases. However, when the normalized NSD_{pl}s of the plumes during the nighttime and the daytime were studied the increase in the diameter of the maximum of the NSD_{pl} increased when the sulfur concentrations decreased. This

implicates that even while the growth potential of the particles is limited by the lowered fuel sulfur content the effect on the final size of the particles is not as large as the size reduction of the primary emission particles during the nighttime.

When the average NSD_{pl} of the nighttime plumes from the sector 1 was compared to NSDs of direct emission measurements NSDs were found to have very similar shapes and two detectable modes. Only the shape of the NSDs from direct emission measurements was a lot sharper. The shapes of the NSDs were almost identical for the particle sizes larger than 100 nm, and after normalizing NSDs to same total concentration of particles in the size range of 108-402 nm it was found that in atmosphere plumes have approximately two orders of magnitude lower concentrations in the particle mode with the smaller particle diameter than the direct emissions. Implicating that a large number of these particles evaporate in atmosphere.

The restrictions of the marine fuel sulfur content had an effect on the background aerosol shifting the maximums of the NSD_{bg}s to smaller particle sizes and reducing the PNC_{bg}s. The PNC_{bg}s were reduced especially in the particle sizes typical for the ship emissions indicating that the large fraction of the marine background aerosol particles was from the diluted shipping emissions. The effect of the later change of the sulfur restriction from 1.00 % to 0.10 % had much clearer effect on the background aerosol than the smaller first change of sulfur restriction from 1.50 % to 1.00 %. This effect of the sulfur restrictions on the PNC_{bg} implicates that the total effect of the particles produced by shipping on the atmospheric total PNC is larger than the direct contribution of 4-8 % and that the change of the total concentrations in the area might be better implication of the effectiveness of the sulfur restrictions than the direct contribution of PNC_{pl} to the total PNC.

REFERENCES

Aakko-Saksa P., Murtonen T., Vesala, H., Nyssönen, S., Puustinen, H., Lehtoranta, K., Timonen, H., Teinilä, K., Hillamo, R., Karjalainen, P., Kuittinen, N., Simonen, P., Rönkkö, T., Keskinen, J., Saukko, E., Tutuianu, M., Fischerleitner, R., Pirjola, L., Brunila, O.-P., and Hämäläinen, E., Black carbon measurements using different marine fuels, *28th CIMAC World Congress on Combustion Engines*, At Helsinki, Finland, Volume: CIMAC (2016), Paper no. 068, 2016.

Agrawal, H., Malloy, Q. G. J., Welch, W. A., Wayne Miller, J. and Cocker, D. R., 2008. In-use gaseous and particulate matter emissions from a modern ocean going container vessel. *Atmospheric Environment,* **42**(21), pp. 5504-5510.

Anderson, M., Salo, K., Hallquist, Å. M., and Fridell, E., 2015. Characterization of particles from a marine engine operating at low loads. *Atmospheric Environment,* **101**, pp. 65-71.

Antturi, J., Hänninen, O., Jalkanen, J., Johansson, L., Prank, M., Sofiev, M. and Ollikainen, M., 2016. Costs and benefits of low-sulphur fuel standard for Baltic Sea shipping. *Journal of Environmental Management,* **184**(Pt 2), pp. 431-440.

Ausmeel, S., Eriksson, A., Ahlberg, E. and Kristensson, A., 2019. Methods for identifying aged ship plumes and estimating contribution to aerosol exposure downwind of shipping lanes. *Atmospheric Measurement Techniques,* **12**(8), pp. 4479-4493.

Boucher, O., Randall, P., Artaxo, P., Bretherton, C., Feingold, G., Foster, P., Kerminen, V.-M., Kondo, Y., Liao, H., Lohman, U., Rasch, P., Satheesh, S. K., Sherwood, B., Stevens, B. and Zhang, X. Y., 2013. *Clouds and Aerosols. In: Climate Change 2013: The Physical Science Basis. Contribution of Working Group I to the Fifth Assessment Report of the Intergovernmental Panel on Climate Change [Stocker, T. F., D. Qin, G.-K. Plattner, M. Tignor, S.K. Allen, J. Boschung, A. Nauels, Y. Xia, V. Bex and P. M. Midgley (eds.)].* Cambridge, United Kingdom and New York, NY, USA: Cambridge University Press.

Brockmann, J. E., (2011). Aerosol transport in sampling lines and inlets. In Kulkarni, P., Baron, A. P. and Willeke, K., 2011. *Aerosol Measurement Principles, techniques, and Applications.* pp. 69-105. Third Edition. Hoboken, New Jersey: John Wiley & Sons, Inc.

Buhaug, Ø, Corbett, J. J., Enderssen, Ø, Eyring, V., Faber, J., Hanayama, S., Lee, D. S., Lee, D., Lindstad, H., Markowska, A. Z., Mjelde, A., Nelissen, D., Nilsen, J., Pålsson, C., Winebrake, J. J., Wu, W. and Yoshida, K., 2009. *Second IMO GHG study 2009.* London, UK.

Castranova, V., (2011). Factors Governing Pulmonary Response to Inhaled Particulate Matter. In Kulkarni, P., Baron, A. P. and Willeke, K., 2011. *Aerosol Measurement Principles, techniques, and Applications.* pp. 793-803. Third Edition. Hoboken, New Jersey: John Wiley & Sons, Inc.

Cheng, Y.-S. (2011). Condensation particle counters. In Kulkarni, P., Baron, A. P. and Willeke, K., 2011. *Aerosol Measurement Principles, techniques, and Applications.* pp. 381-392. Third Edition. Hoboken, New Jersey: John Wiley & Sons, Inc.

Chu Van, T., Ramirez, J., Rainey, T., Ristovski, Z. and Brown, R. J., 2019. Global impacts of recent IMO regulations on marine fuel oil refining processes and ship emissions. *Transportation Research Part D,* **70**, pp. 123-134.

Dall'osto, M., Ceburnis, D., Monahan, C., Worsnop, D. R., Bialek, J., Kulmala, M., Kurtén, T., Ehn, M., Wenger, J., Sodeau, J., Healy, R. and O'Dowd, C., 2012. Nitrogenated and aliphatic

organic vapors as possible drivers for marine secondary organic aerosol growth. *Journal of Geophysical Research: Atmospheres,* **117**(D12).

Dessens, O., Anger, A., Barker, T. and Pyle, J., 2014. Effects of decarbonising international shipping and aviation on climate mitigation and air pollution. *Environmental Science and Policy,* **44**, pp. 1-10.

Di Natale, F. and Carotenuto, C., 2015. Particulate matter in marine diesel engines exhausts: Emissions and control strategies. *Transportation Research Part D,* **40**, pp. 166-191.

Donaldson, K., Mills, N., Macnee, W., Robinson, S. and Newby, D., 2005. Role of inflammation in cardiopulmonary health effects of PM. *Toxicology and Applied Pharmacology,* **207**(2), pp. 483-488.

Ehn, M., Thornton, J. A., Kleist, E., Sipilä, M., Junninen, H., Pullinen, I., Springer, M., Rubach, F., Tillmann, R., Lee, B., Lopez-Hilfiker, F., Andres, S., Acir, I., Rissanen, M., Jokinen, T., Schobesberger, S., Kangasluoma, J., Kontkanen, J., Nieminen, T., Kurtén, T., Nielsen, L.B., Jørgensen, S., Kjaergaard, H. G., Canagaratna, M., Maso, M. D., Berndt, T., Petäjä, T., Wahner, A., Kerminen, V., Kulmala, M., Worsnop, D. R., Wildt, J. and Mentel, T. F., 2014. A large source of low-volatility secondary organic aerosol. *Nature,* **506**(7489), pp. 476-479.

Ehn, M., Vuollekoski, H., Petäjä, T., Kerminen, V., Vana, M., Aalto, P., DE Leeuw, G., Ceburnis, D., Dupuy, R., O'Dowd, C. D. and Kulmala, M., 2010. Growth rates during coastal and marine new particle formation in western Ireland. *Journal of Geophysical Research: Atmospheres,* **115**(D18).

Eyring, V., Isaksen, I. S. A., Berntsen, T., Collins, W. J., Corbett, J. J., Endresen, O., Grainger, R. G., Moldanova, J., Schlager, H. and Stevenson, D. S., 2010. Transport impacts on atmosphere and climate: Shipping. *Atmospheric Environment,* **44**(37), pp. 4735-4771.

Flagan, R. C., (2011). Electrical mobility methods for submicrometer particle characterization. In Kulkarni, P., Baron, A. P. and Willeke, K., 2011. *Aerosol Measurement Principles, techniques, and Applications.* pp. 339-364. Third Edition. Hoboken, New Jersey: John Wiley & Sons, Inc.

Fuglestvedt, J., Berntsen, T., Eyring, V., Isaksen, I., Lee, D. S. and Sausen, R., 2009. Shipping Emissions: From Cooling to Warming of Climate—and Reducing Impacts on Health. *Environmental science & technology,* **43**(24), pp. 9057-9062.

Gao, Y., Zhao, C., Liu, X., Zhang, M., and Leung, L. R., 2014. WRF-Chem simulations of aerosols and anthropogenic aerosol radiative forcing in East Asia. *Atmospheric Environment,* **92**, pp. 250-266.

Gentner, D. R., Lsaacman, G., Worton, D. R., Chan, A. W. H., Dallmann, T. R., Davis, L., Liu, S., Day, D. A., Russell, L. M., Wilson, K. R., Weber, R., Guha, A., Harley, R. A. and Goldstein, A. H., 2012. Elucidating secondary organic aerosol from diesel and gasoline vehicles through detailed characterization of organic carbon emissions. *Proceedings of the National Academy of Sciences of the United States of America,* **109**(45), pp. 18318-18323.

Goldsworthy, B. and Goldsworthy, L., 2019. Assigning machinery power values for estimating ship exhaust emissions: Comparison of auxiliary power schemes. *Science of the Total Environment,* **657**, pp. 963-977.

Goldsworthy, L. and Goldsworthy, B., 2015. Modelling of ship engine exhaust emissions in ports and extensive coastal waters based on terrestrial AIS data – An Australian case study. *Environmental Modelling and Software,* **63**, pp. 45-60.

Hallquist, M., Wenger, J. C., Baltensperger, U., Rudich, Y., Simpson, D., Claeys, M., Dommen, J., Donahue, N. M., George, C., Goldstein, A. H., Hamilton, J. F., Herrmann, H., Hoffmann, T.,

Iinuma, Y., Jang, M., Jenkin, M. E., Jimenez, J. L., Kiendler-Scharr, A., Maenhaut, W., McFiggans, G., Mentel, T. F., Monod, A., Prévôt, A. S. H., Seinfeld, J. H., Surratt, J. D., Szmigielski, R. and Wildt, J., 2009. The formation, properties and impact of secondary organic aerosol: current and emerging issues. *Atmospheric Chemistry and Physics,* **9**(14), pp. 5155-5236.

Hassellöv, I., Turner, D. R., Lauer, A. and Corbett, J. J., 2013. Shipping contributes to ocean acidification. *Geophysical Research Letters,* **40**(11), pp. 2731-2736.

Headey, B., Muffels, R. J. A. and Wagner, G., 2010. Supporting information. *Proceedings of the National Academy of Sciences of the United States of America (PNAS),* **107**(42), pp. 1-7.

Hennig, F., Quass, U., Hellack, B., Küpper, M., Kuhlbusch, T. A. J., Stafoggia, M. and Hoffmann, B., 2018. Ultrafine and Fine Particle Number and Surface Area Concentrations and Daily Cause-Specific Mortality in the Ruhr Area, Germany, 2009–2014. *Environmental health perspectives,* **126**(2).

Hinds, W. C., 1999. *Aerosol Technology Properties, Behavior, and Measurement of Airborne Particles Second Edition.* John Wiley & Sons, inc.

Grythe, H., 2017. *Quantification of sources and removal mechanisms of atmospheric aerosol particles*, Stockholm University.

Hong, Y., Hong, Z., Zhang, Y., Zhang, H., Xu, L., Liu, T., Xiao, H., Chen, X., Chen, J., Li, M., Deng, J., Wu, X. and Hu, B., 2019. Secondary organic aerosol of $PM_{2.5}$ in a mountainous forest area in southeastern China: Molecular compositions and tracers implication. *Science of the Total Environment,* **653**, pp. 496-503.

Hsieh, P. Y., Abel, K. R. and Bruno, T. J., 2013. Analysis of Marine Diesel Fuel with the Advanced Distillation Curve Method. *Energy & Fuels,* **27**(2), pp. 804-810.

Huang, Y., Shen, H., Chen, H., Wang, R., Zhang, Y., Su, S., Chen, Y., Lin, N., Zhuo, S., Zhong, Q., Wang, X., Liu, J., Li, B., Liu, W. and Tao, S., 2014. Quantification of Global Primary Emissions of $PM_{2.5}$, PM_{10}, and TSP from Combustion and Industrial Process Sources. *Environmental Science & Technology,* **48**(23), pp. 13834-13843.

Hyvärinen, A.-P., Komppula, M., Engler, C., Kivekäs, N., Kerminen, V., Dal Maso, M., Viisanen, Y. and Lihavainen, H., 2008. Atmospheric new particle formation at Utö, Baltic Sea 2003-2005. *Tellus B: Chemical and Physical Meteorology,* **60**(3), pp. 345-352.

International Maritime Organization. *AIS transponders*. Available: http://www.imo.org/en/OurWork/Safety/Navigation/Pages/AIS.aspx [6.11., 2019].

International Maritime Organization. *IMO identification number schemes*. Available: http://www.imo.org/en/OurWork/MSAS/Pages/IMO-identification-number-scheme.aspx [20.11., 2019].

International Maritime Organization. *Sulphur oxides (SO_x) and Particulate Matter (PM) – Regulation 14*. Available: http://www.imo.org/en/OurWork/Environment/PollutionPrevention/AirPollution/Pages/Sulphur-oxides-(SOx)-%E2%80%93-Regulation-14.aspx [07.10., 2019].

Corbett, J. J. and Koehler, H. W., 2003. Updated emissions from ocean shipping. *Journal of Geophysical Research - Atmospheres,* **108**(D20).

JI, Y., Qin, X., Wang, B., Xu, J., Shen, J., Chen, J., Huang, K., Deng, C., Yan, R., Xu, K. and Zhang, T., 2018. Counteractive effects of regional transport and emission control on the formation of fine particles: a case study during the Hangzhou G20 summit. *Atmospheric Chemistry and Physics,* **18**(18), pp. 13581-13600.

Jiang, H., Wu, G., Li, T., He, P. and Chen, R., 2019. Characteristics of Particulate Matter Emissions from a Low-Speed Marine Diesel Engine at Various Loads. *Environmental science & technology.*

John, W., (2011). Size distribution characteristics of aerosols. In Kulkarni, P., Baron, A. P. and Willeke, K., 2011. *Aerosol Measurement Principles, techniques, and Applications.* pp. 41-54. Third Edition. Hoboken, New Jersey: John Wiley & Sons, Inc.

Kanakidou, M., Seinfeld, J. H., Pandis, S. N., Barnes, I., Dentener, F. J., Facchini, M. C., Van Dingenen, R., Ervens, B., Nenes, A., Nielsen, C. J., Swietlicki, E., Putaud, J. P., Balkanski, Y., Fuzzi, S., Horth, J., Moortgat, G. K., Winterhalter, R., Myhre, C. E. L., Tsigaridis, K., Vignati, E., Stephanou, E. G. and Wilson, J., 2005. Organic aerosol and global climate modelling: a review. *Atmospheric Chemistry and Physics,* **5**(4), pp. 1053-1123.

Kang, E., Root, M. J., Toohey, D. W. and Brune, W. H., 2007. Introducing the concept of Potential Aerosol Mass (PAM). *Atmospheric Chemistry and Physics,* **7**(22), pp. 5727-5744.

Kattner, L., Mathieu-Ãœffing, B., Burrows, J. P., Richter, A., Schmolke, S., Seyler, A. and Wittrock, F., 2015. Monitoring compliance with sulfur content regulations of shipping fuel by in situ measurements of ship emissions. *Atmospheric Chemistry and Physics,* **15**(17), pp. 10087-10092.

Kholod, N. and Evans, M., 2016. Reducing black carbon emissions from diesel vehicles in Russia: An assessment and policy recommendations. *Environmental Science and Policy,* **56**(C), pp. 1-8.

Kim, S. D., Kim, I., Lee, K. and Lee, S., 2019. Characteristics and health effects of PM2.5 emissions from various sources in Gwangju, South Korea. *Science of the Total Environment,* **696**.

Kivekäs, N., Massling, A., Grythe, H., Lange, R., Rusnak, V., Carreno, S., Skov, H., Swietlicki, E., Nguyen, Q. T., Glasius, M. and Kristensson, A., 2014. Contribution of ship traffic to aerosol particle concentrations downwind of a major shipping lane. *Atmospheric Chemistry and Physics,* **14**(16), pp. 8255-8267.

Kuittinen, N., 2016. *The effect of fuel on the physical and chemical characteristics of particle emissions from marine engine*, Tampere University of Technology.

Kulkarni, P., Baron, A. P. and Willeke, K., (2011). Introduction to Aerosol Characterization. In Kulkarni, P., Baron, A. P. and Willeke, K., 2011. *Aerosol Measurement Principles, techniques, and Applications.* pp. 3-13. Third Edition. Hoboken, New Jersey: John Wiley & Sons, Inc.

Landis, M. S., Norris, G. A., Williams, R. W. and Weinstein, J. P., 2001. Personal exposures to $PM_{2.5}$ mass and trace elements in Baltimore, MD, USA. *Atmospheric Environment,* **35**(36), pp. 6511-6524.

Lehtoranta, K., Aakko-Saksa, P., Murtonen, T., Vesala, H., Ntziachristos, L., Rönkkö, T., Karjalainen, P., Kuittinen, N. and Timonen, H., 2019. Particulate Mass and Nonvolatile Particle Number Emissions from Marine Engines Using Low-Sulfur Fuels, Natural Gas, or Scrubbers. *Environmental Science & Technology,* **53**(6), pp. 3315-3322.

López-Aparicio, S., Tønnesen, D., Thanh, T. N. and Neilson, H., 2017. Shipping emissions in a Nordic port: Assessment of mitigation strategies. *Transportation Research Part D,* **53**, pp. 205-216.

Lu, X., Lin, C., Li, W., Chen, Y., Huang, Y., Fung, J. C. h., Lau, A. K. H., 2019 Analysis of the adverse health effects of $PM_{2.5}$ from 2001 to 2017 in China and the role of urbanization in aggravating the health burden. *Science of The Total Environment*, **652** (2019), pp. 683-695

Mason, T.G., Chan, K. P., Schooling, C. M., Sun, S., Yang, A., Yang, Y., Barratt, B. and Tian, L., 2019. Air quality changes after Hong Kong shipping emission policy: An accountability study. *Chemosphere,* **226**, pp. 616-624.

Sofiev, M., Winebrake, J. J., Johansson, L., Carr, E. W., Prank, M., Soares, J., Vira, J., Kouznetsov, R., Jalkanen, J.-P. and Corbett, J. J., 2018. Cleaner fuels for ships provide public health benefits with climate tradeoffs. *Nature Communications,* **9**(1), pp. 1-12.

Molland, A. F. (2008) *The Maritime Engineering Reference Book A Guide to Ship Design, Construction and Operation. pp. 346-482. Butterworth-Heinemann*

Nguyen, Q. T., Glasius, M., Sørensen, L. L., Jensen, B., Skov, H., Birmili, W., Wiedensohler, A., Kristensson, A., Nøjgaard, J. K. and Massling, A., 2016. Seasonal variation of atmospheric particle number concentrations, new particle formation and atmospheric oxidation capacity at the high Arctic site Villum Research Station, Station Nord. *Atmospheric Chemistry and Physics,* **16**(17), pp. 11319-11336.

Ntziachristos, L., Saukko, E., Lehtoranta, K., Rönkkö, T., Timonen, H., Simonen, P., Karjalainen, P. and Keskinen, J., 2016. Particle emissions characterization from a medium-speed marine diesel engine with two fuels at different sampling conditions. *Fuel,* **186**, pp. 456-465.

Peterson, P. E. and Woessmann, L., 2014. Feature. *The economic journal,* **120**(546), pp. 183-186.

Pirjola, L., Pajunoja, A., Walden, J., Jalkanen, J.-P., Rönkkö, T., Kousa, A. and Koskentalo, T., 2014. Mobile measurements of ship emissions in two harbour areas in Finland. *Atmospheric Measurement Techniques,* **7**(1), pp. 149-161.

Plauškaitė, K., Špirkauskaitė, N., Byčenkienė, S., Kecorius, S., Jasinevičienė, D., Petelski, T., Zielinski, T., Andriejauskienė, J., Barisevičiūtė, R., Garbaras, A., Makuch, P., Dudoitis, V. and Ulevicius, V., 2017. Characterization of aerosol particles over the southern and South-Eastern Baltic Sea. *Marine Chemistry,* **190**, pp. 13-27.

Pope, C. A., 1996. Adverse health effects of air pollutants in a nonsmoking population. *Toxicology,* **111**(1), pp. 149-155.

Potier, E., Waked, A., Bourin, A., Minvielle, F., Péré, J. C., Perdrix, E., Michoud, V., Riffault, V., Alleman, L. Y. and Sauvage, S., 2019. Characterizing the regional contribution to PM_{10} pollution over northern France using two complementary approaches: Chemistry transport and trajectory-based receptor models. *Atmospheric Research,* **223**, pp. 1-14.

Robinson, A. L., Donahue, N. M., Shrivastava, M. K., Weitkamp, E. A., Sage, A. M., Grieshop, A. P., Lane, T. E., Pierce, J. R. and Pandis, S. N., 2007. Rethinking Organic Aerosols: Semivolatile Emissions and Photochemical Aging. *Science,* **315**(5816), pp. 1259-1262

Sager, T. M. and Castranova, V., 2009. Surface area of particle administered versus mass in determining the pulmonary toxicity of ultrafine and fine carbon black: comparison to ultrafine titanium dioxide. *Particle and fibre toxicology,* **6**(1), pp. 15.

Schwartz, J., Dockery, D. W. and NEAS, L. M., 1996. Is daily mortality associated specifically with fine particles? *Journal of the Air & Waste Management Association (1995),* **46**(10), pp. 927.

Seinfeld, J. H., & Pandis, S. N. (2006). *Atmospheric chemistry and physics: From air pollution to climate change*. Hoboken, N. J. J. Wiley.

Singh, N., Murari, V., Kumar, M., Barman, S. C. and Banerjee, T., 2017. Fine particulates over South Asia: Review and meta-analysis of $PM_{2.5}$ source apportionment through receptor model. *Environmental Pollution,* **223**, pp. 121-136.

Solomon, P. A., Fraser, M. P., and Herckes, P., (2011). Methods for Chemical Analysis of Atmospheric Aerosol. In Kulkarni, P., Baron, A. P. and Willeke, K., 2011. *Aerosol Measurement Principles, techniques, and Applications.* pp. 3-13. Third Edition. Hoboken, New Jersey: John Wiley & Sons, Inc.

Spracklen, D. V. and Rap, A., 2013. Natural aerosol–climate feedbacks suppressed by anthropogenic aerosol. *Geophysical Research Letters,* **40**(19), pp. 5316-5319.

Thiruvengadam, A., Pradhan, S., Thiruvengadam, P., Besch, M., Carder, D. and Delgado, O., 2014. *Heavy-Duty Vehicle Diesel Engine Efficiency Evaluation and Energy Audit.*

Tiwari, S., Parya, S., Mohan, M., Verma, S., Bisht, D. S., 2011. Visibility degradation during foggy period due to anthropogenic urban aerosol at Delhi India. *Atmospheric Pollution* Research. **2**(1), pp.116-120.

TSI (2002). *Model 3010 Condensation Particle Counter. Instruction Manual. Available:* https://www.wmo-gaw-wcc-aerosol-physics.org/files/cpc_3010.pdf [3.2.2020].

UNCTAD (2018). *Review of Maritime Transport 2018.* Technical report, United Nations Conference on Trade and Development.

U.S Department of Homeland Security. *Maritime Mobile Service Identity*. Available: https://www.navcen.uscg.gov/?pageName=mtmmsi [20.11., 2019].

Ushakov, S., Valland, H., Nielsen, J. B. and Hennie, E., 2013. Particle size distributions from heavy-duty diesel engine operated on low-sulfur marine fuel. *Fuel Processing Technology,* **106**, pp. 350-358.

Eyring, V., Köhler, H. W., Van Aardenne, J. and Lauer, A., 2005. Emissions from international shipping: 1. The last 50 years. *Journal of Geophysical Research - Atmospheres,* **110**(D17).

Viana, M., Hammingh, P., Colette, A., Querol, X., Degraeuwe, B., Vlieger, I. D. and Van Aardenne, J., 2014. *Impact of maritime transport emissions on coastal air quality in Europe.*

Wang, X., Shen, Y., Lin, Y., Pan, J., Zhang, Y., Louie, P. K. K., Li, M. and Fu, Q., 2019. Atmospheric pollution from ships and its impact on local air quality at a port site in Shanghai. *Atmospheric Chemistry and Physics,* **19**(9), pp. 6315-6330.

Warneke, C., De Gouw, J. A., Goldan, P. D., Kuster, W. C., Williams, E. J., Lerner, B. M., Jakoubek, R., Brown, S. S., Startk, H., Aldener, M., Ravishankara, A. R., Roberts, J. M., Marchewka, M., Bertman, S., Sueper, D. T., McKeen, S. A., Meagher J. F. and Fehsenfeld, F. C., 2004. Comparison of daytime and nighttime oxidation of biogenic and anthropogenic VOCs along the New England coast in summer during New England Air Quality Study 2002. *Journal of Geophysical Research - Atmospheres*, **109**(D10).

Welp, L. R., Keeling, R. F., Weiss, R. F., Paplawsky, W. and Heckman, S., 2013. Design and performance of a Nafion dryer for continuous operation at CO_2 and CH_4 air monitoring sites. *Atmospheric Measurement Techniques,* **6**(5), pp. 1217-1226.

Westerlund, J., Hallquist, M. and Hallquist, Å. M., 2015. Characterization of fleet emissions from ships through multi-individual determination of size-resolved particle emissions in a coastal area. *Atmospheric Environment,* **112**, pp. 159-166.

Wiedensohler, A., Birmili, W., Nowak, A., Sonntag, A., Weinhold, K., Merkel, M., Wehner, B., Tuch, T., Pfeifer, S., Fiebig, M., Fjäraa, A. M., Asmi, E., Sellegri, K., Depuy, R., Venzac, H., Villani, P., Laj, P., Aalto, P., Ogren, J. A., Swietlicki, E., Williams, P., Roldin, P., Quincey, P., Hüglin, C., Fierz-Schmidhauser, R., Gysel, M., Weingartner, E., Riccobono, F., Santos, S., Grüning, C., Faloon, K., Beddows, D., Harrison, R., Monahan, C., Jennings, S. G., O'Dowd, C. D., Marinoni, A., Horn, H., Keck, L., Jiang, J., Scheckman, J., McMurry, P. H., Deng, Z., Zhao, C. S., Moerman, M., Henzing, B., De Leeuw, G., Löschau, G. and Bastian, S., 2012. Mobility particle size spectrometers: harmonization of technical standards and data structure to facilitate high quality long-term observations of atmospheric particle number size distributions. *Atmospheric Measurement Techniques,* **5**(3), pp. 657-685.

Zetterdahl, M., Moldanová, J., Pei, X., Pathak, R. K. and Demirdjian, B., 2016. Impact of the 0.1% fuel sulfur content limit in SECA on particle and gaseous emissions from marine vessels. *Atmospheric Environment,* **145**, pp. 338-345.

Zhang, F., Chen, Y., Tian, C., Wang, X., Huang, G., Fang, Y. and Zong, Z., 2014. Identification and quantification of shipping emissions in Bohai Rim, China. *Science of the Total Environment,* **497-498**, pp. 570-577.

Zhou, S., Zhou, J. and Zhu, Y., 2019. Chemical composition and size distribution of particulate matters from marine diesel engines with different fuel oils. *Fuel,* **235**, pp. 972-983.

Zhu, C., Cao, J., Zhang, N., Zhang, Z., Zhang, T., Liu, S., Zhou, J., Wang, P., Wang, Q., Tao, J. and Su, X., 2018. The impact of biomass burning on total suspended particulate matter in the southeastern Tibetan Plateau. *Atmospheric Environment,* **193**, pp. 33-39.

Zieman, P.J. and Atkinson, R., 2012. Kinetics, products, and mechanisms of secondary organic aerosol formation. *Chemical Society reviews*, **41**(19), pp 6582-6605.

APPENDIX A: TABLES

Table 1 The number of plumes detected from the different sectors the during different sulfur restriction periods.

Sector	Harbor			Nearby shipping lane			Distant shipping lanes		
Sulfur restriction (%)	1.50	1.00	0.10	1.50	1.00	0.10	1.50	1.00	0.10
Plume number	1721	3393	860	2601	4400	1251	3121	3982	631

Table 2 The average PNC_{pl}s from the sectors 1, 2 and 3 during the different sulfur restriction periods, divided into 3 distinct size classes. From the analyzed plumes the first and the last measurement cycles inside the plumes have been removed.

	Particle size (nm)	Sulfur restriction			Relative change		
		<1.50 %	<1.00 %	<0.10 %	Change 1	Change 2	Total change
Units	nm	#/cm^3	#/cm^3	#/cm^3	%	%	%
Sector 1	7-33	972	825	1180	-15	+43	+21
	33-108	1290	1070	613	-17	-43	-52
	108-537	109	96	92	-12	-4	-16
	Total	2371	1991	1885	-16	-5	-21
Sector 2	7-33	505	506	613	0	+21	+21
	33-108	1033	1064	631	+3	-41	-39
	108-538	104	89	67	-14	-25	-36
	Total	1646	1660	1312	+1	-21	-20
Sector 3	7-33	370	330	350	-11	+6	-5
	33-108	936	945	584	+1	-38	-38
	108-538	131	131	102	0	-22	-22
	Total	1437	1406	1037	-2	-26	-28

APPENDIX B: NUMBER SIZE DISTRIBUTIONS OF PLUMES WITH THE FIRST AND THE LAST MEASUREMENT CYCLES REMOVED

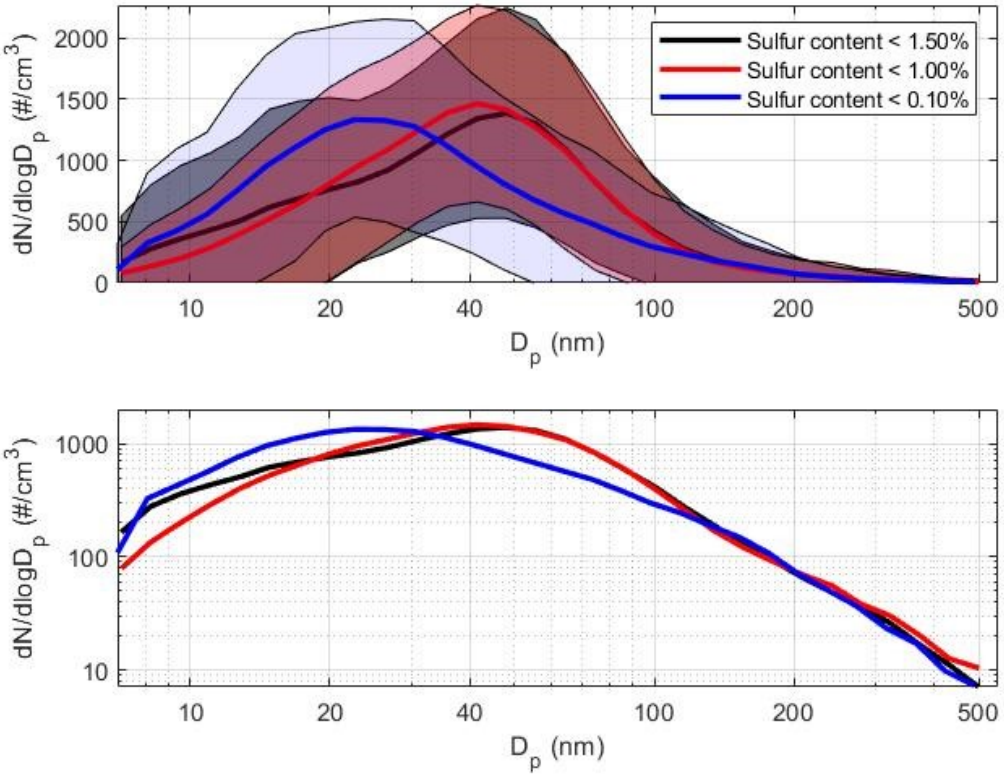

Figure 1 The NSD$_{pl}$s of the plumes from the sector 1 during the 3 different sulfur restriction periods. From the analyzed plumes the first and the last measurement cycles inside the plumes have been removed.

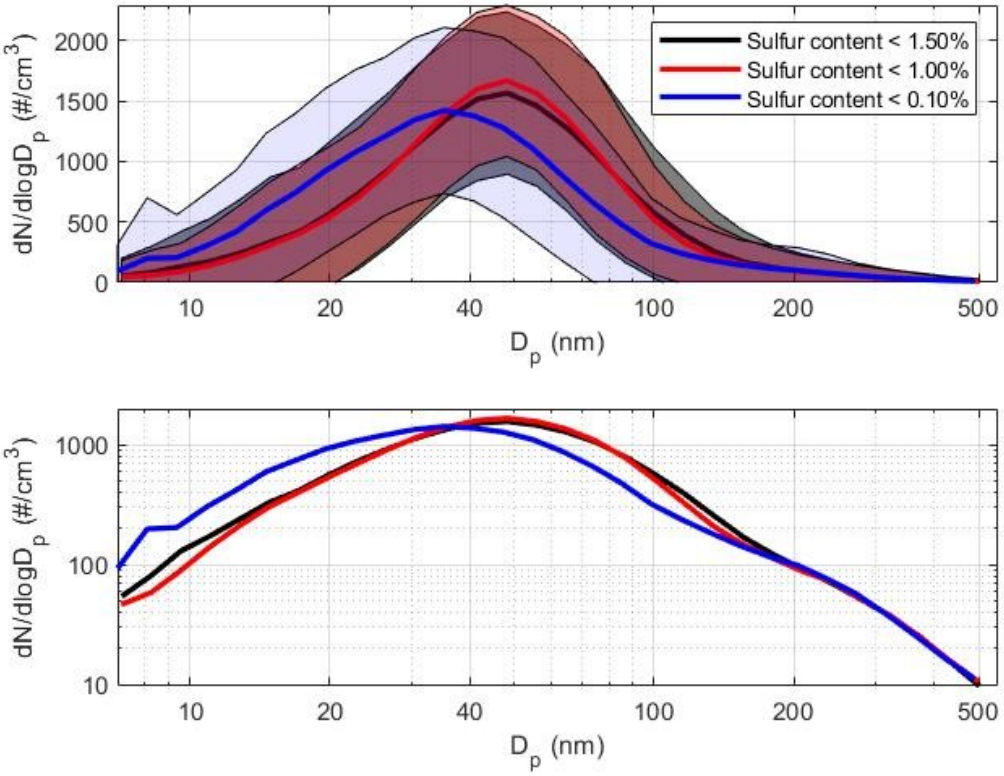

Figure 2 The NSD$_{pl}$s of the plumes from the sector 2 during the 3 different sulfur restriction periods. From the analyzed plumes the first and the last measurement cycles inside the plumes have been removed.

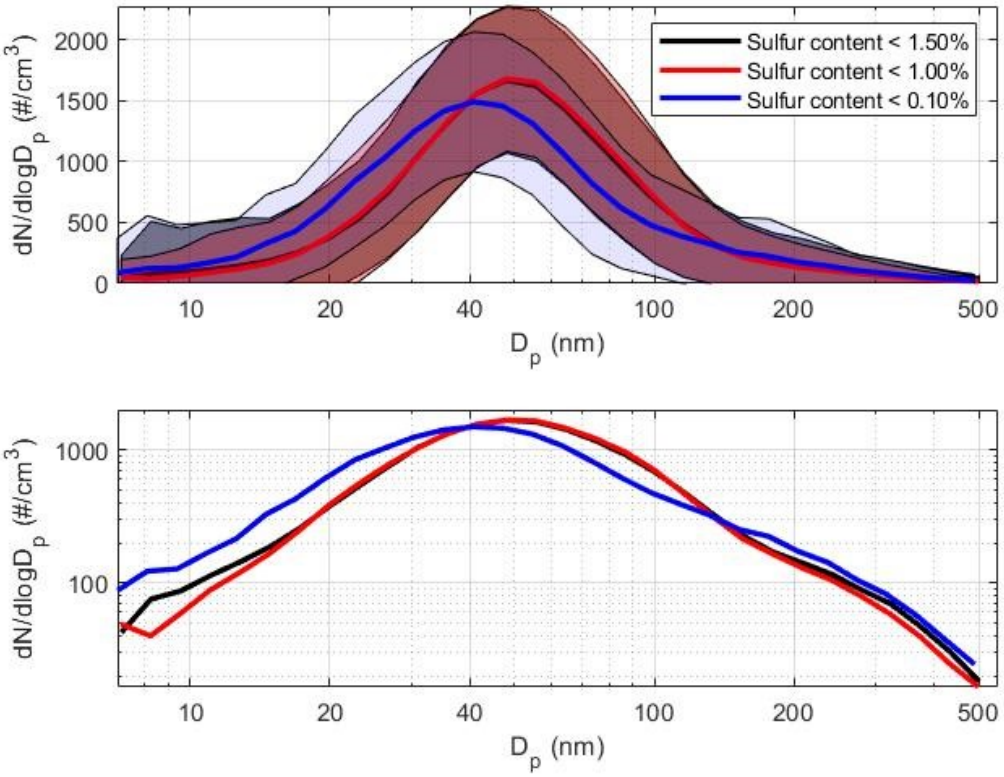

Figure 3 The NSD$_{pl}$s of the plumes from the sector 3 during the 3 different sulfur restriction periods. From the analyzed plumes the first and the last measurement cycles inside the plumes have been removed.